Fire Safety Journal 140 (2023) 103871

Contents lists available at ScienceDirect

Fire Safety Journal

journal homepage: www.elsevier.com/locate/firesaf

A review of thermal exposure and fire spread mechanisms in large outdoor fires and the built environment

Alexander I. Filkov [a,*], Virginie Tihay-Felicelli [b], Nima Masoudvaziri [c], David Rush [d], Andres Valencia [e], Yu Wang [f], David L. Blunck [g], Mario Miguel Valero [h,p], Kamila Kempna [i], Jan Smolka [j], Jacques De Beer [k], Zakary Campbell-Lochrie [l], Felipe Roman Centeno [m], Muhammad Asim Ibrahim [n], Calisa Katiuscia Lemmertz [m], Wai Cheong Tam [o]

[a] Faculty of Science, the University of Melbourne, 4 Water st, Creswick, 3350, Australia
[b] Université de Corse, Campus Grimaldi, 20250, Corte, France
[c] University at Buffalo, 206 Ketter Hall, Buffalo, NY, 14228, USA
[d] School of Engineering, University of Edinburgh, United Kingdom
[e] Department of Civil and Natural Resources Engineering, University of Canterbury, 20 Kirkwood Avenue, Upper Riccarton, Christchurch, 8041, New Zealand
[f] State Key Laboratory of Fire Science, University of Science and Technology of China, Hefei, 230026, Anhui, China
[g] Oregon State University, Rogers 314, Corvallis, OR, USA
[h] Wildfire Interdisciplinary Research Center, Department of Meteorology and Climate Science, San Jose State University, San Jose, CA, USA
[i] Faculty of Safety Engineering, VSB-Technical University of Ostrava, 630/13, Lumirova, 70030, Czech Republic
[j] Faculty of Safety Engineering, VSB-Technical University of Ostrava, 630/13, Lumirova , 70030, Czech Republic
[k] Department of Fire Protection Engineering, University of Maryland, 4356 Stadium Dr, College Park, MD, 20742, USA
[l] School of Engineering, The University of Edinburgh, 190 Mayfield Road, Edinburgh, United Kingdom
[m] Department of Mechanical Engineering, Federal University of Rio Grande do Sul, Sarmento Leite Street, 425, Porto Alegre, 90050-170, RS, Brazil
[n] Department of Biology and Environmental Science, Linnaeus University, Stuvaregatan 2, 392 31, Kalmar, Sweden
[o] Fire Research Division, National Institute of Standards and Technology, 100 Bureau Drive, Gaithersburg, MD, USA
[p] Department of Fluid Mechanics, Universitat Politècnica de Catalunya, Barcelona, Spain

ARTICLE INFO

Keywords:
Exposure mechanisms
Large outdoor fires
Wildfires
WUI
Built environment
Communities
Structures
Resilience

ABSTRACT

Due to socio-economic and climatic changes around the world, large outdoor fires in the built environment have become one of the global issues that threaten billions of people. The devastating effects of them are indicative of weaknesses in existing building codes and standard testing methodologies. This is due in part to our limited understanding of large outdoor fire exposures, including the ones from wildland to communities and within communities. To address this problem, the Ignition Resistance Committee (IRC) of the International Association of the Fire Safety Science working group 'Large Outdoor Fires and the Built Environment' was established. This manuscript is the result of one of the IRC's initiatives to review current knowledge on exposures associated with large outdoor fires, identify existing knowledge gaps, and provide recommendations for future research. The article consists of two sections: the wildland fire exposure to the built environment and the settlement fire exposure to structures. Each section presents a comprehensive review of experimental and numerical studies of exposure mechanisms (flame contact and convection, radiation, and firebrands). The review concludes with a discussion on data consistency and existing knowledge gaps to highlight future directions for each of the three fire exposure mechanisms.

* Corresponding author.
E-mail addresses: alexander.filkov@unimelb.edu.au (A.I. Filkov), tihay_v@univ-corse.fr (V. Tihay-Felicelli), nimamaso@buffalo.edu (N. Masoudvaziri), d.rush@ed.ac.uk (D. Rush), andres.valencia@canterbury.ac.nz (A. Valencia), yuwang@ustc.edu.cn (Y. Wang), David.Blunck@oregonstate.edu (D.L. Blunck), mm.valero@sjsu.edu, mm.valero@upc.edu (M.M. Valero), kamila.kempna@majaczech.cz (K. Kempna), jan.smolka@majaczech.cz (J. Smolka), jdebeer@umd.edu (J. De Beer), z.campbell.lochrie@ed.ac.uk (Z. Campbell-Lochrie), frcenteno@mecanica.ufrgs.br (F.R. Centeno), asim.ibrahim@lnu.se (M.A. Ibrahim), calisa.lemmertz@ufrgs.br (C.K. Lemmertz), waicheong.tam@nist.gov (W.C. Tam).

https://doi.org/10.1016/j.firesaf.2023.103871
Received 7 September 2022; Received in revised form 26 June 2023; Accepted 24 July 2023
Available online 28 July 2023

1. Introduction

Over the past 15 years, there has been a significant increase in the number of large outdoor fires impacting the built environment worldwide [1]. These devastating infernos can be wildfires that spread into communities (known as Wildland-Urban Interface, or WUI fires) or purely urban blazes such as earthquake fires or informal settlement fires. Although these fires threaten populations across the world [2], scientific research on large outdoor fires and possible ways to mitigate the loss of structures when exposed to external fire has lagged far behind research on building fires [3].

To reduce the number of homes lost during large outdoor fires, building structures with higher resilience to fire ignition is necessary. Building codes and standards already include requirements intended to reduce the ignition risk of structures. However, the devastating effect of current large outdoor fire events is revealing weaknesses in existing building codes and standard testing methodologies based on which building codes are developed [4]. It is therefore necessary to improve existing and propose new testing methodologies. To do so, it is important to understand the performance of various structures that are exposed to a range of ignition sources during large outdoor fires.

The general categories of outdoor fire exposures, and the mechanisms of their impact on structures, are well known [5]: radiant exposure, flame impingement or convection, and flying embers or firebrands. Radiation and convection both involve heat transfer directly from the flame. However, unlike radiation heat transfer, convection requires the flame to be in contact with the structure [6], whereas ignition by radiation can occur at a distance substantially greater than the distance to which flames generally extend [7]. Fires can also ignite structures within a built environment through exposure to firebrands. Firebrands can be generated by either burning vegetation or burning structures, and may land on structures, residential materials or adjacent vegetation, causing ignition at such a distance (potentially multiple kilometres) that heat transfer by radiation and convection from the primary fire can be negligible.

Post-fire investigations indicate that the exposure mechanisms leading to the loss or damage of structures vary from fire to fire. For example, during the 2007 Witch and Guejito fires [8,9], 2003 Canberra fire [10] and Fort McMurray fires [9,11] at least 50% of destroyed structures were ignited by firebrands. Direct flame contact impacted 37% of all houses during the 2017 Pedrógão Grande fire, Portugal [12]. Direct flame contact was also identified as an ignition mechanism in the 2012 Waldo Canyon fire in Colorado, USA [13] and the 2009 Black Saturday fires in Victoria, Australia [14]. There have been several studies regarding post-fire investigation of urban fires. However, they have mainly focused on understanding the effectiveness of fire protection or suppression [15], or firebrand generation [16,17]. Only in Ref. [18] the authors indicated that firebrands and radiation from burning structures are the main mechanism of house loss. Thus, to reduce buildings' vulnerability to fire, it is necessary to understand which exposure mechanisms are present in the wildland-urban or rural areas, and to understand the risks each mechanism poses.

The strategy currently being implemented to reduce the ignition potential of structures is to reduce or even eliminate fuel around them (based on the concept of a 'home ignition zone') and to harden structures based on exposure levels [19,20]. However, the distances established by different regulations around the world and the methods for determining exposure levels and construction materials, respectively, vary from place to place. This confirms the need to better understand the different modes of fire exposure in order to come to an agreement about best practices and codes. Therefore, the aim of this study is to review current knowledge on exposures associated with large outdoor fires, identify existing knowledge gaps, and provide recommendations for future research.

To this end, we considered two scenarios: *firstly*, wildfires transition to WUI fires and *secondly*, fire spread in urban settings. This approach led to the following article structure:

Section 1: Wildland fire exposure to the built environment.

- Flame contact and convection,
- Radiation, and
- Firebrands

Section 2: Settlement fire exposure to structures.

- Flame contact and convection,
- Radiation, and
- Firebrands

We reviewed experimental and numerical data and presented a discussion on data consistency and existing knowledge gaps in order to highlight future directions for each of the three fire exposure mechanisms.

The review was conducted by members of the Ignition Resistance Committee of the International Association of the Fire Safety Science working group 'Large Outdoor Fires and the Built Environment' [21]. Literature for the review was selected based on searches of citation databases and the expertise of each committee member.

2. Wildland fire exposure to the built environment

2.1. Flame contact and convection

One of the three exposure mechanisms is flame contact and convection [5,22]. Direct flame contact can occur when a structure is exposed to the flames from a wildfire, ornamental vegetation or other combustible elements near the structure, or neighbouring properties [22]. For instance Ref. [13], found that some ignitions of decking, leading to structure loss during the Waldo Canyon fire, occurred due to direct flame contact with overhanging decks from spot fires in nearby woodlands [14]. attributed also some home losses during the 2009 Australian 'Black Saturday' to flame contact. Despite this, there is currently a lack of studies on flame contact and convection in the WUI [5].

Endeavours to investigate flame dynamics and convective heat transfer in wildland fires can be categorized in four topics: 1) Laboratory experiments; 2) Large-scale field experiments; 3) analytical and numerical studies; and 4) post-incident investigations. Temperature, height and time of residence are among the features that are commonly explored to characterize flames. Sometimes, parameters such as heat flux and surrounding air flow of a fire are examined when considering the convective mode of heat transfer. Several studies have also investigated the response of specific structural components exposed to flames. Such studies are usually at component-level and consider the effect of variables (e.g., fuel load, spacing, etc.) on fire behaviour and the corresponding response of the structural component (e.g., a wall subject to fire load).

2.1.1. Experimental studies

Numerous experimental studies have measured convective heat fluxes both in the laboratory and in the field [23–30] (Appendix, Table 1). At smaller scales, this has included detailed study of the role of high frequency convective bursts as a result of the buoyancy-induced flame dynamics [31,32]. In recent years, convective heat transfer measurements have been a critical component in recent large-scale experimental campaigns [33–36]. Peak convective heat fluxes vary greatly depending on the type of fuel, weather conditions and scale of the fire. Values between 4 kW/m^2 and 300 kW/m^2 have been reported in medium-scale surface fire field experiments [25,27,37,38], whereas maximum sensible (vertical) heat fluxes of up to 3 $MW\ m^{-2}$ were estimated by Ref. [39] and further discussed in Ref. [40].

Measuring the flame temperature in both laboratory and field

experiments has been a long-standing interest. Such measurements are primarily performed via point measurements, e.g., fine wire thermocouples. For example [41], observed an average flame temperature of 815 °C for a variety of forest fuel types but few experimental details were provided [42]. suggested possible flame temperature assumptions for both dry (980 °C) and wet fuels (870–925 °C), based on a compromise between the measurements of [41]; and the greater flame temperatures observed by Ref. [43]. Peak temperatures measured within a wildfire exceed 1000 °C (e.g., 1017 °C measured by Ref. [44] and 1159 °C measured by Ref. [38]), with average temperatures usually being between 600 °C and 700 °C [36,38].

Additionally, past authors have observed variations in flame temperature with height, consistent with the presence of different regions as is typical for buoyant plumes [45,46]. In a series of field experiments within dry eucalypt forests (conducted during Project Vesta [47]) [46], measured flame temperatures at various heights, observing flame tip temperatures of around 200–400 °C and significantly higher flame temperatures at lower thermocouples which ranged from 676 °C to 1184 °C.

The effect of fuel moisture content (FMC) on flame temperature has been studied at the laboratory scale [48]. observed an inverse relationship between FMC and average flame temperature in a number of flame spread experiments in pine needle beds. This rate of change in average flame temperature ranged from 24 °C to 42 °C per % rise in FMC, across the three pine needle species studied. A significant effect of FMC on the resulting flame temperature was also observed by Mendes-Lopes [45] in 2003 in Pinus pinaster needle beds at various slope angles.

The effect of fuel structure and fuel loading must also be considered and can directly affect the flame characteristics. During a series of stationary burns [48], observed a significant effect of porosity on the resulting flame length and on the combustion behaviour (burning rate). Given the complex nature of wildland fuels, varying the porosity (bulk density, packing ratio etc.) can alter both the vertical buoyant flow profile (e.g., altered combustion dynamics due to change in oxygen availability) and the convective heating within the fuel layer (since the permeability of the fuel bed and resulting drag profile may also be altered) [49–51]. The effect of fuel loading on the radiant and total heat flux has been studied in past laboratory-based flame spread studies [52–55], and a positive trend between fuel loading and heat flux was observed within the pre-heating region.

In addition to quantitative measurements of convective heat fluxes, flame geometry and temperature, other studies have focused on the characterization of the air flow patterns that drive convective heat transfer. For example [23], conducted an extensive set of wind-tunnel fire experiments and identified exponential decays in the temperature of the air with the distance from the fire front in the presence of wind. Additionally, maximum air temperatures decreased as the wind speed, packing ratio (of the fuel) and fuel moisture increased. The characteristic distance of the exponential decay increased with the wind speed and decreased with the packing ratio and surface-area-to-volume ratio of the fuel. Furthermore [39], found that the air motions during crown fires had energy-containing scales on the order of meters with timescales of fractions of a second. They also estimated that the motions that occur frequently throughout a crown fire can include updrafts between 10 and 30 m/s, downdrafts between −10 and −20 m/s, and horizontal motions between 5 and 15 m/s. These results are consistent with more recent studies [44].

It is also important to understand the response of structures to given exposure conditions. A USDA Forest Service research team conducted a series of experiments to validate the Structure Ignition Assessment Model (SIAM), a physics-based model they developed (discussed later), and to gain better understanding on the ignitability of structures [56–58]. [56] described the development of the ignition module within SIAM based upon bench-scale experiments (cone calorimeter, Lateral Ignition and Flame Travel (LIFT) apparatus, and Ohio State University (OSU) calorimeter). The time to ignition of samples was correlated with the applied radiant heat flux in order to determine the critical heat flux. The ignition module also considers the potential for the critical heat flux to be exceeded if flame impingement occurs. Flame impingement was studied in a small additional series of gas burner tests involving wall sections covered with hardboard siding. Ignition of the hardboard siding was observed after a sufficient period of flame exposure (circa. 1 min) with self-extinguishing of the flame after removal of the gas burner flame. Continued smouldering was observed (and burning under wind exposure) in certain cases with the flame impingement period determined to be the most important parameter for sustained burn. In Ref. [59] study, the influence of a surface fire front on the ignition of wooden fences was examined. The researchers observed that fences without gaps between boards had a greater flame exposure compared to those with gaps. Additionally, the back surface of the fences was found to be the most affected by the flaming fire front.

2.1.2. Numerical studies

The advancement of computational power has facilitated expanded efforts to develop models to understand the behaviour of wildland fires and their exposures. In recent years, several physics-based models have been developed [60–65]. These models account for sophisticated reactions in solid phase combustion, such as thermal degradation [66], volatilization [67,68], char formation [69] and gas phase reactions [70–72]. These models consider fuel chemistry [73,74] of various wildland fuels, such as wood, grasses, leaf litter, twigs, bark, and shrubs, and evaluate the energy (in the form of heat) released from the fuel. The subsequent heat transfer to the surrounding unburnt fuel is determined with the effect of atmospheric and topographic interactions, including wind speed and direction [75,76], temperature [77,78], humidity [79], fuel slope, structure, and load [80,81].

Numerical tools have been used to study a broad range of factors, such as investigating various fire ignition modes and inter-relationship of flame dynamics and surrounding structures, etc (Appendix, Table 2). For example [82,83], utilized CFD modelling to study the thermal response of a structure exposed to fire. A diffusion flame was used to represent burning vegetation. For cases involving convective heating, variations of the flow patterns were observed around the structure, altering the flame geometry and resulting heating. The relative importance of radiative and convective heating mechanisms varied across the structure boundaries, with convective heating becoming significant in plume contact regions [84]. studied the effect of two- and three-dimensional simulations of fires at WUI. The findings indicate that 2D simulations are suitable for order-of-magnitude analyses due to their short computing times. However, their effectiveness in accurately predicting building and human response is limited, as the differences are considerable. Therefore, for critical simulations, 3D modelling should be employed.

[85] evaluated the Australian Standard AS 3959 (Construction of buildings in bushfire-prone areas) using CFD simulations. The primary objectives were to assess the sensitivity of the heat load on a structure when variables were changed, including wind speed. Specifically, they compared the heat loads on a structure in buoyancy-dominated and wind-dominated fires. It was found that increasing wind speed over flat ground causes the vertical plume (which makes the radiation to be the dominant mode) to incline forward. This shift reduces the flaming area and radiative heat flux while increasing the preheating of the unburnt fuel ahead of the fire [85].

The USDA Forest Service fire research team developed a physics-based Structure Ignition Assessment Model (SIAM) as a practical tool for considering threats from WUI fires. The model was evaluated through several bench-scale and field-scale experiments whose results were discussed earlier in Section 2.1, [56–58]. The model accounts for fire characteristics and general features of the structure and topography, and estimates the ignitability of structures exposed to different heat transfer mechanisms. It is emphasized that although radiative heat flux

contributes significantly to the transferred energy, flame impingement is also important, because simulations that consider only radiation require larger fires and longer residence times compared to field experiments. To account for uncertainties and various scenarios, the flame is assumed to be planar in SIAM and parallel to the wall of the structure. The model shows that flames can cause ignitions when adjacent to structures. As a result, it is argued that when structures are sufficiently close together, they may replace the wildfire as the main source of ignition. The implementation of this ideology can be found in recent studies focusing on the behaviour of burning structures and their contribution of the fire spread in the built environment [86,87].

In [88,89] authors conducted a study on the effects of wildfires on building ignition under various conditions. The forest was represented as a porous reactive medium, and the problem was formulated using standard nonstationary three-dimensional Reynolds equations for flow in a multiphase reactive medium. The equations were solved numerically using the finite volume method. Their study revealed that convection plays a significant role in increasing the risk of house ignition during wildfires. For instance, an increase in wind speed from 6 to 10 m/s resulted in a rise in building surface temperature from over 100 °C to above 300 °C.

[90] reviewed the modelling of fire and wind interaction and its effects on structures. They found that the focus in previous studies was primarily on evaluating fire damage to structures and fire safety engineering of buildings, with little attention given to the interactions between disturbances and structures. They stated that knowledge on wind characteristics and forced convection it generates is crucial to gain a better understanding of fire behaviour as wind largely influences the severity of fires. At the Wildland-Urban Interface (WUI), simulations must consider the coupling effects between structural and wildland fuels, as the combination of these two fuel types has a significant impact.

Ghodrat, Edalati-nejad, and Ghaderi recently conducted numerical modelling to examine the impact of fire intensity and sloped terrain on a simplified structure [91–95]. The simulation employed the FireFOAM solver, which is a transient solver for fire dynamics that utilizes Large Eddy Simulation (LES) and is derived from the OpenFOAM platform. This solver is specifically designed to simulate fire dynamics in large-scale fires. According to the simulations, the presence of a building affects the growth and formation of buoyant instabilities, which directly affect the behaviour of the fire's plum [92]. As the upslope terrain angle and fire intensity increase, the temperature of the ground near the building and the surface of the building increases [91–95].

Summary. Previous experimental studies have mainly focused on measuring flame temperature and size/shape, leading to a wide range of peak temperatures from 200 °C to 1200 °C due to the lack of a standard protocol and measurements at different flame locations. Furthermore, the complex nature of wildland fuels alters both the vertical buoyant flow profile and convective heating within the fuel layer. While convective heat transfer measurements have become critical in experiments over the last two decades, there is still limited data with varying values among studies. For instance, medium-scale field experiments report peak convective heat fluxes ranging from 4 kW/m^2 to 300 kW/m^2 with updrafts up to 30 m/s.

Recent advancements in computational power have allowed for the development of physics-based models that help understand fire ignition modes and flame dynamics. CFD modelling has been used to study the thermal response of structures to fire and the impact of wind speed on heat loads. Convective heating was found to be significant in regions of plume contact, and increased wind speed can lead to a substantial increase in building surface temperature. Understanding the coupling effects between structural and wildland fuels is also crucial in accurately simulating fire behaviour, as is recognizing how the presence of a building affects the growth and formation of buoyant instabilities that influence the behaviour of the fire's plume.

Future research in convective heat transfer in fire science can focus on more detailed studies of the role of wind gusts and fire atmosphere interactions. Studies can also investigate the relationship between fuel properties and flame dynamics, such as the effect of fuel moisture content and structure on flame temperature and convective heat transfer. The development and use of improved instrumentation for measuring convective heat fluxes in combination with 3D modelling should be employed to predict building response to fire more accurately.

2.2. Radiation

Measuring the radiant heat fluxes of wildland fires is necessary to understand fire behaviour and impacts [34,35] and to correctly design wildland firefighter safety zones [96], as well as defensible spaces around structures [8]. The approaches used to study radiant heat transfer in wildland fires can generally be classified into three categories: laboratory and field experiments, and numerical modelling.

2.2.1. Laboratory scale experiments

At the laboratory scale [97–104], studies concerning radiation emissions usually use in-situ measuring devices (Appendix, Table 3) placed at the edges of the fire [48,105]; Mell et al., 2009 [52,54,106–109],). Peak radiation fluxes reported in laboratory scale studies are typically much lower than those found in full scale fires due to the large difference in size. Nonetheless, laboratory-scale studies provide an opportunity to collect repeated measurements for well characterized boundary conditions and can be used to assess simulations. The measurements can be heat fluxes (HF), heat release rates (HRR), radiant and convective fractions, flame emission or flame temperature [110–112]. [109] reported peak heat fluxes near 8 kW/m^2 for beds of pine needles, which is consistent with values reported by Ref. [52]. [113] burned individual Douglas-fir trees that were 2–5 m tall. Peak heat fluxes were near 20 kW/m^2 for 2 m tall trees but increased to near 50 kW/m^2 for 5 m tall trees, depending on the location of the measurement. These values are consistent with the work of [114]; who notes that values from literature range from 15 to 50 kW/m^2, although no references are provided. Certainly, the nature of the fuel influences peak radiant heat fluxes.

Studies have also measured the heat release rate during static fires and as the fire front propagates [52,54,108,110,114–116]. These data are generally obtained by oxygen consumption calorimetry or are calculated from mass loss rates. Values between 4.5 and 400 kW have been recorded depending on the fuel nature and quantity.

Knowledge of heat release rates can be used to determine the amount of radiation emitted if the radiative fraction is known. The radiant fraction is the ratio of the energy transferred to the surroundings through infrared radiation normalized by the total heat released by burning the fuel [117]. Measuring this quantity, and knowing the heat release, is one approach to quantifying the radiation emissions and facilitating scaling of results. At the laboratory scale, the radiant fractions found in the literature are in the range of 0.1–0.4 [48]. obtained radiant fractions between 0.1 and 0.4 for pine needle fuel beds with a size between 0.04 and 0.09 m^2. By using the gas temperature rise (GTR) calorimetry [118], found a radiant fraction of 0.298 for pine wood [105]. reported a mean radiant fraction of 0.124 for biomass fires across fuel beds of 80 × 210 cm. While [52] measured radiant fractions ranging from 0.17 to 0.22 for pine needle fuel beds of 1 m × 2 m under no slope conditions, others have reported global radiant fractions closer to 0.25 and 0.39, depending on the slope of the fuel bed [54]. Increasing the slope tends to increase the radiant fraction and the contribution of radiation heating. However, beyond a certain slop angle convective heating becomes more important than radiative heating in causing fire spread [108]. reported that this transition occurs near a slope of approximately 20°.

It is also noted that the contribution of radiation and convective heat transfer to fire exposure depends on the location. Radiation dominates heat transfer in the preheating region (at some distance from the fire front) while both convection and radiation both contribute closer to the

flame front [52]. According to Ref. [119]; the radiation from the burning embers through the fuel bed to the unburnt fuel is about 3 times higher than the radiation from the overhead flame to the same particles. Furthermore, the contribution to radiation emissions from the flames (in contrast to fuel surfaces) tends to increase with fuel loading [52,54].

Laboratory-scale radiation research has also considered radiation emissions from vegetation flames [120,121]. demonstrated that flame emission is governed by combustion-produced hot gases with a low-intensity background radiation from soot, as the small-scale flames in these experiments were optically thin. The corresponding spectral emission is far from that of a blackbody [120,121]. However, as the depth of the flame increases, it becomes optically thick with emissivity tending to 1 [122]. In parallel, they showed that the spectral absorption of the vegetation varies with the wavelength, indicating a non-gray behaviour [121]. [123]; in their study on flames from a cylindrical forest fuel burner, showed that radiation was dominated by emissions from soot in the spectral range of the camera, but radiation from gaseous products of the combustion was not negligible.

Another quantity studied by the scientific community is the flame emissivity. Several studies have demonstrated that the emissivity values were correlated against flame thickness. [48] has demonstrated that only flames thicker than 3.2m exhibit an emissivity value close to that of a blackbody (0.9). Anderson obtained measurements showing flame emissivity between 0.16 and 0.28.

2.2.2. Field scale experiments

Field scale experiments dealing with radiant exposures in wildland fires have been quite diverse. The first studies across vegetative fuels appear in the early 20th century [97,124,125]. From 1990s, scientists evaluated either prescribed burns [126,127]; Viegas et al. [58,128]; De Luis et al. [24,25,33,44,46,83,129–137]; or fire propagations in cut fuels or fuel beds [131,138,139]. This led to great variability in the burned area - ranging from 25 m^2 to more than 400 ha. The vegetation of relevant studies has varied from: trees (pine, oak, eucalypt), to shrubs (strawberry tree, broom, heather, sagebrush, asphodel, cistus, tea shrub, broad leaved brown pea, huckleberry, blueberry), to herbaceous layers (grass, wheat crop), vegetable litters (pine needles, leaves), and wood wool. Regarding ignition, two methods are reported: in-line ignition performed with drip torches or strip ignition with delayed-ignition devices dispensed via helicopter. A great variability in the experimental conditions is also noted. For example, the slopes considered varied between 0 and 37° and the wind speeds between 0 and 8.05 m/s.

A variety of quantities have been measured and reported during field scale fire experiments. In some of the first related work [126,127,140], only information on the characteristics of the fire front (rate of spread, fire front geometry, flame duration) or the temperatures was provided. Starting in 2000s, the fireline intensities of the fires, generally calculated with Byram's equation, have been reported [33,44,46,129,133,134,137–139,141–143]. Since this quantity depends on the vegetation, fuel load, and the fire's rate of spread, fire line intensity values ranging from 207 to 93,476 kW/m are reported in the literature. Heat flux measurements started to be reported in 2004 (Table 4). Different measurement devices, such as heat flux gauge, radiometer, or long-wave infrared camera, can be used to collect such measurements. The sensors are placed either in the fire or at the fire's periphery by using towers, remotely piloted aircraft systems or satellites. The values of measured radiant heat fluxes can range from 1.5 to 300 kW/m^2. Thus, fireline intensity and radiant flux values can vary by a factor of 200 or more from one study to another, mainly due to differing experimental conditions (burn area, position of the sensors, fuel load, etc.).

It can be challenging to compare laboratory-scale to field-scale data. The size of the fire has a considerable impact on the magnitude of its heat release rate and radiant emissions. At the laboratory scale, oxygen consumption calorimetry makes it possible to precisely measure the heat release rate of burning vegetation. Unfortunately, this technique cannot be used on a field scale. To estimate such a fire's power, scientists resort to determining the fireline intensity, generally calculated with Byram's equation. Although this formula provides a good estimate of the fire's power [144], showed that fireline intensity could be overestimated by about 20% because Byram's equation did not take into account combustion efficiency. Regarding radiative fluxes, the only parameter that can be compared between scales is the radiant fraction. At the field scale [145], found radiant fractions close to 0.20 for wildfires while [138] found radiant fractions between 0.13 and 0.22 during the burning of 8 × 8 m plots of leaf litter from oak-dominated stands. These values are in the same range as those obtained at laboratory scale.

In the context of fires at the WUI, it is important to quantify the impact of wildfire fires on adjacent structures. In 2004 [128], studied the ignition of a wood wall due to a crown fire in jack pine and black spruce forest. The wood wall measured 1.2 m × 1.2 m and had a roof section 1.22 m wide. The wooden structure was placed at the middle of the downwind side of the burn plot 10, 20, or 30 m away. Heat flux sensors were placed in the middle portion of the wall's front surface, 1.22 m from the wall-eave junction. Thermocouples were placed at the wall base, the eave soffit-wall corner, and the outer eave edge in order to detect when flaming ignition occurred. Walls that ignited did not sustain flaming after the crown fire burned. The burning wall did not generate sufficient heat to maintain flames without the crown fire. Walls that did not ignite but charred, did not char under the eaves because of the eave blocking the radiation. In 2007 [83], performed experiments in a wind tunnel. The vegetation was represented by a 2 × 3 meter litter bed made with wood wool (fuel load of 1.32 kg/m^2) or Douglas pine needles (fuel load of 2.575 kg/m^2). The structure was made up of Syporex blocks and was 2.04 m high, 1.38 m wide, and 7 cm thick. This structure was placed at the end of the tunnel 1 m from the end of the vegetation fuel bed. A wind speed of 1.2 m/s was applied during the experiments. The thermal impact on the structure was evaluated from temperature measurements using three thermocouples embedded in the wall. No flux measurements were performed. Temperatures of 190 °C were measured on the concrete structure, when the fire plume was in contact with the upper part of the structure.

2.2.3. Numerical modelling

Numerical simulations of fires in vegetation fuels typically take radiation into account in a simplified form, or use the radiative transfer equation (RTE) [63,107,108,113,114,146–152]. The RTE, which governs the propagation of radiation through an absorbing and emitting medium, is a multi-dimensional partial differential equation with spectrally dependent properties [153]. Solving such an equation is exceedingly difficult, and the numerical complexity is exacerbated by the strong spectral dependence of the radiative properties of non-gray gases, such as water vapor and carbon dioxide [121,154,155]. In addition to gaseous species, particulates such as soot also emit and absorb infrared radiation. Even though the Rayleigh limit [156] is often being considered in the RTE, in which the complex Lorenz-Mie calculations [157] for the evaluation of scattering effects can be neglected, the absorption behaviour of soot is still a strong function of wavelength. Nevertheless, since the spectral behaviour of soot is generally monotonic and is proportional to the source temperature, the radiative properties of soot can be evaluated analytically through closed form expressions [158].

The spectral behaviour of non-gray gases, such as water vapor, is highly irregular and is described by more than ten thousand spectral lines. Detailed spectral evaluation accounting for different line structures is typically required to evaluate the total emissivity/absorptivity. It is well known that the Line-by-Line (LBL) method [159,160] provides the most accurate predictions of the spectral properties (i.e., 1-D emissivity and absorptivity) of non-gray gases. However, this method requires high-resolution spectroscopic databases [161] and lengthy computation times. Even with today's powerful computers, the LBL method can only be used to generate benchmark solutions.

In order to overcome the numerical bottleneck for practical

engineering applications, approximate methods such as narrow band models [162–164], gray gas models [165–167], and total emissivity chart models [168] have been developed. Narrow band models (NB) provide predictions for the average spectral absorption coefficient near a narrow spectral band. The results generally agree well with those generated from the LBL models. However, the NB results must still be integrated over the wavelength from the entire spectrum to generate the total emissivity/absorptivity. The direct use of NB models in today's physics-based models, such as WFDS [63], is still limited and additional mathematical simplification is often required. Gray gas models are more computationally efficient. It assumes that the spectral behaviour of a non-gray gas (i.e., water vapor and CO_2) over the entire spectrum can be described by an "equivalent" gray absorption coefficient. However, previous studies [169,170] showed that treating gas absorption coefficients as gray in high temperature applications can lead to temperature under-predictions of 375 K or more. In addition, gray models require an extensive database for the "equivalent" gray absorption coefficients. Therefore, the use of gray gas models is generally not recommended if modelling accuracy is a concern. Total emissivity chart models are established on the basis of measurements and total (spectrally integrated) emissivity data, with various path-lengths, species concentrations, and temperatures, typically formulated into empirical charts/correlations. The emissivity charts are generally utilized in analytical models [6,107,146,152] in which the geometrical condition of the fire can be simplified with limited information about the thermal conditions and the species concentration of the non-gray gases. However, if the source temperature (i.e., flame) and the gas temperature (i.e., gas medium in between the emitting source and the receiving area) are substantially different, the use of the emissivity charts can lead to significant errors [171,172]. Therefore, validation efforts are vital to assess model accuracy.

As the RTE is an integro-differential equation for which exact solutions are not available for wildland fires, several methods with varying degrees of approximation have been developed to solve it [173]. The major solution approaches include statistical or Monte Carlo methods, zonal methods, flux methods including the discrete-ordinates approximation, moment methods, spherical harmonics approximation and hybrid methods. The Monte Carlo (MC) approach simulates the histories of a finite number of photons which originate from specified elements, propagate in all directions, and are absorbed and scattered based on local values for absorption and scattering coefficients. However, in order to obtain a converged solution, a significantly large number of emitting photons are needed, and this requires a lengthy computational time and resources. Therefore, the MC approach is often being used to obtain benchmark solutions.

In the zonal methods (ZM), the computational domain is divided into zones, each having uniform temperature and radiative properties. This makes it possible to write an energy balance for each zone. The radiative heat flux generated by the exchange between the zones is determined using a radiosity method based on appropriate view factors. In the case of an absorbent-emitter medium, the calculation of the direct exchange areas is complicated due to the attenuation of the radiation along a path connecting two zones. However, ZM becomes computationally inefficient when coupled with the finite volume reactive fluid flow approaches usually used in full combustion models.

Flux methods are based on separating the angular dependence of the radiation intensities, coming from the spatial dependence of the in-scattering source term. Assuming uniform intensities over defined intervals of the solid angle, the RTE can be simplified into a series of coupled, linear, differential equations expressed in terms of average radiative intensities or fluxes. There are different flux models depending on the number of solid angles used to approximate the directional dependence of the radiant intensity such as six-flux or eight-flux models for three dimensions.

For the moment methods and spherical harmonics approximations, the radiative intensity is expressed as a series of products of angular and spatial functions. An integral part of the equation can be eliminated and a series of equations in terms of different orders of moments can be generated. If the angular dependence is expressed using a Taylor power series expansion, the method is called the moment method, and if spherical harmonics are used to express the intensity, it is called the spherical harmonics (PN) approximation results. The P1 approximation is particularly simple, as it can be expressed in a single second-order differential equation, but this simplicity comes at the expense of accuracy.

Finally, combinations of various methods for solving the RTE (described above) have been used to formulate hybrid methods, which attempt to compensate for the flaws of one approach with the strengths of another. The most widely used physical models for modelling wildland fires use different resolution methods for the RTE. For example, FIRESTAR employs the discrete ordinates method. WFDS uses the finite volume (FV) method, which solves the grey gas form of the RTE in a participating media. FireFoam employs a Finite Volume Discrete Ordinance method (fvDOM).

The main advantage of simulations over experiments lies in their ability to provide data, such as radiative heat transfer, from across the whole of the computation domain and not only at certain measurement locations. Moreover, parameters such as the fire behaviour and exposure levels can be determined in conjunction with the radiative behaviour. Table 5 in Appendix presents numerical studies involving the radiation impact of a wildland fire on structure. In 1996 [6], proposed a thermal radiation and ignition model to estimate structure ignition potential using designated flame characteristics and flame-to-structure distances. The flame was represented by a rectangular radiator at 1200 K with an emissivity of 1. The flame-wall configuration was modelled by centred parallel plates. At 3 m from the fire, heat fluxes between 20 and 110 kW/m^2 were obtained depending on the vegetation. They highlighted also the influence of the tree density on the incident radiant heat flux. Model results indicate that ignitions from fire radiation are unlikely to occur beyond 40 m from a structure.

In 2005 [82], estimated the thermal impact on structures exposed to a fire. The RTE was solved by the finite-volume method using a local angular mesh refinement to accurately describe radiative transfers in the structure direction. The pyrolysis products were modelled by CO and soot formation was considered. A grey gas assumption was used for the absorption coefficient. The burning vegetation was represented by a burner of 1 m × 2 m with a fire intensity of 5 MW/m. Two wind speeds were tested: 3 and 5 m/s. A concrete structure (0.2 m × 2 m × 2 or 5 m) was located at 5 m from the burner. Radiant heat fluxes up to 8 kW/m^2 were obtained on the structure.

In 2008, Zárate et al. worked on the determination of the safety distances for wildland fires by using a solid flame model coupled with the calculation of view factor. They highlighted that the heat fluxes were higher than 4.7 kW/m^2 for a distance between 3 and 6 times the flame height. Safety distances between 7 and 65 m were proposed depending on the considered material for the house (wood or plastic), the type of fuel and the fires (surface or crown fires). In 2011 [174], used a solid flame model coupled with a Monte Carlo method to estimate the radiant heat flux from wildland fire. They evaluated, in particular, the merits of a 50-meter clearing distance around constructions. They modelled a 10m × 10m x 6m house surrounded by vegetation and calculated the radiant heat fluxes on the house. Values up to 20 kW/m^2 were obtained on the house walls. They concluded that a 50-m-radius "fire wise" treatment zone around each housing unit is not sufficient to ensure safety. Rossi et al. (2011) used a solid flame model to calculate the acceptable safety distance for flame lengths and inclinations. They also proposed a simplified analytical expression to determine the safety distance for people and houses [175]. studied the effects of fire intensity and wind speed on the ignition of wooden buildings. The optical properties were independent of radiation wavelength and a diffusion approximation for radiation flux density was used for the mathematical description of radiation transport during forest fires. Temperature fields,

velocity and mass fractions of the different phases were obtained numerically. Temperatures between 320 and 600 °C were obtained on the house wall for a fire at 10 m, depending on the wind speed and the house dimension. Based on their data, the maximum fire-to-structure distance within which ignition is possible was determined for various configurations.

[176] studied in 2017 the potential damage to a house during a fire at WUI with ornamental trees surrounding the construction. For this, they used EcoSmartFire software. The trees in fire are modelled by cylinders and the heat flux calculations is based on the direct line-of-sight radiative heat transfer from the cylindrical to the surface element in question, while adjusting for the blocking of that line of sight from other trees and other parts of the structure, and including ground reflections of the radiative heat flux. They provided heat fluxes and temperature fields on the house walls and determined the percentage of damage by using a temperature criterion. Heat fluxes above 65 kW/m^2 and temperature above 600 °C were obtained on the house wall. In 2019 [177], evaluated the effects of radiant heat flux from wildfires on structures in an urban environment by using a solid flame model and considering the heat obstructions of non-combustible structures. In particular, they used two case studies featuring several houses to compare their results to existing approaches employed in Australian standards.

In 2021, Ricci et al. (2021) proposed a methodology for the evaluation of safety distances between storage tanks and vegetation that may be affected by a wildfire. For this, they used a solid flame model and considered grassland fires, shrubland fires and crown fires. The incident radiation on the tank was employed to calculate the time to failure as a function of the distance. Two references times (5 and 15 min) were considered to define the safety distances ranging between 15 and 405 m depending on the type of tank and fire. In 2022 [95], investigated the combined effects of slope and fire intensity on an idealized building with FireFOAM using a Finite Volume Discrete Ordinance method. The impact of the fire on the structure was evaluated by using the temperature distribution. Temperature variation up to 1500 K were obtained for the highest fire intensity (18 MW/m) and the steepest sloped terrain (30°).

Perez-Ramirez et al. (2022) characterized the heat exposure on a dwelling for two Mediterranean WUI scenarios by using WFDS. A defensive zone was modelled around a house followed by a high-density cork oak forest. The litter and shrubs were modelled by a boundary fuel model coupled with a linear pyrolysis sub-model for the thermal degradation of the solid-phase. For trees, the fuel element model was used combined to an Arrhenius type model for solid-phase degradation including char oxidation. The gases were assimilated to grey medium. The vegetative fuels were assumed to be spherical, non-scattering and perfectly absorbing. A finite volume method was used to solve the grey form of the RTE. Total heat fluxes above 120 kW/m^2 were obtained on walls exposed to the fire.

Summary. Compared to other types of exposures, there has been relatively thorough research conducted on the radiant heat exposure of wildfires to structures. Just like convection, the type of fuel has an impact on the level of radiant heat flux. In laboratory-scale studies, the radiant fractions documented in literature typically range from 0.1 to 0.4. Research has shown that radiation is the primary mode of heat transfer in the preheating area, which is located at some distance from the fire front, while both convection and radiation contribute closer to the flame front. Laboratory and field experiments exhibit substantial variability in their values for various reasons. In laboratory-scale experiments, peak radiation fluxes are typically much lower than those seen in full-scale fires, owing to the substantial size difference. At the field scale, this variability stems from a range of factors, including the extent of the burned area (spanning from 25 m^2 to 400 ha), the types of vegetation present (including trees, grass, and litter), as well as the experimental conditions such as terrain, weather or the position of the sensors. As a result, fireline intensity and radiant flux values may vary significantly from one study to the next by a factor of 200 or more. Additionally, because the laboratory and field experiments measure different parameters due to the nature of the experiments, it is incredibly challenging to understand the scale effect.

The primary focus of numerical modelling of radiant exposure is to compute the safety distance around a structure based on the estimated level of radiant heat flux. Radiant heat flux is typically considered in a simplified form, or by using the radiative transfer equation (RTE). However, solving RTE is a challenging problem, and several approximation methods have been developed to solve it. Nevertheless, all these methods have their limitations. Due to the use of different models, initial conditions, and computational techniques, various safety distances (ranging from 7 to 405 m) and heat flux values on the structure (8–110 kW/m^2) have been obtained, which makes it challenging to compare results across different studies.

Further research is required to improve the methods used for measuring radiant heat fluxes in wildland fires. This requires a comprehensive study into different types of measuring devices and their optimal placement relative to the fire. To gain an in-depth understanding of radiant exposures in wildland fires, it is essential to conduct field-scale experiments. Future studies should prioritize the simultaneous measurement of fireline intensities and radiant heat fluxes across diverse vegetative fuels and experimental conditions. By comparing data obtained from laboratory-scale and field-scale observations, we can unravel the scale-dependent radiant exposure. Future research should also concentrate on the development and refinement of radiative transfer models. Understanding radiant heat fluxes holds significant importance in assessing the impact of fires, designing safety zones for firefighters, and establishing defensible spaces around structures.

2.3. Firebrands

During wildland and structural fires, a large number of burning and glowing/smouldering particles can be generated and then transported by the convective column of a fire front and by the wind. Usually, these particles are referred to as firebrands and/or embers (firebrands hereafter), and consist of pieces of structural materials and vegetation (bark, leaves and twigs) (Fig. 1a). Firebrands can ignite vegetation or structural materials ahead of the fire front (known as spotting) and significantly contribute to house loss in the Wildland-Urban Interface (WUI) [9–11]. To make communities more resilient to firebrand exposure the fire community needs to better understand the phenomenon of spotting, which consists of three main processes (Fig. 1b):

1. Firebrand generation (how many particles of different mass, size, shape and material type are produced by fire);
2. Firebrand transport (how far and in what combustion mode [i.e., flaming or smouldering/glowing] particles can travel);
3. Firebrand deposition/Ignition potential (what is the remaining energy/temperature of a particle upon landing and its potential to ignite fuel).

This section is organized according to the three factors that contribute to spotting.

2.3.1. Generation

The generation of firebrands is the least understood of the three processes leading to spotting. While the majority of studies considering generation have been conducted in laboratory settings [179], the few studies of firebrand generation in field conditions have proven quite insightful (Appendix, Table 6). For example, one field study was conducted as a part of “Project VESTA: Fire in Dry Eucalypt Forest” [180]. This study sought to quantify short distance firebrand production and spotting in Western Australian forests. They found that a large proportion of firebrands are small flakes of jarrah bark and that firebrand densities were greater at older plots of trees. They also found that more

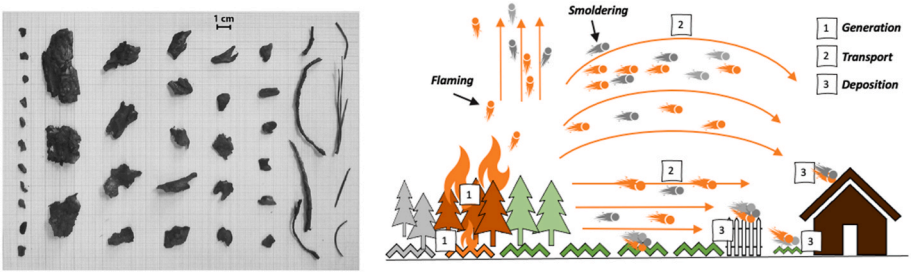

Fig. 1. a) Examples of collected firebrands [178], b) illustration of the three processes of spotting.

intense fires resulted in higher bark consumption.

A number of publications were produced as an outcome of the "Evaluation and Optimization of Fuel Treatment Effectiveness with an Integrated Experimental/Modelling Approach" project [181]. Specifically, a series of prescribed fire experiments were used to understand and estimate short-distance firebrand generation [178,182]. [178] found that fine fuel with diameter <4 mm contributed to firebrand generation in a shrub layer. The authors concluded that the fire-induced draft is an important influence for firebrand production and transport of bark. Similar to Refs. [178,180] reported that the majority of firebrands produced in the field were bark flakes, and the rest were twigs [182]. developed algorithms to process infrared videos for firebrand diagnostics. The authors observed that for low intensity surface fires, the firebrand velocity is consistent with the ambient wind speed. The method was further developed in Refs. [183,184] to measure firebrand characteristics and flux, and correlate results to fire intensity. The authors measured the firebrand flux (number of firebrands fallen on one square meter of area per second) and found that the occasional crowning (21,000 kW/m) increases firebrand flux significantly (3–10 times) compared to surface fire (180–12,590 kW/m) [185]. continued to investigate firebrand generation in pine forests during a series of field experiments. Consistent with the work of [180]; higher numbers of firebrands were found at sites with higher fire intensity [186]. [187] monitored mature pine trees to examine the effects of varying solar exposure on bark moisture and peeling. They found that bark moisture and flakiness is highly dynamic on short time-scales and these diurnal changes likely influence the probability of firebrand production during fire events.

Investigations after wildfire incidents provide insights into firebrand generation characteristics. For example [188], analysed the burn marks on trampolines and plastic sheeting after fires to estimate firebrand sizes at the time of landing. More than 95% of holes are less than 0.5 cm^2. These results confirm the findings of [189] from the Angora Fire, where more than 85% of all firebrand holes measured were less than 0.05 cm^2. Firebrand production was also found to be dependent on fire severity with more severe fires resulting in more firebrands [188].

Much of our understanding of firebrand productions has resulted from laboratory-scale studies. For example [190,191], investigated firebrand generation on Douglas-fir trees through a series of experiments where the size and mass distributions of generated firebrands were measured. They found that (i) Douglas-fir trees generated firebrands only at moisture content levels below 30% in the absence of wind, (ii) the majority of generated firebrands were cylindrical with an average size of 4 mm in diameter and 53 mm in length, and (iii) the surface area of the generated firebrands increased linearly with firebrand mass.

[192,193] conducted comprehensive laboratory experiments at a relatively large-scale investigating firebrand generation from wildland and structural fuels. They developed statistical frameworks and introduced generalizable distributions of different variables (e.g., firebrand size and mass) for firebrand generation. In agreement with [191,192] found a very strong correlation between firebrand mass and projected area. Additionally, the mean and median travel distances of firebrands, along with their projected area and mass, increased with wind speed. A comparison of the mass and projected area of firebrands generated from building materials and firebrand generators [193] showed significant variation because of differences in the properties (e.g., material type or moisture content) of the fuels.

[194] also examined firebrand generation for different vegetation species by measuring the time required for the fuel to generate the firebrands. Interactions between different parameters (e.g., the concurrent effects of wind and moisture content) were considered. They found that the diameter of the samples had the greatest effect on the time to generation and the fuel species had the second greatest effect. These conclusions suggest that fuel morphology is one of the most significant factors influencing firebrand generation.

Simulations have proven useful for helping to bridge the gap in our understanding between laboratory- and field-scale studies of firebrand generation [195]. developed a model to predict the breaking of twigs when exposed to fire. Their analysis suggested that laboratory- and field-scale firebrands were similar enough in size that one could serve as a reasonable analogue for the other. The model predicted that the surface area of firebrands tends to scale with the mass of the firebrand to a power of 2/3, consistent with results from experiments. The size of firebrands is influenced by the combustion behaviour and failure mechanics of the limb. In related work [196], developed a model to predict the generation of firebrands by considering the mechanics of branch breakage and a fuel decomposition model. By coupling the breakage model to a plume model, generation and transport of firebrands were predicted. The authors identified an optimal diameter for generating and lofting/transporting firebrands.

2.3.2. *Transport and spot fire distance*

One of the factors important when determining the threat to structures from firebrands is the maximum distance over which spot fires can occur (Appendix, Table 7). This distance is generally considered as a function of the type of firebrand (size, density, shape, and material), the local conditions (plume dynamics, updraft, local weather and topography), and the ignition potential of the area where the firebrand(s) landed [197]. Spotting can be classified into three categories, depending on the distance and the distribution density: short distance spot fires (up to 750 m), average distance spot fires (1000–1500 m) and long-distance spot fires (>5000 m) [198]. The type of fuel influences the distances at which firebrands are most likely to cause spotting. For example, eucalypt species with fibrous bark (e.g., Eucalypt obliqua, *E. marginata*, and E. macrorrhyncha) are more likely to cause short-range spotting while eucalypt species with smooth decorticating bark (e.g., Eucalyptus viminalis, E. globulus, and E. delegatensis) are optimal for long-range spotting [198]. Intense short-range spotting results in rates of fire spread varying between 68 and 153 $m.min^{-1}$ and average fireline intensities up to 88,000 kW/m [198].

[199] studied flight behaviour of eucalypt bark in the vertical wind tunnel in the laboratory. He found that the terminal velocity of the bark is a linear function of the species, how the bark spins, and the density of the surface. The combustion behaviour of the bark strongly depended on the size of the particle and ignition time [180]. studied spotting distance in the field and observed that the intensity and distance of short-distance

spotting, both for moving fires and for fires reaching firebreaks, increases with fuel age. They found that distribution of spot fires decreases rapidly with distance downwind of the fire, and suggested that an exponential function is likely to roughly approximate the decrease in number of spot fires [200]. analysed data collected by the National Infrared Operations (NIROPS) program on spot fire distance. Most spotting distances calculated were ≤500 m. However, a combination of high wind speeds and substantial fire growth increased the likelihood of observing spotting distances in excess of 1 km.

Long-range spotting (>5 km) is caused by a strong convection plume leading to the transport of firebrands over considerable distances. A distance of 33 km ahead of the main fire front was recorded during Black Saturday fires in Australia [198]. Long range spotting was also reported in the Bastrop Complex fire in the USA [188] where the distance from fire line points to firebrand production and subsequent fire spread was 24 km.

[201] analysed spotting >500 m from 251 wildfires between 2002 and 2018 in south-eastern Australia. They found that there was significant variation in spotting distances between regions. This sensitivity it could be related to changes in rainfall, terrain ruggedness and fuel types. For example, the regions with the highest annual rainfall, the most rugged terrain, the highest canopy height and the highest proportion of bark had the most intense spotting.

A variety of models, both analytical and physics based, have been applied to predict firebrand transport [202]. introduced one of the first models for firebrand transport. It is an analytical model assuming that the mechanism of transport comprises lifting of brands in thermals and their throw-out. It was noted in the study that due to the simplifying assumptions, some of which cannot be validated (at the time of publication), the model should not be used in practice; instead, it was intended as a means to conduct research on the matter [203]. measured and calculated free fall characteristics of objects with shapes similar to those of firebrands (e.g., disks, cylinders, etc.). It was argued that physics-based transport models should include 6° of freedom and consider lift and rotational force to be more accurate [204]. used Fire Dynamic Simulator (FDS) to simulate firebrand generation, transport, and deposition near a structure. A single tree was burned in the simulations. No firebrands reached the structure for the wind speeds considered (≤12.5 m/s). Buoyancy forces were insufficient to transport the firebrands high enough to eventually reach the structure with a single burning tree. It was argued that the model is a tool that can be used for further analysis [205]. simulated a small spot fire and studied the transport of firebrands and their deposition. They found that the temperature of larger particles at the moment of deposition is higher than smaller ones [206]. performed a series of free fall experiments on non-burning rod-like debris to test the transport model of [207]. They found that the model could predict statistics of the flight in the free fall experiments and suggested that the firebrand transport models must contain the full six degrees of freedom to avoid underestimation of the firebrand flight distance.

2.3.3. Firebrand deposition/ignition potential

The potential of firebrands to ignite recipient fuels has been studied primarily through laboratory studies (Appendix, Table 8). Numerous experimental studies have used the National Institute of Standards and Technology (NIST) Firebrand Generator (or NIST Dragon) [208] to assess the impact of firebrands on structural and natural fuels. For example [209], conducted eight full-scale experiments to study the potential of firebrand showers to ignite decking assemblies under a continuous wind speed of 8 m/s. They found that the mass of firebrands required for flaming ignition was one order of magnitude lower than the firebrand mass reported in previous studies under a wind speed of 6 m/s (10 g vs. 100 g) [210]. Their study of firebrand accumulation in front of obstacles [209] showed that wind speed influences not only the spatial location and extent of the accumulation firebrands, but also the intensity at which firebrands smoulder [211]. studied the effect of radiation on the ignition of fuel beds subject to firebrand showers and found that radiant heat flux can play an important role in firebrand ignition under winds of 6 m/s, while little effect was observed under 8 m/s winds [212]. experiments confirmed the influence of surrounding airflow (velocity and direction with respect to particle orientation) on the combustibility of particles.

Additional studies have further characterized the behaviour of firebrands and the subsequent influence on ignition of recipient fuels [213]. showed that, regardless of the species of firebrands, there is a negative exponential relationship between particle weight loss and temperature. In Refs. [214–218], the authors designed laboratory experiments to investigate heat transfer from single firebrands and firebrand piles to fuel bed [214]. compared flaming and glowing firebrands in different surrounding conditions and the time required to ignite the fuel bed. His work showed that the fuel moisture content and wind speeds can have a dominate effects [217]. investigated the heat transfer from firebrands to surfaces. Their research showed that a single firebrand could generate heat fluxes ranging from 30 to 105 kW/m^2. The magnitude and duration of the heat exposure were found to be dependent on factors such as the firebrand's geometry, wind speed, and the orientation of the wind speed in relation to the firebrand [215–218]. studies were focused on comparing the thermal behaviour of a firebrand pile to that of a single particle by varying firebrand properties. They concluded that the mass of the pile (or number of firebrands) is an important and influencing factor of ignition [216]. showed that artificial firebrands produced higher heat fluxes than natural firebrands. This difference was attributed to the presence of a unique ash layer in natural firebrands, which was absent in artificial firebrands [218]. Wind speed, firebrand length, and firebrand aspect ratio (length-diameter interaction) were identified as other factors that significantly impacted the heat flux. The researchers suggested that firebrand aspect ratio affects pile porosity, which in turn regulates heat fluxes.

[219] studied smouldering time and temperature of pine bark firebrands in order to determine their potential to cause ignition. The authors found that the firebrand temperature of 190°C can be used as a threshold value, below which the particle lost its ignition potential. The interaction of smouldering pine bark and twig firebrands with pine needle fuel beds were studied in Refs. [220,221]. Increases in the wind speed and number of firebrands led to increased probability of fuel bed ignition, while an increase in the density of fuel bed decreased the probability of ignition [221]. studied the effect of heated air flow on the probability of ignition and showed that the temperature of the air flow has a significant effect on ignition [222]. tested in the field conditions a firebrand flux and condition system (emberometer) to measure and analyse firebrand properties, such as temperature and area, during their deposition. Distinct periods of higher firebrand deposition were observed during their experiments. Their results indicate that there can be large spatial variability in firebrand deposition due to factors such as fire behaviour and plume dynamics.

The vulnerability of wooden structures to an accumulation of firebrands at particular locations (e.g., roofs or decking) is a concern and has been considered [223]. collected data from prescribed fires and replicated firebrands in laboratory conditions to evaluate ignition of building materials/geometries. She found that 13 g of smouldering firebrands were able to ignite redwood panels in a flat configuration while 8 g in the same conditions did not result in ignition at all. The critical conditions leading to the ignition of decking slabs used in French dwellings from flaming firebrands were determined by Ref. [224]. They found the critical amount and mass of firebrands needed to ignite the decking slabs. The critical mass varied from 0.31 g to 1.30 g for wooden slabs and from 0.8 g to 1.80 g for thermoplastic slabs. Wooden slabs required fewer firebrands to ignite, ranging from 1 to 39, while for thermoplastic slabs the number ranged from 1 to 47. No ignition occurred when firebrands were on the decking surface, but it occurred when firebrands were located in crevices and against the thermoplastic slab [224]. [86] have incorporated these experimental findings into

SWUIFT, a streamlined fire spread model for WUI communities, such that ignition due to firebrands depends on the total mass of accumulated particles over a particular area.

Computational modelling has provided useful insights into physical processes associated with firebrands and ignition [225]. conducted a numerical simulation of heat transfer from firebrands to fuel beds and investigated the effect of thermal conduct resistance. The model shows that the maximum temperature in a fuel bed increases as the relative contact pressure increases. It also shows that with surface irregularities (which cause poor and local contacts) higher temperatures are observed in the fuel bed. This is due to radiation becomes another mechanism of heat transfer to the fuel bed; producing higher heat flux compared to only conduction. A 3-D simulation of fuel bed ignition by glowing twig and bark firebrands was conducted and compared with experimental tests in Ref. [226]. Irrespective of experimental conditions, single bark firebrand ($\leq$30 mm) could not initiate fuel bed ignition. The analysis of the simulated results shows that firebrand length can be a major factor in the initiation of ignition. An analytical model was created in Ref. [227] to predict the burning of firebrands, and six different models for predicting char oxidation were assessed. The model that utilized the heat and mass transfer Reynolds analogy produced the most accurate outcomes for a single firebrand. Nevertheless, significant discrepancies were detected for firebrand piles, which might be attributed to the intricate flow field generated by adjacent firebrands that were not considered in the model.

[228] summarized the findings from a multi-faceted research effort considering spot fire ignition from a variety of sources (e.g., hot metal particles, sparks, and firebrands). Ignition occurs when the temperature and energy of small particles is sufficient. Natural fuels were more difficult to ignite than the (idealized) fuel bed composed of cellulose. This difference in ignition propensity indicates the importance of understanding fuel bed characteristics, including the chemical composition [229]. noted that considering ambient humidity and fuel bed moisture content further complicates ignition prediction.

[179] recently compiled a summary of the available knowledge about physical processes related to firebrand mechanisms on large outdoor fire spread. Specifically, they reviewed previous literature about experiments, models and simulations related to firebrand generation, lofting, burning, transport, deposition, and ignition of materials. Based on their review, a number of key research areas requiring considerable further efforts have been identified: (i) the development of well-controlled experiments on firebrand transport and deposition under different fuel bed morphologies; (ii) the design of new experimental methodologies to characterize firebrand flux; (iii) additional experimental data regarding the ignition of structural elements; (iv) improved measurement methodologies to characterize firebrand generation from real fire sources; and (v) improved understanding of the combined effects of firebrands, radiant and convective heat.

Summary. Most of the research on firebrands has been conducted in laboratory settings, and the process of firebrand generation is the least understood of the three processes that lead to spotting. However, there has been a significant increase in firebrand studies over the last two decades, which has led to a better understanding of spotting.

The generation of firebrands is influenced by various factors. Specifically, higher fire intensity, fire-induced draft and wind speed are associated with a greater number of produced firebrands. Bark flakes and twigs are the primary types of firebrands observed, with a majority of them measuring smaller than 0.05 cm^2 in size. The findings indicate the considerable influence of fuel morphology on firebrand generation. Additionally, a strong correlation between the mass of firebrands and their projected area has been established.

Regarding the transport of firebrands, the type of fuel directly impacts the distance at which spotting occurs. As the distance from the fire increases, the distribution of spot fires decreases rapidly. Moreover, the combustion duration of firebrands during transport is influenced by variables like particle size and fuel type. To accurately model these processes, it is essential for physics-based transport models to incorporate six degrees of freedom, lift, and rotational force.

In terms of ignition potential, wind speed and firebrand mass exhibit a negative correlation with ignition likelihood, indicating that higher wind speeds require less firebrand mass for ignition to occur. Additionally, the temperature of the airflow plays a significant role in determining the success of ignition. A negative exponential relationship exists between particle weight loss and temperature. The accumulation of firebrands significantly impacts ignition success, emphasizing their importance in the process. It is noteworthy that flaming firebrands exhibit a higher rate of ignition success compared to smouldering or glowing firebrands.

Despite the significant progress in understanding of spotting, the overall knowledge is still immature, and more efforts are required to gather data on spotting and develop robust and comprehensive models. In particular, further studies are needed to improve our understanding of firebrand generation, especially in field conditions. Research should explore the factors influencing firebrand production, such as fuel type, fire intensity, and weather conditions. Investigations into the size, mass, combustion mode and composition of firebrands generated from different fuel sources would be valuable. Additionally, the development and refinement of laboratory-scale experiments and simulation models can help bridge the gap between laboratory and field studies. To establish the relationship between generation results and transport and ignition potential, it is necessary to measure the HRR or fire intensity for specific fuel structures in order to develop their dependencies.

Research should also aim to improve our understanding of firebrand transport and the distances over which spot fires can occur. This involves studying the characteristics of firebrands that influence their transport, such as size, shape, density, and material. Laboratory experiments are constrained by the large scale of the problem, while field experiments face limitations in terms of available measurement equipment and technics. As a result, modelling remains the main tool for investigating firebrand transport and should incorporate effects of wind, plume dynamics, and their interaction with the atmosphere. This approach can offer valuable insights into the behaviour of firebrands under different weather conditions and terrain types.

Laboratory studies using firebrand generators and experimental setups can continue to investigate the ignition potential of firebrands on recipient fuels. Research should focus on understanding the effects of firebrand properties (e.g., mass, size, shape, single or pile, flaming or glowing) and environmental factors (e.g., wind speed, fuel moisture content) on ignition. The additional effect of radiant and convective heat flux on ignition should also be explored. Further investigations into heat transfer from firebrands and firebrand piles to fuel beds and surfaces can provide valuable insights into ignition mechanisms.

3. Settlement fire exposure to structures

3.1. Flame contact and convection

This section reviews studies and findings regarding direct flame contact of settlement fires on structures. Specifically, this section focuses exclusively on literature dealing with fire source fuel elements that are components of the urban infrastructure (e.g., building/house/settlement, deck, fence, vehicle and ornamental/landscaping plants). In real outdoor fires, those components can be the origin (ignition location) or part of the fire spread pathway [230]. Only studies dealing with experimental work were found to be relevant for this section.

Vehicles are a common element of the built environment with a high burning and hazard potential, mainly due to their highly flammable composition including foam, rubber, PVC (Polyvinyl chloride) and in most of the cases liquid fuel. Research into vehicle burning behaviour involves both large outdoor and enclosed urban fires involving one or more vehicles. Among the relevant literature, the majority of studies consider radiation as the dominant (in some cases the only) fire spread

mechanism, and do not include explicitly flame impingement in their analysis [231–235]. To our knowledge, only two full-scale experimental studies have described the observations associated with vehicle fire spread mechanisms via flame impingement [236,237].

One of the experimental studies of vehicle-to-vehicle fire spread was conducted by the Department for Communities and Local Government [236]. In this work, eleven full-scale fires fuelled by a total of sixteen cars were performed using a highly instrumented car park platform. The diagnostics used in this study and summarized in Table 9 included calorimetry, thermocouples, heat flux gauges, load cells, gas analysis, infrared imaging, and video recording. The test platform dimensions were 12 m × 6 m x 2.9 m (L x W x H), with some vents along two of the walls. The experiments involve a minimum separation distance between cars of 50 cm. Two main fire spread mechanisms via direct flame contact between vehicles were experimentally identified. First, it was observed that flames can be "ejected" through the openings of the burning car during high intensity fire stages, resulting in flame impingement and subsequent ignition of adjacent cars. Second, it was observed that direct flame contact can also occur from burning spilt fuel and/or molten plastics escaping from one car and spreading towards another. A similar fire spread mechanism was observed by Ref. [237] during an experimental campaign involving two full-scale fire burns instrumented with thermocouples, infrared imaging and video recording. It is worth noting that none of those mechanisms were identified as the only source of fire spread, but as contributors to the combined exposure mechanisms leading to ignition.

Decking and fencing assemblies as well as roofing materials attached or in close proximity to the main structure have been identified as typical structural elements of the built environment that can be conducive to ignition. Once ignited, flames can spread from the point of ignition towards or into the main structure to which these assemblies are attached. A variety of materials used to build decks and fences are commonly inherently flammable. Research related to the ignition and flame spread from decks and fence materials includes both laboratory- and full-scale testing. Decking material ignition in the built environment has been extensively studied, but our understanding of flame spread across decking boards and thermal exposure from burning decking assemblies is still limited [238]. studied under-deck and above-deck ignition scenarios and found that board orientation with respect to flame spread direction drastically affects the flame exposure. It was noted that in both ignition scenarios, a maximum thermal exposure of about 50 kW/m^2 was recorded, and the heat flux from the decking increased as the airflow velocity increased. The National Institute of Standards and Technology has led several experimental campaigns specifically looking at flame spread across privacy fences and the thermal exposure from burning fencing assemblies to adjoining structural materials. It was found that the mulching material at the base of the fence is required to sustain flaming ignition and subsequent flame spread along the fencing material at lower air flow velocities and during the initial stage of a test [239]. The thermal exposure of fencing materials to adjoining structural materials has been noted to be affected by separation distance as well as air flow velocity, with smaller gap sizes increasing the heat exposure from a fencing assembly.

Residential fuels such as toy houses, tables, chairs and tricycles have been also identified as common hazardous materials actively involved in the development of urban fires [240]. This type of fuel is commonly found nearby main structures (e.g., backyards) or inside secondary structures (e.g., garages). Their composition can vary from petroleum-based to wooden materials, spanning an extensive range of burning behaviour properties with potential of playing major roles throughout the development of structural fires [241]. studied experimentally the burning behaviour and spread mechanism of residential fuels. They used calorimetry, thermocouples, heat flux gauges, load cells, gas analysis, infrared imaging, and video recording in their experiments. Peak of heat release rate and radiative heat flux (1.5 m measurement distance) over 2.5 MW and 20 kW/m^2 were measured during the experiments, showing potential for fire ignition of nearby flammable materials. Two potential mechanisms of fire spread via flame impingement were identified during their work. The first relates to the hazards posed by the flame heights measured during the experiments (2.65 m–3.60 m) which could potentially ignite materials (e.g., roofing systems, rolling shutters, dead vegetation, etc.) at some elevation in the main structure via direct flame impingement. The second spread mechanism is associated with an increase in the effective burning area due to the melting during the combustion process, which for some fuels can double [241]. suggested increasing the safety distances between these fuels, the structure being protected, and other flammable elements as a risk mitigation measure.

Summary. The review findings indicate that there is limited and mostly qualitative research on the effects of direct flame contact and convective heat in settlement fires. Many studies primarily focus on radiation as the dominant (and sometimes the only) mechanism of fire spread. However, when flame impingement is considered, two key mechanisms of settlement fire spread are identified: a) flame contact resulting from the expansion of the burning area and subsequent fire propagation; b) flame "ejection" from structural openings, leading to significant increases in flame length and the potential for spreading to adjacent combustible targets.

Structural fires involve a wide array of combustible elements, including decking, fencing assemblies, roofing materials, vehicles, and residential fuels like toy houses, tables, and chairs. These elements exhibit a wide range of compositions, from petroleum-based to wooden materials, resulting in varying peak HRR ranging from 20 kW/m^2 (for residential fuels) to 50 kW/m^2 (for decking materials). The unique properties of these elements contribute to distinct fire behaviours. For instance, some residential fuels have a tendency to melt, increasing the effective burning area and intensifying exposure levels. The orientation of deck boards relative to the direction of flame spread impacts flame exposure and rate of spread. The presence of additional fuel, such as mulch, at the base of a fence is critical to sustain flaming ignition and facilitate subsequent flame spread along the fence.

Further investigations are needed to understand the specific mechanisms and characteristics of flame impingement in vehicle fires, including observations of flame ejection through openings, flame lengths, and exposure distances. Additionally, investigations into flame spread across privacy fences and the thermal exposure from burning fencing assemblies to adjoining structures are necessary. Despite extensive studies on ignition, there remains a limited understanding of flame spread across decking boards and the thermal exposure from burning decking assemblies, particularly when considering different board orientations and airflow velocities. It is imperative to conduct comprehensive research on the burning behaviour and spread mechanisms of residential fuels. These studies should encompass an analysis of peak heat release rates, radiative heat flux, and flame lengths. Furthermore, the potential for flame impingement and the increase in effective burning area resulting from the melting process during combustion must be explored. Developing a standardized method to quantify critical metrics, such as impingement frequency and minimum flame size for ignition, is essential for understanding the underlying nature of exposure and the burning mechanisms involved with different fuels in such fires and to develop mitigation measures.

3.2. Radiation

This section will look specifically at how radiative heat transfer from ornamental vegetation to structures and between structures has been measured in experiments and modelled using various software programs. The aim of this section is to provide a detailed review of current literature regarding radiation at the built environment and from structure to structure. Table 10 (Appendix) presents selected papers of experimental research about fire exposure due to thermal radiation, which are briefly described below.

3.2.1. Small scale experiments

A reasonable first approach to understand radiation emissions is through experiments in small-scale, which in general are performed inside the laboratory and under controlled ambient conditions.

[242] performed experiments in a small compartment of 0.5 m (cubic shape) made from ceramic board (4 cm thick) with a façade of 1.0 m × 2.1 m and a door (different sizes were tested: 0.2 m × 0.2 m, 0.2 m × 0.1 m). A target wall of 0.9 m × 1.8 m, representing a neighbouring dwelling or building, was positioned at distances varying 0.1 m–0.3 m from the fire room. They used a propane gas burner of 0.2 m × 0.1 m with different flow rates, providing heat release rates (HRR) ranging from 11 kW to 32 kW. A relationship between the ventilation factor ($V_F = A_o\sqrt{H_o}$) and the critical heat release rate (HRR_{crit}, heat release rate at which emerging flames occur) was found. Heat fluxes on the façade and opposite wall ranged from 13 kW/m^2 to 47 kW/m^2. External flames and radiative heat fluxes were longer and higher (respectively) as the distance between the fire room and the target wall decreased.

A small cubic room (0.5 m × 0.5 m x 0.5 m) made from ceramic fiberboard walls with a façade wall (0.8 m × 2.5 m) and a parallel opposite wall (target wall, 0.8 m × 2.5 m) was also employed in Ref. [243]. The window, placed at the façade wall, was varied in size between 0.1 m × 0.25 m, 0.2 m × 0.2 m, and 0.25 m × 0.1 m. The distance between the façade wall and the target wall (D) varied from 0.1 m to 0.5 m, and experiments without the target wall were also performed. A propane sandbox burner was used, providing HRR in the range of 20–50 kW. During the experiments, they observed flame heights from 0.6 m to 1.0 m, the maximum heat fluxes on the façade wall ranged from 18 kW/m^2 to 68 kW/m^2, and on the target wall from 4 kW/m^2 to 61 kW/m^2. They found that the maximum heat fluxes were located at about 0.4 flame heights and the flame height decreased for distances between façade wall and target wall up to 0.3 m, then became constant. The total radiation outputs from the enclosure and the flames corresponded to about 50%–65% of the total HRR and their contribution to radiation outputs from the opening was 1–3 times that from the ejecting flames.

[244] employed the data of a model-scale industrial facility experiment aiming to study flames ejecting from ceiling openings and to understand how a neighbouring building would be affected by them. A compartment of 6 m × 3 m x 0.7 m (reduced-model of an industrial premise) made from calcium silica boards and having both vertical wall openings and horizontal ceiling openings was built. The fire source was centred on the floor, burning wood cribs of two different sizes (80.8 kg and 105.4 kg), providing maximum heat release rates of 3.68 MW and 3.8 MW, respectively. Measurements of heat fluxes were made in 10 positions outside the compartment, at distances ranging from 0.5 m to 3.0 m from the external walls, always 25 cm above the ceiling. Heat fluxes ranged between 1 kW/m^2 and 46 kW/m^2, depending on the distance from the ceiling openings. Calculation methods for incident radiation heat fluxes (single point source radiation model and solid flame radiation model) were tested against model-scale data. The single point source radiation model performed better than the solid flame radiation model (which uses view factors).

While other works study fire exposure to a neighbouring dwelling opposite the burning dwelling [245], tried to understand fire exposure to a neighbouring dwelling located on the side of the fire source dwelling. Experiments were performed using a small-scale cubic compartment (side 0.4 m) with a façade wall (dimensions 1.2 m × 1.6 m) insulated internally with ceramic fibre board and 3 ventilation conditions (window sizes: 25 cm × 10 cm, 25 cm × 12.5 cm, 25 cm × 15 cm). Propane gas burned in a square porous burner (side 0.2 m) with a total HRR of 3.07 kW–92.24 kW was used. A radiometer was placed at the side of the compartment to measure the radiative heat flux of the ejecting flames. Results found radiation fluxes of up to 1.04 kW/m^2 and radiative fractions ranging from 0.08 to 0.28 (it was calculated using the single point source method). Flame radiative fraction decreased as the excess-HRR (outside the opening) increased. Measurements were fitted in an empirical correlation to predict radiative fraction from external flames as a function of external-HRR, ambient conditions and ventilation sizes.

According to Ref. [246]; the fully-developed, post-flashover stage of a compartment fire is the most critical scenario to a neighbouring building [247]. studied both experimentally and numerically the heat release rate required to reach flashover within and heat fluxes to the surroundings of a small-scale compartment (0.6 m × 0.9 m x 0.6 m) made from 0.5 mm thick corrugated steel sheets and with a door of 0.2 m × 0.5 m. Polypropylene fuel in a 0.4 m × 0.4 m fuel tray to simulate different fuel loads of 24, 32, 40, 80 MJ/m^2 was used, providing maximum heat release rates from 55 kW to 90 kW. Incident radiative heat fluxes were measured using TSCs outside the compartment: in front of the door opening (distances 20 cm–60 cm from the opening) and at the side wall (distances 15 cm–45 cm from it). Maximum heat fluxes in front of the door were in the range of 3 kW/m^2 (at 60 cm distance) and about 2 kW/m^2 on the side wall (45 cm distance), showing that fire spread to a neighbouring side-dwelling would be a concern (as studied in Ref. [245]), since heat fluxes were of the same order of magnitude.

External flames and radiative heat fluxes from doors and window openings of the fire source dwelling are known as the main fire spread modes to neighbouring buildings or dwellings [248]. quantified the effect of adding horizontal openings to the roof, with the aim of reducing fire spread hazards by decreasing external flames and radiative heat fluxes from the original door opening. The same small-scale compartment used in Ref. [247] was adopted, but horizontal openings were cut in its roof, with areas ranging from 0.0025 m^2 to 0.16 m^2, located at the corners of the roof (4 square openings) or at its centre depending on the test. Fuel was 1 kg of polypropylene placed in a 0.4 m × 0.4 m tray, equivalent to 80 MJ/m^2. Maximum HRR ranged between 100 kW and 120 kW, and peak radiative heat fluxes ranged from 5 kW/m^2 to 15 kW/m^2, depending on the roof configuration. Horizontal openings reduced radiation heat fluxes in front of the door by about 60–70%, which proved to be an effective way to reduce fire spread between dwellings, with the central slot horizontal opening being more effective than openings at the corners of the roof. However, the time to flashover decreased as the area of the roof opening increased.

3.2.2. Full-scale experiments

Small-scale experiments are important to obtain insights about fire phenomena, but their ability to simulate real-scale fires is limited. Therefore, full-scale experiments are needed in order to obtain radiation heat flux data more similar to real fires.

Lin [249] conducted several experiments in a full-scale double storey reinforced concrete building specifically built for the fire tests. The fire compartments were 2.64 m × 3.64 m in floor area and 3.0 m (ground floor) or 2.93 m (first floor) high. Both compartments had a door and window, where the door opening was 0.75 m wide and 1.8 m high, and the window dimension was either 2.64 m (W) x 1.72 m (H), 1.72 m × 1.72 m or 1.64 m × 1.64 m. A 5.1 m wall was built above the first-floor compartment. Three fuel loads of 15, 25, and 40 kg/m^2 were used. The radiant fluxes were measured at distances of 2, 3, and 5 m from the ground floor opening and 0.6 m above the openings. Radiant heat fluxes at 2 m from the first-floor opening ranged from 15 to 22.5 kW/m^2 depending on the fuel load with the door closed and 15–40 kW/m^2 with the door open. The higher fluxes indicated larger external flame lengths and higher flame temperatures. During the double room experiments, fluxes at 2 m ranged from 12 to 47 kW/m^2. Based on the results, a new model to determine the flux from the flames emitted from the window opening was proposed [249].

Building construction materials, opening positions and sizes, separation distances between buildings and weather conditions have a major influence on fire exposure to a neighbouring building [250]. investigated fire exposure to a neighbouring wall for two different construction materials: regular construction (layers of drywall, wood studding,

oriented strand board, weather wrap, and vinyl siding) and including a fire-resistant barrier (a layer of ½ inch drywall between the oriented strand board and the weather wrap). The dimensions of the compartment fire were 3.7 m × 4.3 m x 2.4 m, with a window of 0.6 m × 0.9 m facing the target wall and a vent of 1.8 m × 0.3 m on the opposite wall (inlet for fresh air). The neighbouring (target) wall (4.9 m × 4.9 m) was 1.8 m away from the compartment fire (as required by building codes in the USA). Since this experiment intended to be as close as possible to a real fire scenario, fuel was based on typical living room arrangement (sofa, armchair, coffee table, table with a lamp and bookcase, curtain, interior walls covered with wood panelling, carpeted floor), with a total fuel mass of 312.5 kg, and fuel load of 19.7 ± 0.5 kg/m^2. Results showed that temperatures inside the compartment fire reached 800 °C, and heat fluxes reached 140 kW/m^2 at 4.9 m, exceeding 50 kW/m^2 for most of the fire. After the flame exited the window of the compartment, it took less than 80 s to ignite the target wall made from regular construction material. The fire-resistant construction slowed down fire spread, even avoiding the ignition of the target wall, clearly demonstrating the impact of construction materials on fire spread between buildings.

[246] conducted full-scale experiments using a 5.95 m × 4.4 m x 2.75 m compartment made of non-combustible, insulated walls. They conducted experiments for several window sizes (2.55 m × 1.45 m, 1.45 m × 1.45 m, 1.10 m × 1.45 m) and several separation distances between the target wall and the compartment fire (ranging from 2.4 m to 4.0 m). Propane and wood cribs (1000 kg of wood in each experiment, fuel load of 38 kg/m^2) were used in their experiments. The radiative heat fluxes and temperatures on the target wall ranged from 12.67 kW/m^2 to 28.75 kW/m^2 and 160 °C–405 °C, respectively. The maximum temperature and radiative heat fluxes were located between the centre of the window and just above the soffit of the target wall. The contribution of external flame above the soffit to the radiation flux ranged from 21% to 63% [246]. also developed a model to predict radiation heat flux on the target wall from post-flashover compartment fire.

Aiming at testing simple calculation methods for predicting radiative heat fluxes from compartment fires [251], performed full-scale experiments using a room of 4 m × 3 m x 2.75 m with natural ventilation (6 window dimensions were tested: from 3 m × 1.5 m–1 m × 1 m) and an external façade 5 m high. Propane burners were employed, for which HRR ranged from 1 MW to 5 MW, spanning from fuel-to ventilation-controlled fires. A target wall was positioned 3 m or 5 m away from the window of the fire room. Heat fluxes on the target wall ranged from 3 kW/m^2 to 20 kW/m^2, while temperatures ranged from 600 °C to 1030 °C inside the compartment and from 760 °C to 1150 °C at the window opening. Evaluation of two calculation methods, when the flame was modelled as a vertical plane (area method) and as a point source (single point source radiation model), showed a significant underestimation relative to measured heat fluxes.

[252] studied the shielding effect of a water curtain from sprinklers placed between a compartment fire and a target wall, as a measure to attenuate heat fluxes on the latter. A full-scale compartment made from cement boards, thermally insulated, with dimensions 3 m × 4 m x 3 m and a façade extending 3 m above the compartment front wall, was used for this investigation. A target wall (dimensions 4.9 m × 4.9 m) was positioned at 3 m and 4 m from the compartment fire. A propane burner was used with different gas flow rates leading to fire sizes of 2 MW, 3 MW and 4 MW. For tests in which sprinklers were not activated, average heat fluxes on the target wall ranged between 7.44 kW/m^2 and 19.24 kW/m^2. Heat fluxes were reduced by up to 80% in tests with sprinklers activated.

[253] conducted two three-dwelling experiments, where each dwelling was 3 m × 3 m x 2.3 m. The experiments consisted of three steel or timber cladding structures arranged in a row, with each structure presenting a door and a window arranged at a 90° angle. Pine wood with a load of 770 MJ/m^2 (45 kg/m^2) was used as fuel. Timber cladding of structures increased the fuel load to 1315 MJ/m^2, with a predictable effect on the heat fluxes. The maximum heat fluxes found in the timber cladding dwellings at the doors were 145 kW/m^2, 260 kW/m^2, and 215 kW/m^2 (compared to 156 kW/m^2, 153 kW/m^2, and 133 kW/m^2 for the steel cladding) for the 1st, 2nd, and 3rd dwellings respectively. At 1 m distance the maximum heat fluxes were higher in the timber cladding dwellings due to the additional radiation from the cladding (150 kW/m^2, 273 kW/m^2 and (no data)) compared to the steel cladding dwellings (59 kW/m^2, 79 kW/m^2 and 66 kW/m^2). At 2 m the heat fluxes for the steel cladding dwellings dropped to 46 kW/m^2, 35 kW/m^2, and 55 kW/m^2. The authors proposed using Beer's law to determine the radiation at a distance and obtained a good agreement, but they later published a corrigendum stating that Beer's law is not suitable for this purpose [254]. also conducted two single dwelling (3 m × 3 m x 2.3m) experiments on a steel and a timber cladding full-scale compartments, both lined with cardboard. The fuel load was the same as in Ref. [253]. The average heat fluxes for the timber cladding dwelling were 93 kW/m^2, 43 kW/m^2, 88 kW/m^2, and 50 kW/m^2 at the door, 1 m from the door, at the window, and 1 m from the window, respectively. The maximum flux at the door was recorded as 106 kW/m^2. For the steel cladding structures, the average heat fluxes were 95 kW/m^2, 32 kW/m^2, and 80 kW/m^2 at the door, 1 m from the door, and at the window, respectively. It is important to note that Cicione [253,254] did not differentiate between radiative and total heat flux, and measurements taken at the door and window may have been affected by flame and hot gas impingement. However, based on the images presented in the paper, the fluxes measured at distances of 1m and 2m are more likely to be radiative fluxes.

In [255] the authors proposed a new heat flux sensor, named as FOA-013-01, in which total heat flux measurements can be collected in the range of 0–630 kW/m^2. Calibration against prescribed heat fluxes of 20 kW/m^2 and 40 kW/m^2 showed a good agreement. The sensor was used to measure heat fluxes adjacent to a diesel pool fire of 1.48 m in diameter, placed 2 m, 4 m and 6 m from the fire. The maximum heat fluxes reached up to 30 kW/m^2 for the closer position, decreasing to 1.5 kW/m^2 and 1 kW/m^2 for the other two positions. The authors stated that it is not appropriate to adopt heat flux as the sole criterion with which to analyse fire spread between buildings and suggested that the ignition temperature of the materials of the neighbouring building be used instead.

[256] conducted a single full-scale fire spread experiment of a mock informal settlement with 20 dwellings in a 4 row by 5 column arrangement (each column had four dwellings). This was conducted outdoors where the wind fluctuated between 15 and 25 km/h (4–7 m/s) Each dwelling was 3.6 m × 2.4 m x 2.2 m, with rows separated by 1 m, and columns separated by either 1.2 m or 2.2 m. At the extremities of the gaps between columns, 2.4 m wide x 2.2 m high steel walls were erected again at 1 m separation distance. Each dwelling was lined with cardboard and had a door and window. All dwellings were covered with 0.5 mm galvanized steel sheeting roof panels, with 14 dwellings having galvanized sheeting as wall cladding and 6 dwellings cladded with 12 mm thick timber planks. Fuel load in each dwelling was 392 MJ/m^2. Incident radiant heat fluxes were measured using TSCs. The fire was initiated by igniting the first 4 dwellings in the first downwind column of the arrangement. Heat flux values of 50–100 kW/m^2 were observed on the wall of the downwind dwelling when there was an opening in the upwind dwelling (the opening working as a radiation emission source). Sensors located at the roof level recorded lower heat fluxes, but higher temperatures due to being upwind of the fire plume. The steel clad dwellings exhibited the highest heat fluxes opposite the openings, while the timber clad dwellings did not show a significant difference between the maximum heat fluxes near openings and those on neighbouring walls. Besides that, the influence of the height above the ground on measured heat fluxes was more important for wood clad dwellings than for steel clad ones. The ignition of dwellings located upwind occurred at relatively low heat fluxes (<30 kW/m^2). When several structures burned simultaneously, the heat fluxes ranged between 100 and 250 kW/m^2, and in some cases they were directly related to flame impingement, i.e.,

the data may not be recording pure radiative flux, but a form of total heat flux from the fire.

[257–259] conducted two series of experiments totalling 13 burns. Twelve experiments used single dwellings with identical dimensions to ISO 9705 room (3.6 m × 2.4 m x 2.4 m). The floor was covered with 8-mm-thick cement boards. The walls and ceiling were made of 0.51 mm thick corrugated galvanized steel sheets attached to the timber frame. The design and materials were adopted to model common informal settlement dwellings typology. Two openings were designed including a door (2.0 m (H) x 0.8 m (W)) and a window (0.6 m × 0.6 m). One of the 12 experiments did not have a window. The 13th experiment used two dwellings with openings facing one another and the structures separated by 1 m, with one being initially ignited and spread to the second. The fuel load was approximately 25 kg/m^3 or 437.5 MJ/m^2 made from pine timber cribs. The heat fluxes, measured with TSCs, at a distance of 2 m from the door and window (1.6 m height) were approximately 12–18 kW/m^2 and the fluxes at the side wall were 5–25 kW/m^2 and 7 kW/m^2 at 0.5 m and 1 m, respectively. Reducing ventilation (no window) or moving the window to a wall that does not contain the door, both reduced the fluxes recorded opposite the door and window (by about 4–5 kW/m^2). Increasing ventilation (by either doubling the height, the width, or adding a second window) had no noticeable effect on the measured fluxes. In the double dwelling experiment, the heat fluxes at the door and window peaked at 25 kW/m^2 and 15 kW/m^2, respectively.

Cicione and colleagues [260,261] conducted several outdoor experiments in South Africa, where the wind speed varied between 3 and 18 km/h (1–5 m/s) during all experiments, but never exceeded 10 km/h in any individual experiment. Each experiment involved 2 dwellings: the fire origin dwelling and the target dwelling. All dwellings were 3.6 m × 2.4 m x 2.3 m. The fire origin dwelling had a single door opening (0.85 m × 2.05 m), while the target dwelling had a door of the same dimensions, and a window of 0.85 m × 0.6 m (W x H). In 4 of the experiments the dwellings were separated by 1 m (door of the fire origin dwelling facing the back wall of the target dwelling), with a freestanding wall situated 2 m from the target dwelling (door of the target dwelling was facing the freestanding wall). The other experiments considered a separation distance of 1.75 m between fire origin and target dwellings, and a distance of 1.5 m between the target dwelling and the freestanding wall. Pine timber cribs with fuel load 30 kg/m^2 (17 MJ/kg) were used for all the experiments. The peak radiative heat fluxes measured varied between 39 and 66 kW/m^2 opposite the doors, with higher fluxes being recorded on the freestanding wall, with peak fluxes of 14–22 kW/m^2 measured at 2 m and 4 m from the window. It is worth noting that the radiative flux measurements obtained in the experiments conducted under the influence of wind, burning of multiple dwellings, and close proximity of structures and freestanding walls should be interpreted with caution. The flux measurements may have been influenced by convection and the potential impact of flame impingement, which could affect the accuracy of the measurements.

The experimental results must be considered in terms of the risk of ignition of neighbouring structures, so the material properties of the external facades of these structures must be well detailed, both for piloted and spontaneous ignition. For example [7,262], indicate that piloted ignitions (such as a small flame or a firebrand) often occur in conditions where the radiation level is above 12.5 kW/m^2, with spontaneous ignitions (for wood) occurring at 33.5 kW/m^2 and above [263]. developed a database of piloted ignition fluxes and times of materials commonly found on or around the exteriors of informal settlement dwellings in Cape Town, South Africa. He reported critical heat fluxes as low as 6 kW/m^2.

3.2.3. Numerical modelling and tools

Numerical studies are important for developing knowledge about the contribution of thermal radiation to fire propagation among dwellings. The following paragraphs discuss such studies, first for fire dynamics in a single dwelling and then for fire propagation between multiple dwellings. Table 11 in the Appendix provides an overview of selected papers on numerical modelling research focused on fire exposure resulting from thermal radiation, which are briefly described below.

3.2.3.1. Single dwelling. Cicione et al. [254] modelled numerically their two single dwelling experiments using both FDS [264], and OZone [265] - a two-zone fire model software. For the FDS model, an area size of 5 m × 5 m x 3 m and a cell size of 50 mm were used. The two-zone fire model (OZone software) was used employing the McCaffrey method. The simulations focused on the post-flashover steady-state analysis of internal and external fire dynamics of the dwelling. Both the FDS and OZone were able to accurately capture the temperature increase in the steel clad dwelling, but there were difficulties with the timber clad dwelling because of the complex changes in ventilation that occur as the cladding burns. For the steel clad dwelling, the temperature was slightly overpredicted using OZone and underpredicted using FDS. The FDS also predicted heat fluxes relatively well during steady state burning and captured a high peak for the cardboard flashover observed visually but not observed in the experimental data. The temperature was initially overpredicted for the timber clad dwellings, but while it continuously rose in the two-zone model, the FDS model showed a sharp decrease shortly after the flashover. Heat flux trends were generally captured in the FDS model. It captured the peak heat flux when the cardboard was fully ignited but did not capture the heat flux when the timber cladding was fully ignited, overpredicting by 20%. The authors suggest that the errors arose from assumptions made about material properties (e.g., combustion efficiency) and ventilation modelling.

Beshir et al. [247] studied the heat release rate necessary to reach flashover inside a small compartment and the heat fluxes to surroundings using FDS. The fire was modelled using the simple pyrolysis model (prescribing the rate of heat release per unit area). The validation analysis showed satisfactory agreement for the hot gas layer temperature and good agreement for the velocity and radiative heat fluxes (outside the door and side wall). The authors performed a parametric study analysing heat transfer by conduction, convection, and radiation to/from the walls using 6 different thermally thin materials and 4 ventilation factors. Thermal radiation from internal walls was shown to determine the heat release rate to achieve flashover for the compartment with thermally thin walls, and a new semiempirical correlation was established for the heat release rate to achieve flashover as a function of internal wall surface temperature, hot gas layer temperature, wall emissivity, surface area, and opening size.

In a subsequent work using the same small-scale compartment [248], studied the effect of horizontal roof openings as a means of reducing fire spread to neighbouring dwellings by reducing external flames and radiative heat fluxes from the original door openings. The FDS was used with a mesh size of 5 cm, and cases with roof openings less than 5 cm were modelled with a 2.5 cm mesh. The FDS results are in good agreement with experimental data regarding the compartment fire dynamics and radiative heat flux values. Although gas concentrations decreased as the roof slot area increased, gas temperatures and radiative heat fluxes were well predicted. The authors stated that this verification work can be used in future studies to better understand the effects of scaling (e.g., in terms of scale from small to real) and to improve the proposed empirical correlation for the ventilation factor covering both horizontal and vertical openings.

In a compartment fire, the post-flashover stage is the most likely to spread fire to an adjacent dwelling, so it is important to determine the conditions for the start of the flashover [266]. performed a numerical study to determine the minimum heat release rate required to instigate a compartment flashover in the presence of wind outdoors [266]. used FDS to study thermally thin and thermally thick walled small compartments (0.6 m × 0.9 m × 0.6 m), considering wind velocities from 0 m/s to 3 m/s. A mesh size of 5 cm was chosen after comparison with more fine and coarser meshes. The results showed that the minimum

heat release rate needed to achieve flashover is between 25 kW and 70 kW, being the lower range applicable for thermally thick compartments and the upper range for thermally thin. In addition, when wind velocity was increased, the heat release rate necessary to achieve flashover increased for thermally thin compartments, whereas for thermally thick compartments, the effect of wind velocity was the opposite. Based on this, the authors concluded that the thermally thick compartments present a greater risk of fire spread to an adjacent dwelling because of the higher probability of reaching flashover compared to thermally thin compartments.

[267] used FDS to model the 13 experiments mentioned in section 3.2.2, with leakage modelled through HVAC vents due to the small vent areas resulting from construction gaps in the informal settlement dwellings studied. They also used a simple pyrolysis model to model the wood cribs and made other computational efficiency modelling choices, such as using a time shrink factor. The modelled heat fluxes out of the openings were compared to those observed in the experiments, with the maximum heat flux measured and modelled (2m from the door and 1.6m from the ground) generally matching well. However, the form of the curve did not always match, with experimental values rising more sharply to the peak than the modelled values, which took longer to reach the peak values. This discrepancy was partly due to the use of a time shrink factor, as shown in Ref. [267].

In their study, [267]; also modelled single dwellings in windy conditions and analysed the impact of wind-based parameters (such as aerodynamic roughness and Obukhov length) on the time to flashover. They found that at 3m from the door and 1.6m from the ground, heat fluxes varied from 4 to 24 kW/m^2 for thermally thin structures under wind speeds of 1 and 25 m/s, respectively, and from 1.5 to 12.5 kW/m^2 for thermally thick structures under the same wind speeds.

[261] used a two-zone model, namely the BRANZ fire program B-RISK [268], to understand the influence of ventilation changes (specifically the introduction of a large horizontal opening in the roof) and to perform a parametric study of the effect of window openings on the time to flashover and the maximum velocity at the door of the escaping gases (and hence flames). The models followed the general trends of the experiments presented in the paper relatively well, but they were mostly limited to internal dynamics rather than external fluxes and the effects of wind, etc.

4.2.3.2. Fire spread between structures. [269] modelled 3 experimental timber and steel dwellings using FDS. A 12 m × 4.6 m x 3 m domain with a mesh size of 0.1 × 0.1 × 0.1 m^3 was used. Three meshes (one per dwelling) were used. Burners with a prescribed HRR were defined. The first dwelling was ignited, and the subsequent dwellings were ignited using the critical heat flux from the SFPE handbook [270], and the ignition temperature of the material to find the time to ignition. In the baseline model, the first two dwellings ignited but the fire did not spread to the third. The ignition problem was caused by determining the leakage in the compartment, which allows hot gases to be transported but does not allow thermal radiation to pass through. To overcome this, the T_{ig} was reduced from 263 °C to 220 °C for the cardboard lining (other material properties were considered, but they had little effect on fire spread). Overall, the steel-clad dwelling model overpredicted the measured heat fluxes by 10–52%, underestimating them by 15% at the door of dwelling 3 and by 26% at 1 m from the door of dwelling 2. The overall trends were well captured, but the magnitude of simulated fluxes was poorly reflected. The timber cladding introduced a lot of uncertainty, and the predictions of heat fluxes were poor, both in trend and magnitude. A sensitivity analysis of the material properties (conductivity, specific heat capacity, and emissivity) showed that only the emissivity had an effect on the rate of spread between the dwellings, and no other material properties affected either the fire spread or the heat fluxes observed outside the doors. Soot yield and radiative fraction were also evaluated, with soot yield having no significant effect on the results, but radiative fraction did affect both the propagation rate and the simulated external fluxes.

[260] developed analytical equations to describe the radiation received by the target informal settlement dwellings from the emitting surfaces (i.e., from the opening, hot walls, hot gases and flames of an adjacent burning dwelling). This study also examined the time to ignition based on the radiation received under the assumption of piloted ignition. The heat flux emitted to the target dwelling was shown to be dominated by the thermal radiation emitted from flames and from hot gases of the adjacent burning dwelling, with the incident radiative heat flux estimated to be approximately 40 kW/m^2 and 18 kW/m^2 at 1.0 and 2.0 m, respectively, which agrees well with the experimental data presented in Table 10.

Using a process similar to that used for his single dwelling models [271], simulated two dwellings under different wind conditions. The first dwelling was ignited, and fire spread was simulated to the second structure which was separated by a distance of 1.0m. When the wind speed was 10 m/s, the modelled fluxes at the door of the second structure (which was lined with cardboard) reached 90 kW/m^2, whereas the fluxes at the ends of the alley between the two structures were generally around 10–15 kW/m^2, with one instance of reaching similar values.

In [272], exploratory FDS wind modelling was conducted on 4 and 8 structure arrangements using the same FDS model as [271] but without cardboard lining. The study varied wind direction and speeds, as well as separation distances between structures. Results from the four structure models showed peak heat fluxes at the nearest neighbouring structure (at 0.9m separation) to the ignited structure at 39 kW/m2, when a 10 m/s wind was blowing down the alley between the two structures, which was consistent with findings from Ref. [260]. Similar to Ref. [273], Rush also reported that heat fluxes increased up until a point (dependent on direction) and then started to decrease again. It was hypothesized that while low wind speeds increase flame length and combustion efficiency of ejected gases, high wind speeds lead to dominant convective cooling. Therefore, wind may have a significant impact on fire behaviour.

A computational model was developed by Ref. [274] for studying fire exposure in densely built urban areas. Two major sub-models are considered in this computational model, one related to fire dynamics inside buildings and another one focusing on fire spread to neighbouring buildings. The inside building sub-model is a one-zone model, considering each room of the building as a control volume and governing equations for mass, energy and chemical species are solved. The fire spread sub-model considers thermal radiation, fire plumes, and firebrands from the building on fire to neighbouring buildings. The onset of fire spread is a function of incident heat fluxes on the neighbouring surfaces, surface temperature of the neighbouring walls and materials, and firebrand deposition on combustible surfaces of the neighbouring building.

[275] modelled the fire exposure within informal settlements using the software B-RISK (a two-zone fire modelling software) [276]. Fire exposure is modelled using a point source model for radiant fluxes from the ignited dwellings, with ignition being determined by the Flux-Time Product and critical heat flux of the materials. Wind was also incorporated by modifying the point source model by uniformly tilting the flame. Each structure had a prescribed heat release rate based on the Babrauskas' crib model [277]. The HRR model was developed using a heat of combustion of 16.8 MJ/kg and an assumption that the structure would collapse after 7.1 min. The HRR of timber dwellings has also been increased by 20%, 50%, and 100% to account for timber facades. The sensitivity analysis of ignition criteria shows how important this parameter is for fire spread. The study also looked at dwelling spacing and other fire exposure scenarios and settlement layouts, examining high-risk settlements in Cape Town, South Africa. Unfortunately, the time histories of fluxes from the point source model were not presented to see if they were consistent with the experimental data.

Summary. This section emphasizes the key factors of thermal

radiation that should be taken into account when analysing heat transfer between structures and ornamental vegetation, as well as between structures themselves. The separation distance between objects is crucial since radiative heat flux decreases significantly as the distance increases. The size of the radiating source also affects the magnitude of the heat flux received by the target. Flames emerging from openings in a structure generally contribute more to radiation than hot surfaces, such as a hot steel wall in an informal dwelling. The presence of wind can impact the shape of flames and, consequently, the magnitude of radiative heat flux at a distance. The review reveals that compartment dimensions and HRR ranges used in small and full-scale experiments do not follow a scaling trend, even though radiative heat fluxes are of the same order of magnitude. Additionally, the scaling related to ventilation conditions (doors and windows) and boundary thermal behaviour (e.g., surface radiation absorption and reflection, conduction through wall/ceiling thickness) is not well understood.

Most of the literature relies on the FDS software, although a few papers utilize other models such as B-Risk, OZone, and analytical models. Surprisingly, popular software like FireFOAM or Ansys Fluent have not been utilized in the identified research. It is worth noting that FDS simulations, which employ simple gray gas models for radiation by default, may result in discrepancies in external heat flux and temperature predictions. Modelling studies indicate that a minimum heat release rate of 25 kW–70 kW is required to achieve flashover in a single dwelling fire, and thermally thick compartments pose a greater risk of fire spread to adjacent dwellings. In the case of fire spread between structures, the heat flux emitted to the target dwelling is predominantly influenced by thermal radiation from flames and hot gases of the adjacent burning dwelling. Higher wind speeds result in higher radiant exposures. However, radiant heat fluxes peak at a certain value of wind speed (dependent on direction) and then begin to decrease.

Further experimental research is needed to better understand scaling from small to large structures, considering the influence of wind and environmental conditions like terrain and slope. Exploring the effect of different construction materials on fire spread between buildings and exposure levels is necessary. Conducting experiments with a range of fuel loads to cover realistic scenarios and assessing their impact on fire spread and radiation heat flux would be valuable. Collecting data on radiation heat flux at various distances from the fire source and different heights above openings is also recommended. Additionally, investigating the effectiveness of fire mitigation measures, such as water sprinklers, in reducing heat fluxes on target walls is important.

Although there are various methods available for modelling radiative heat flux and fire exposure in complex areas, several issues still need to be addressed in future research. Alternative radiation models, such as the weighted-sum of gray gases (WSGG) model or wide band model (WBM), could be employed, although they are more time-consuming. Other parameters related to radiation modelling, such as radiative fraction, soot yield, and solid angle discretization, require further investigation in the field of settlement fire exposure. Simple radiation calculation methods, like the single point source radiation model and solid flame radiation model [244,251,274], could be explored for predicting radiation fluxes emitted from entire dwellings instead of just the flame, considering the focus on fire spread between settlement structures caused by radiation.

3.3. Firebrands and fire spread among structures

A review of literature on the risk of fire spread caused by firebrands was conducted using the keywords “Ember” OR “Firebrand” OR “Settlement fire” on the Scopus database, which resulted in 441 articles. Based on this literature review, a concise summary of experimental studies and numerical studies on the topic is presented in sections 3.3.1 and 3.3.2, respectively.

3.3.1. Experimental work

Firebrands generated from building structures have the potential to ignite neighbouring buildings downwind, leading to more severe large outdoor fires [179]. There is relatively less research on the exposure of firebrands compared to other fire exposure mechanisms, such as radiant heating and flame contact, in urban and informal settlements. This is because the phenomenon of firebrand exposure is arguably more complex. Historically, researchers have tended to focus more on other mechanisms, such as window ejected flames or radiation analysis, which have been considered as the primary fire exposure mechanisms [278]. At present, however, the risk of ignition posed to neighbouring structures by firebrands is attracting more and more attention from researchers due to the increasing number of urban fires or fires in settlements. Experimental efforts to understand firebrand generation from structures began with work by Ref. [279] in which five residential houses were burnt and the firebrands were collected using polyurethane sheets. It was found that roof collapse caused the largest number of firebrands. As has been observed in recent experimental studies, the collapse of a glass façade/window or weak wall/roof is common in modern structures and informal settlements, resulting not only in fire, but also in large numbers of firebrands [256,280,281]. Interestingly, post incident analysis of the Shurijo Castle fire in Japan [17] showed that, despite the large number of firebrands generated, not a single spot fire was registered. It should be noted that wood is the material that will produce firebrands in an actual fire, and is commonly used as a surrogate for fuel load and firebrand generation material [208].

Based on scale, experimental studies related to firebrands can be categorized into two categories, laboratory and field (full-scale). Recently, a full-scale three-story wooden school was burnt in Japan and the travel distance, size and mass of the firebrand were recorded [282]. It was found that over 60% of the firebrands were 1–3 cm in size regardless of location from the fire. Recently, systematic series of experiments have been conducted at different scales to study firebrand generation under well-controlled experimental conditions [211,283,284]. These studies indicated that the firebrands can be generated at different scales both in the field and in the laboratory [179].

When embers or firebrands reach building structures, they can ignite structural materials such as wooden roofs, walls and fences, or ornamental vegetation and litter on decks or eaves. In addition, firebrands can enter buildings through open (or broken) windows or vents [285–287]. Studies of these vulnerabilities in urban fires can be found in Refs. [5,288]. It should be noted that the situation in informal settlements, in which one billion people live, is much more complicated. According to a study by Ref. [263] in South Africa, combustible materials in informal settlements include tires on the roof, hanging clothing between dwellings, plastic sheeting between structures, firewood outside, wooden walls/roofs, crossing electrical wires over/among dwellings, etc. These materials are very flammable with relatively low ignition criteria (critical heat flux, ignition time), and some materials, such as tires placed on the roof, can cause the large number of firebrands observed in both laboratory [263] and full-scale field experiment [281], potentially increasing fire spread exposure in informal settlements. More research is needed to understand firebrand ignition in settlements. In particular, careful consideration must be given to wind conditions, which have a significant effect on fire exposure in settlements (5 min for a burnout of 20 dwellings when downwind versus 16 min for 12 dwellings when upwind) [281].

To protect structures from wind-blown firebrands, the creation of a protective space can be supplemented by interceptors, such as installing an external water spray system [289], using woven wire screens [290–292], or employing fire-resistant construction [293]. Intercepting firebrands with water sprays is effective only for firebrands <5 mm in size and fluxes $>100\ m^{-2}\ s^{-1}$, and it requires 0.1 mm water droplets at a flow rate of $0.1\ L\ s^{-1}$ per meter of building perimeter [289]. This means that ~259,000 L ($260\ m^3$) of water would be required to protect an 8 m $\times$ 15 m building for 3 h, and it calls into question the practical

applicability of such systems because a large volume of water would be required over a relatively long period of time.

3.3.2. Numerical work

Simulation work related to firebrand ignition in settlements can serve to supplement experiments. A review of literature shows that excellent efforts have been made in the areas of model development and numerical research. Based on a mathematical approach, firebrand models can either be deterministic or probabilistic in nature. The limiting factor of deterministic models is that simulations can only be performed for a selected set of conditions (e.g., certain power of fire source, particular particle size of firebrands, certain level of turbulent flow field, etc). There are also several oversimplified modelling assumptions, which usually cause either under or overestimation of risk, and for this reason some researchers prefer the probabilistic approach [195,294–296]. Probability-based models are often preferred because of their ability to include supplementary non-technical factors, such as occupant intervention characteristics in the model [297]. However, probabilistic firebrand models are not exempted from validation errors and often hold validity only under certain conditions. An example is the firebrand model of [296]; which is not valid when spotting is relatively rare (i.e. a scenario when fire spread rate is not firebrand driven).

In general, numerical modelling of firebrand dispersal is challenging because of the complex nature of the physical processes and several (typical) oversimplified modelling assumptions. For example, it is common to assume in numerical simulations that firebrands are spherical in shape [298,299]. In reality, however, firebrands are highly irregular in shape, and because of distinct aerodynamic characteristics, their transport distances vary greatly. Other common non-spherical shapes that were numerically studied in the past include disk-shaped [295,300,301] and cylindrical firebrands [295,301]. One of the reasons for modelling firebrands as spherical particles is the convenience it lends to drag force calculations. The drawback, however, is that spherical firebrands are physically the most difficult to transport because they have the largest volume to surface ratio, thus simulated results can deviate from reality [295]. Similarly, it is common to assume that the mass and shape of firebrands do not change during flight and that the temperature of firebrands has no effect on air flow [298,299]. In some cases, this is a reasonable assumption, as some studies have shown that for firebrands that stay in the thermal plume longer, the distance travelled upon landing is independent of the initial particle diameter and pyrolysis temperature [302,303]. However, in other situations the aforementioned assumption is not valid. An additional common assumption in firebrand simulation is that the relative velocity of firebrands with respect to local winds is always equal to their terminal velocity [295,304]. This assumption is more appropriate for simulating smaller firebrands than larger firebrands [295]. Similarly, the assumption of minimal interaction between the wind field and the thermal plume can lead to a significant change in the predicted range [305]. Ultimately, highlighting these common assumptions emphasizes that results obtained with numerical simulations should be interpreted with caution.

Practical usability of simulation results is another endpoint based on which numerical simulations of firebrands can be grouped into two categories: those meant for post-fire investigations [274] and those meant for monitoring ongoing firefighting operations [306]. The fire jump model of [306] is a firebrand model that can provide acceptable wildfire propagation results within 1 min and can assist in safe firefighting operations. In this regard, the most fundamental work has been done by Ref. [307]; in which algebraic equations were used to quickly and reasonably estimate the risk posed by firebrands. Recently [308], presented a meshless discrete model to help first-responders in real-time and has the capability to track the trajectory of airborne hot particles/embers.

Researchers have made both qualitative and quantitative conclusions about firebrand transport based on numerical simulations of firebrand transport. For example [205], concluded that the lift height of the firebrands carried from the peripheral part of the convective plume is lower compared to the firebrands carried from the axial zone. Numerical simulations show that for firebrands with the same initial mass, disk-shaped firebrands can travel further than cylindrical and spherical firebrands, and therefore disk-shaped firebrands (which represent bark) are more favourable to initiate spot fires [295,309]. As for the travel distance, simulation results show that the firebrands can travel up to 400 m [299] and up to 530 m when axial and radial distribution of the fuel is considered [295].

Summary. Firebrand exposure in settlement fires has received relatively less research attention compared to other exposure mechanisms and firebrand exposure in wildland fires. In the past, flame impingement and radiation were considered the primary exposure mechanisms, but this perception has changed in the last two decades. Recent experiments have revealed that structural fires can generate significantly larger firebrands compared to wildfires. For example, a wooden structure fire produced firebrands ranging from 1 to 3 cm in size, accounting for over 60% of the firebrands. The highest volume of firebrands is generated when structural components collapse, such as roofing and facade elements. It is important to note that firebrands can be produced at various scales. The diverse range of fuels found in settlements, particularly in informal settlements where highly combustible materials are prevalent, poses challenges for studying firebrands.

Probabilistic models are commonly used to simulate firebrands due to their ease of implementation. Physical models, on the other hand, make several assumptions to simplify the problem, such as considering firebrands as spherical with constant mass and shape. Modelling studies have indicated that firebrands can travel distances exceeding 500 m, with disk-shaped firebrands posing the greatest danger in terms of travel distance and their potential to ignite new spot fires.

To gain further insights into the role of firebrands in large outdoor fires, additional numerical and experimental investigations are required to examine their generation, transport, and ignition mechanisms. Special attention should be given to studying firebrands in informal settlements, where ongoing research on fire exposure and propagation mechanisms is still needed. Specifically, research is required to understand the generation and ignition of firebrands from structural materials commonly used in informal settlements, given their high flammability and potential to contribute to fire spread and exposure. Wind conditions must be carefully considered, as they have a significant impact on firebrand exposure in settlements. More research is warranted to evaluate the effectiveness of protective systems, such as water spray systems and woven wire screens, in mitigating firebrand attacks.

4. Discussion: knowledge gaps and direction for research

A review was carried out to examine the exposures resulting from wildland and settlement fires. Recent studies on flame contact and convection, radiation, and firebrands were analysed from both an experimental and numerical perspective. The main findings from these studies are presented, along with existing research gaps, and future research areas for investigation are proposed.

The spatial and temporal scales at which fire characteristics and heat transfer must be measured vary greatly with fuel type, ambient conditions and fire size. This partly reflects the wide variation in the results of previous studies. Detailed measurements of flame, airflow dynamics, radiation and firebrands are few and often based on diverse methodologies. Furthermore, heat transfer is usually characterized using macroscopic averaged variables. These limitations hinder the detailed analysis of convective and radiative heat transfer and the further development of physics-based models and analysis.

The research area that is most sorely lacking in data is that relating to the impact of fires on structures. There are indeed very few studies on this subject [56–58,83,310,311]. Thanks to the use of detailed fire models, numerical studies make it possible to obtain data (temperature,

velocity field, power, emitted flux) that can be used to study the vulnerability of structures. However, these simulations must be supported by experimental data. Without this data, it is difficult to know whether the constructions are really vulnerable or not. Platforms have emerged across the world in recent years for the purpose of evaluating fire among structures [312,313]; One House in Australia [314] and EXPLORII in France [315]).

Analysis of post incident data showed that current concepts of defensible space do not account for the hazards of burning primary structures, the hazards presented by firebrands, or those hazards outside of the home ignition zone [316]. Also, the collection of structure damage data to enable the identification of structure ignition vulnerabilities is limited [9]. mentioned the problem of distinguishing home ignitions due to result of firebrands from the wildland fire and via structure generated firebrands. Post fire investigation should incorporate specific actions when performing WUI and urban post-fire assessments, including evaluation of all structures, quantifying fire and firebrand exposure in space and time [316]. Fuels that should be considered should include wildland fuels and structural/residential fuels such as wood roofs, fences, combustible decks, etc. A better understanding of exposure and structure vulnerabilities needs to be developed, including definitions for high and low fire and firebrand exposure areas. Exterior fire protection methods in the WUI areas, in combination to those developed for use within buildings, could be used [5].

In their examination of risk management practices in the US [8], found a lack of specification of WUI fire exposure conditions. A significant gap in risk management strategies lies in the assessment and measurement of exposure levels and vulnerabilities specifically related to protected structures. Considering the escalating severity and frequency of wildfires due to climate change, it is crucial to anticipate that exposure conditions may worsen over time. Therefore, it becomes imperative to incorporate this factor into future studies and assessments.

The analysis of wildfire exposures reveals that different studies have employed various parameters to characterize these exposures. Flame and convective exposure have been characterized by flame temperature and convective heat flux, radiative exposure by radiant heat flux, firebrand exposure by firebrand flux, number of firebrands with specific material, shape, and size, as well as the mode of firebrand combustion (flaming or smouldering/glowing), among others. This lack of uniformity in parameters makes it challenging to standardize the problem.

However, a potential approach to describing wildfire exposures lies in examining fire behaviour, which can be characterized by parameters such as ROS, HRR, and amount of fuel consumed. These factors can be combined to form an index of the energy produced by the fire, such as fire intensity or fireline intensity. Fireline intensity can then be used to establish relationships between each wildfire exposure and their respective parameters, as well as the probability of structure damage and loss.

Currently, there is a lack of consistency and limited data in this field, making it extremely difficult to establish robust relationships. Nevertheless, we believe that by recording exposure parameters in conjunction with fireline intensity, it will be possible to establish connections between exposure parameters and the probability of house loss, ultimately leading to the development of relationships between fireline intensity and house loss. This approach has the potential to improve our understanding of wildfire exposure and its potential impact on structures.

In the subsequent sections, we will delve into a more comprehensive analysis of these considerations, addressing each type of exposure in detail. By doing so, we aim to provide valuable insights and recommendations to enhance risk management practices and mitigate the potential impacts of wildfire exposure on structures.

4.1. Flame contact and convection

The characterization of flame exposure using thermocouples has commonly relied on flame temperature as a key parameter. However, certain issues have been identified in this approach. For instance, previous studies have reported air temperatures at various locations within a burn area, without characterizing the flame characteristics and the thermocouple location relative to the flame envelope [317]. While this may provide insight for fire effects considerations, it complicates efforts to extract a characteristic flame temperature, given the compounding factors involved, e.g., proximity of sensors to flames, local variation in fuel availability, vertical location within flame/fire plume. If the aim is to obtain flame temperature measurements in order to characterize exposure (e.g., to equipment or structures) then it will be particularly important to ensure that a relevant measurement location has been chosen. If a conservative value is desired, then this may also place greater emphasis on the use of absolute peak flame temperatures. An additional consideration for flame temperature measurements is the magnitude of the measurement error. This is relevant wherever a thermocouple is used within a gas stream, where energy losses may occur as a result of radiative losses or conductive losses (from thermocouple junction through wires).

Over the past two decades, researchers have begun to measure convective heat in wildfire and WUI experiments. However, this is still not a common practice, and there is currently no standardized protocol for conducting such measurements. This is partly due to the complexity of the measurements and the lack of robust equipment available for this purpose.

In settlement fires, flame impingement and convection have only recently started to be considered, and very few experimental studies have been conducted. It has been found that settlement fires can produce additional mechanisms for fire spread, such as the expansion of the burning area and flame “ejection” from openings in structures and urban elements. However, the review identified that there is currently no standardized method for quantifying critical metrics such as impingement frequency and minimum flame size for ignition, which are essential to understanding the underlying nature of this exposure and the burning mechanism of different fuels involved in such fires.

CFD modelling could serve as a useful tool to better understand flame dynamics in settlement fires. However, [90]; in a recent review on simulation of fire-wind interactions in settlements, raised several issues in the modelling of fire exposure. In particular, it is necessary to simulate the forced convection produced by wind. Investigations of the impact of fire on wind and wind on fire in WUI and urban areas are not adequately conducted and require further exploration. Knowledge about wind and convective heat is extremely important for correctly predicting firebrand impact, as wind and convective heat carry firebrands and maintain them in a combustible mode. Small-scale modelling of smoke is also under-investigated, and with climate change, more fires are expected, making smoke impact a significant problem in the future.

Fire behaviour in settlements is extremely dynamic, and the rate of spread and fire intensity change rapidly in space and time due to the complex fuel matrix and heterogeneity of fuel [84]. demonstrated that high-accuracy 3D modelling, especially at small scales, should be used to characterize fire exposures in the WUI. Additional research is required to develop more comprehensive models for fire exposure and risk of property loss in both the WUI and the built environment.

4.2. Radiation

Concerning radiation heat transfer, field-scale experiments are needed in order to have data representative of real fires considering that the size of the fires significantly influences the data relating to radiation. At present, there is little data on the characterization of thermal exposure to structures. It is therefore necessary to continue research in this field. Concerning methods to measure radiant heat transfer, they can be classified into two categories: in-situ and remote sensing methods, which present both strengths and weaknesses. While both types of techniques rely on the same physical phenomena (radiant heat), their

different implementation in practice produces some important differences in the resulting datasets. In-situ measurements typically provide highly accurate estimations of the radiant flux received at a certain point and its evolution with time, but these measurements are difficult to extrapolate spatially. Several methods to measure the fluxes have been used, namely radiometer, Schmidt-Boelter gauge, Gardon gauge, steel plate gauge and Thin Skin Calorimeters [318]. All of these deal with convective and radiative heat fluxes differently and need to be considered, in particular with respect to how heat losses and background radiation are incorporated (or not). The data measured with these sensors can only be obtained at particular locations. In addition, the windows and view factors of radiometers can significantly skew the data, giving values lower than the total radiation emissions.

On the contrary, remote sensing methods have succeeded in estimating spatially explicit fields of fire radiative power and energy, at the expense of typically coarser spatial and temporal resolution and added uncertainty due to required transmissivity corrections. In addition, oblique view angles and significant flame lengths limit precise estimation of the fire front location on the ground, especially at large distances from the observation points [36]. Similarly, identification of head fire, flanks and backfire is challenging and there is no quantitative definition for those terms. Therefore, measuring radiation with both in-situ and remote sensing methods seems to be the most promising approach. In addition, the use of flexible experimental configurations should be favoured in order to mitigate the effects of changing meteorological conditions over the course of experimental campaigns. It is also necessary to use a sufficient temporal resolution of the measurements to properly capture radiative and convective heat transfer. While most previous works acquired samples at 1 Hz, recent studies showed that such a sampling rate may be insufficient [24].

Modeling the radiative impact of a fire on a structure is complicated because it involves processes with a wide range of temporal and spatial scales. Chemical reactions occur on the scale of molecules, while phenomena relating to radiation or turbulence occur on scales ranging from millimeters to kilometers [319]. The choice of spatial and spatial temporal discretization is therefore crucial to try to best capture the different phenomena while keeping reasonable computation times. Most studies dealing with the radiant impact of a fire on a structure use the solid flame approach to determine the flux received by a target element. This approach requires approximating the flame front by a simple shape and defining an emissive power generally calculated from a flame temperature. The emissive power of the flame and the atmospheric transmittance are often equal to 1. These assumptions considerably simplify the radiation calculations, however, this implies less precise results. With the development of increasingly powerful calculation servers, studies of the radiant impact on structures are beginning to be carried out using detailed physical models calculating the radiative transfer equation. The calculation of radiation in CFD codes leads to an increase in CPU time: about 20% for WFDS according to Ref. [320]. However, this type of approach makes it possible to take into account the chemistry of combustion (gas, soot) but also the shape of the flame. This therefore increases the precision of the simulations. The current limit of this type of approach is the computation time which can become very important for large computation domains, small meshes or more sophisticated computation methods for the RTE (gray gas or non-gray gas model, number of calculation angles, etc).

4.3. Firebrands

Regarding firebrand exposure, one of the main challenges observed in numerical and experimental studies is validating the findings. Given the complexity of the physics of spotting, involving numerous (often) coupled parameters is extremely challenging. When it comes to numerical research, several assumptions need to be made to simplify the boundary conditions or input parameters. For example [198], highlighted that current fire operational models do not aim to describe such key aspects such as the spotting dynamics and fire-atmosphere interactions. In experimental studies, a major challenge is that of replicating the real fire environment. Experiments should incorporate longer firebrand exposure times. Research could continue on collection of firebrands from real and prescribed fires, including different vegetation, structures, winds, etc. Due to the size limit of facilities and equipment capabilities, it is very challenging to replicate extreme conditions. Hence, there always remains the question of whether the findings of a particular work can be extrapolated to more extreme, and in many cases more realistic, conditions. Moreover, the high number of parameters affecting the behaviour of firebrands (e.g., shape, size, mass, combustion mode, ambient conditions, etc.) at different stages (generation, transport and ignition), and their interactions, mean that it requires a tremendous effort to account for all of the combinations. Another limitation of literature is that studies have not considered all three stages of spotting, and in most cases one of them (generation or transport or ignition) has been the focus of a research work.

5. Conclusion

Despite the considerable amount of literature, there are still critical gaps in knowledge and inconsistencies between the data in each section. Most papers have studied either radiative, convective, or firebrand exposures, which makes understanding the overall fire exposure very difficult. Sensor locations and types vary from study to study and between laboratory and field experiments, making it extremely difficult to compare studies and verify results. For example, flame temperatures and radiative heat fluxes can differ several times under similar conditions. Firebrand studies are mostly limited to laboratory conditions because of complexity of prescribed or wildfire experiments. This raises the question of extrapolating results to more extreme and therefore more realistic conditions. There are very few studies in the literature on firebrand generation and how firebrand generation is influenced by materials and extreme conditions. Moreover, previous studies have not addressed all three stages of firebrand spotting (generation, transport, and ignition) simultaneously. There is a significant lack of experimental data in the impact of fires on structures and transition of fire between structures. Although numerical studies have been relatively successful and have provided the essential data (temperature, velocity field, heat release rate, radiative flux, etc.), they are not fully validated with experimental data and their applicability is limited. Data are needed for quantitative risk analysis, such as wildfire exposure conditions or the reaction of components to these conditions. There is also a lack of post incident data, especially the distinction between house fires resulting from wildfire exposure or from structure-to-structure exposure. All of this prevents improvements in existing building codes and standard testing methodologies. A coordinated effort by researchers around the world is needed to solve this global issue.

Contribution

Alexander I. Filkov: manuscript coordination, writing and editing, subsection 2.3 coordination, writing section 2.3, discussion, editing.

Virginie Tihay-Felicelli: subsection 2.2 coordination, introduction, writing section 2.2, discussion, editing.

Nima Masoudvaziri: subsection 2.1 coordination, writing sections 2.1 and 2.3, discussion, editing.

David Rush: subsection 3.2 coordination, writing section 3.2, discussion, editing.

Andres Valencia: subsection 3.1 coordination, writing section 3.1, discussion, editing.

Yu Wang: subsection 3.3 coordination, writing section 3.3, discussion, editing.

David L. Blunck: writing sections 2.1, 2.2 and 2.3, discussion, editing.

Mario Miguel Valero: writing section 2.1 and 2.3, discussion, editing.

Kamila Kempna: writing sections 2.2 and 2.3, discussion, editing.
Jan Smolka: writing section 2.1 and 2.3, discussion, editing.
Jacques De Beer: writing section 3.1, discussion, editing.
Zakary Campbell-Lochrie: writing section 2.1, discussion, editing.
Felipe Roman Centeno: writing section 3.2, discussion, editing.
Muhammad Asim Ibrahim: writing section 3.3, discussion, editing.
Calisa Katiuscia Lemmertz: writing section 3.2, discussion, editing.
Wai Cheong Tam: writing section 2.2, discussion, editing.

Declaration of generative AI and AI-assisted technologies in the writing process

During the preparation of this work the authors used ChatGPT in order to improve the coherence and readability. After using this tool/service, the authors reviewed and edited the content as needed and take full responsibility for the content of the publication.

Declaration of competing interest

The authors declare the following financial interests/personal relationships which may be considered as potential competing interests: Alexander Filkov reports financial support was provided by Australian Research Council. Asim Ibrahim reports financial support was provided by KK-stiftelsen, Åforsk and Swedish Institute. Yu Wang reports financial support was provided by National Natural Science Foundation of China and USTC Research Funds of the Double First-Class Initiative. Felipe R. Centeno and Calisa K. Lemmertz reports financial support was provided by Brazilian National Council for Scientific and Technological Development (CNPq) and Higher Education Personnel Improvement Coordination (CAPES). David Rush reports financial support was provided by Engineering and Physical Sciences Research Council.

Data availability

No data was used for the research described in the article.

Acknowledgements

Many people were involved in the production of this manuscript, giving advice, editing, and consulting. We would like to thank Torin Christensen for providing editorial feedback, Samuel Manzello and Sayaka Suzuki for their thoughtful comments and constructive feedback, Rafal Porowski for advising on the structure of subsection 3.3, and Daniel Gorham for initially managing subsection 2.1. We also acknowledge the funding from many organizations to enable the studies considered in this work. Specifically, Alexander I. Filkov was supported by the Australian Research Council (Grant No. DP210102540), Muhammad Asim Ibrahim was supported by KK-stiftelsen [grant number 817-2.1.9], Åforsk [grant number 21-106] and Swedish Institute [grant number 00119/2022], Yu Wang was supported by National Key R&D Program of China (2022YFC3003100) and USTC Research Funds of the Double First-Class Initiative (YD2320002005), Felipe R. Centeno and Calisa K. Lemmertz were supported by the Brazilian National Council for Scientific and Technological Development (CNPq/Brazil) and Higher Education Personnel Improvement Coordination (CAPES/Brazil), David Rush was supported by Engineering and Physical Sciences Research Council (IRIS-Fire project of UK, Grant No. EP/P029582/1).

Appendix

Table 1
Summary of experimental studies related to the characteristics of flame contact and convection.

Scale	Experimental Conditions	Fuel	Measured quantities and values	Findings	Reference
Field or laboratory?	Specifics of the experiment, such as variables of the experiment, their values and conditions	Particular vegetation, structural fuel or gas burner?	What is measured/investigated?	What are the conclusions on flame and convection?	
Laboratory	Fire Type: Fire Propagation Area: 1.4 m^2 Slope: −15–15° Wind velocity: −3–3 m/s Location of thermocouple measurements: At heights of 0, 125, 350, 375, 500 & 1000 mm above the bench.	Pinus pinaster	Height: 6.1–46.9 cm Flame Angle: 28–174° Max Flame Temp: ≈325–≈1025 °C RoS: 0.124–7.231 cm s^{-1}	Dependence of flame angle and flame height on wind velocity, fuel bed slope, and fuel moisture content. Reduction of max. flame temperature at greater Fuel Moisture Content. Variation in flame temperature with height.	[45]
Laboratory	1: Hardboard siding Thickness: 11 mm Density: 620 kg m-3 Moisture content: 9% 2: Walls made of the same siding Two nailing configurations Exposed to: 160 KW for 2 min and 40 KW for 10 min	Propane flame	Ignition time and sustainability Critical heat flux Critical ignition time	Flames self-extinguish after removing the source. When comparing the flames, exposure time seems to dominate the intensity. Wind-aided smouldering is an important factor.	[56]
Field	Natural and prescribed fires in various locations.	Various	2 s averaged convective fluxes from 15 to 20% of peak radiative fluxes measured for crown fires in lodgepole pine. (Peak radiative fluxes of 300 kW m-2 measured beneath crown fires). Peak convective heat fluxes ranged from 20 to 70% of peak radiant heat flux for sagebrush fires.	Greater temporal variation in convective heat flux magnitude than radiation (which increased almost monotonically as flame front approached followed by exponential decay after flame arrival).	[27]
Field	Experimental fires Radiant & convective heating/cooling measurements. Sensors at 0.5 m above ground level.	Various	RoS: 0.10–0.51 m/s Flame Heights: 0.3–1.8 m Flaming Zone Depth: 0.3–3.0 m Peak Radiant Heat Flux: 18.8 kW/m^2 Peak Total Heat Flux: 36.7 kW/m^2	Emphasises highly fluctuating environmental conditions and difficulty of meaningfully measuring energy transport. Provides important data for lower	[38]

(*continued on next page*)

Table 1 (*continued*)

Scale	Experimental Conditions	Fuel	Measured quantities and values	Findings	Reference
Field or laboratory?	Specifics of the experiment, such as variables of the experiment, their values and conditions	Particular vegetation, structural fuel or gas burner?	What is measured/investigated?	What are the conclusions on flame and convection?	
				intensity fire spectrum. Convective heating similar in magnitude to radiant heating and linked with ignition highlighting the need to measure both radiant and convective fluxes.	
Laboratory	Phase 1: Window dims: .61 × .61 × .0048 m Configurations: single/double panes & plate/tempered Heat flux: 9.3, 13.6, 17.7 KW m-2 (duration: 300 s) Phase 2: Window dims: .91 × 1.5 × .006 m Windows in wooden walls of 2.5 × 3.4 m Flames of up to 1.3 × 3.1 × 0.8 m	Phase 1: Propane flame Phase 2: Wood fuel cribs	Breakage/collapse of windows (both phases) Incident heat flux (phase 2) Ignitability of walls (phase 2)	Phase 1: Tempered glasses are more resistant to fire exposure, and double pane configuration improves their integrity. Phase 2: For 50 KW m-2, all windows collapsed and walls ignited.	[57]
Laboratory	Fire type: static fire and fire propagation Location of thermocouple measurements: Centre of fuel bed, ½ inch above fuel surface, for propagation test. (Array moved to keep in flame). For static fire (pine wood), held in flame.	Propagating Fires: Pinus resinosa needles Static Fires: Pinus strobus wood	Propagating Fires: Fire Intensity: 15 BTU/sec-ft Flame Height: 1 ft. Flame Thickness: 4 in. Avg. Flame Temp: 765–1023 °C Estimated Zero Diameter Thermocouple Temp: 1093 °C RoS: 0.3 cm s^{-1} Static Fires: Flame Height: 3–4 ft. Flame Thickness: 18 in. Avg. Flame Temp: 833–951 °C Estimated Zero Diameter Thermocouple Temp: 988 °C	Measurements of flame temp with thermocouples can involve significant error particularly in smaller flames. The measurement error is roughly proportional to the thermocouple diameter. Based on these experiments, and existing sources, a minimum flame thickness of 5 ft was suggested, as the critical thickness for the flame to be opaque to thermal radiation.	[321]
Laboratory	Fire Type: Fire Propagation Area: 0.05–0.09 m^2 Slope: 0° Location of Thermocouple Measurements: In flame at 2, 11 & 22 in. above fuel surface.	Pinus ponderosa needles Pinus monticola needles Pinus contorta needles	Flame Depth: 0.06–1.61 m Flame Length: 0.2–1.7 m Residence Time: 55–76 s Flame Temp: 613–916 °C Avg. Flame Temp: 779–867 °C RoS: 0.1–0.6 cm s^{-1}	Avg. flame temperature, flame length and flame depth, all decreased with increasing FMC.	[48]
Laboratory	Location of Thermocouple Measurements: Held within luminous flame region above fuel.	Various forest fuels	Average flame temp for variety of forest fuels: circa. 815 °C	Fons proposed what is widely accepted to be the first detailed mathematical model of wildland flame spread. Model involved a simple film conductance approach to convection using empirical values for cylinders of various diameters (0.0004–3.75 inches) and an assumed flame temperature of 815 °C (1500 °F).	[41]
Laboratory	Porous array of fine fuel Fuel bed width: 1 m Fuel bed length: 7.5 m Fuel bed depth: 0.03–0.15 m Wind velocity: 0–2.68 m s-1	Regular *excelsior* Aspen wood (Populus tremuloides) shavings Ponderosa Pine (Pinus ponderosa) needles Course *excelsior* Aspen wood (Populus tremuloides) shavings	Convective heating Gas temperature Local gas speed	Characterization of near-surface flow profile as a function of applied wind speed, fuel properties and distance from flame front. Identifying three distinct surface flow regimes at different distances from the flame front with region boundaries varying with applied wind speed. Temperature of gas phase ahead of flame front decreased exponentially with distance from flame front. The maximum temperature (at flame front) varied negatively with packing ratio, moisture content and initially with applied wind speed (no effect for wind speeds > circa. 1 m/s). Exponential decay was slightly affected by packing ratio, surface-to-volume ratio and was proportional to wind speed.	[23]
Field	Seven tests Walls of 2.44 × 2.44 m at 10 m from the burn plots Panels of 1.4 × 1.22 m at 20 and 30	Jack pine	Heat flux and exposure of the walls Occurrence/Status of ignition on walls	None of the panels ignited. Average flux-time integral (FTP) is calculated for the walls at 10 m. Ignited walls did not sustained flames.	[58]

(*continued on next page*)

Table 1 (*continued*)

Scale	Experimental Conditions	Fuel	Measured quantities and values	Findings	Reference
Field or laboratory?	Specifics of the experiment, such as variables of the experiment, their values and conditions	Particular vegetation, structural fuel or gas burner?	What is measured/investigated?	What are the conclusions on flame and convection?	
	m from the burn plots Burn plots of 150 × 150 m				
Field	Fire Type: Prescribed burning Area: 4 ha plots Wind Velocity: 1.1–2.4 m/s Location of thermocouple measurements: On towers at 0.5 m, 1.0 m, 2.0 and 3.0 m above the ground. (Additional at roughly 2 m intervals on a max. 12 m tall cable) Ignition Line Length = 120 m Towers located 100–150 m form ignition line at plot center line, and 50 m either side of centre line.	Eucalyptus marginata Taxandria parviceps Bossiaea ornate	Fireline intensity: 710–10,570 kW/m Flame Height: 1.1–14.2 m Flame Length: 1.1–14.4 m Flame Angle: 55–104° Flame Depth: 1.0–14.5 m Residence Time: 20–63 s (Mean = 37 s) Max Flame Temp: 676–1184 °C Visible Flame Tip Temp: 200–400 °C RoS: 0.04–0.34 m/s	For lowest TC (0.5 m), peak temperature was found to be significantly correlated with ROS, fire intensity, flame length, and surface fuel bulk density, and marginally sig. correlations for under-forest canopy wind speed and fire intensity.	[46]
Field	Fire Type: Pile Burning Area: 4.5 acres Pile Arrangement: 36 piles (of 7–10 ft height and 47 ft^2 area) spaced 25 ft apart. Location of Temperature Measurements: Bare thermocouples in piles (7 &20 ft above soil), shielded unaspirated thermocouples in between piles and nearer to plot edge (7 & 20 ft height), shielded aspirated thermocouples in between piles s (7, 20 & 50 ft height)	Pinus monophylla Juniperus californica	In-Pile Max Temp (Unshielded, Unaspirated): >1450 °C (Beyond typical working range of thermocouple) Between Pile Max Temp (Shielded, Aspirated) = 1090 °C Between Pile Max Temp (Shielded, Unaspirated) = 760 °C Soil temperatures also measured.	Higher max. flame temperatures were observed than in many previous studies involving lighter fuel loadings. Suggests it may be necessary to assume flame temperatures of >1425 C when studying large fires. Significantly lower temperatures measured by shielded, unaspirated thermocouples compared to shielded, aspirated thermocouples. Observed two peaks in temperature profiles attributed to initial period of rapid combustion and a subsequent lower intensity period during the combustion growth phase of larger fuel elements.	[322]
Field	Fire Type: Prescribed Burning Area: 0.1–0.15 km^2 Location of Temperature Measurements: Thermocouples at 1, 60 and 160 cm above soil surface.	Mixed (Cerrado vegetation types)	Max Air Temp: 840 °C (Location and duration of thermocouple within flame envelope is unclear)	Considerable variations in measured air temperatures, but the relative location of flame and thermocouple is unclear.	[317]
Field	Fire Type: Natural and Prescribed Fires (Mix of surface fires, brush fires and crown fires)	Various fuel types: Surface fires primarily involved mixed grasses, Ponderosa pine, Longleaf pine and needle cast. Sagebrush and various other brush also present in brush fires. Crown fires involved various grasses, Lopdgepole Pine and needle cast.	Peak Radiative Flux: 20–300 kW/m^2 Peak Convective Flux: 13–140 kW/m^2 RoS: 0.05–0.8 m/s Flame Length: 0.39–30 m Flame Depth: 0.22–40 m Flame Angle: 0–53° Residence Time: 4–50 s Fuel Consumption: 0.17–5.25 kg/m^2	Experimental measurements from 13 natural and prescribed wildland fires. Radiative energy accounted for 79% or variance in fuel consumption. Convective heating at the sensor surface varied from 15% to values exceeding radiative flux.	[24]
Field	Prescribed burn in coniferous fuels Focus was on the effect of sampling rate on heat flux measurements.	Test area dominated by ponderosa pine and Douglas fir fuels.	Peak Radiative Flux: 50 kW/m^2 Peak Convective Flux: 110 kW/m^2	Large peak heat flux measurement uncertainties appear to occur for sampling rates lower than 20 Hz for radiative heat flux and less than 200 Hz for convective heat flux. Yet time averaged values valid even at sampling rates as low as 1 Hz.	[25]
Field	Plot Area: 9 plots with approx. 2ha (ca. 130 × 120 m) Slope: 20°, 17°, 26°, 24°,	Cereal crops - wheat, barley, and triticale crops	Gas Temperature, Heat Flux, Flame Velocity, Pre-Fire and Post-Fire Thermal Features, Air turbulence	It is suggested, these field-scale stubble fires were consistent with laboratory results that convective heating plays the crucial role in heating fuel particles to ignition in wind-driven wildland flame spread.	[29]
Field	Plot Area: 30 × 130 m Avg. Slope Terrain: 28 ± 2° Linear Ignition Radiant & total heat flux pairs at 0.5 m height and 6, 11, and 16 m from upper limit of plot. Thermocouples at 1, 6, 11 and 16 m from upper limit of plot.	Genista salzmanniin	Gas Temperature, Heat Flux, Rate of Spread, Wind Speed/Direction, Ambient Air Properties ROS: 0.423 - 1.136 m/s	Before time of flame front arrival at upper limit of plot, negligible total and radiative heat fluxes were measured. Total and radiative initially almost equal with increased divergence as flame front approaches (attributed to convective heating). In this scenario, convective heating was identified as dominant pre-heating mechanism.	[30]

(*continued on next page*)

Table 1 (*continued*)

Scale	Experimental Conditions	Fuel	Measured quantities and values	Findings	Reference
Field or laboratory?	Specifics of the experiment, such as variables of the experiment, their values and conditions	Particular vegetation, structural fuel or gas burner?	What is measured/investigated?	What are the conclusions on flame and convection?	
				Strong numerical agreement between experimental and predicted (FireStar2D numerical model) time averaged radiative:total heat flux ratio.	
Laboratory	Fuel bed: 7 m (l) x 3 m (w) Slope: 0° and 30°	Fuel Density: 780 kg/m^3 Fuel Load: 0.2, 0.4 and 0.6 kg/m^2 Fuel depth: 10, 17, 18, 22, 21, 23 kg/m^2	Particle Image Velocimetry - PIV CCD camera, Heat Flux, Gas Temperature, Rate of Spread, Flame Angle, Flame Height	Under no slope conditions, the preheating of the fuel particles was dominated by radiation from the flame. The fire-generated wind was blowing away from the fire and the flow was partially attached over the inclined surface. The downstream heating of the unburnt fuel, that governs fire spreading up steep slopes, was shown to depend on both radiative and convective heating mechanisms. The rates of heat transfer received ahead of the fire front increased with increasing slope and fuel load. The downstream convective mechanisms resulted from the interaction between the upstream air entrainment and the fire-generated buoyancy forces.	[55]
Laboratory	Fuel bed: 6m (l) x 3m (w) Slope: 0° and 30°	Fuel Density: 780 kg/m^3 Fuel Load: 0.4, 0.6 and 0.8 kg/m^2	Particle Image Velocimetry - PIV CCD Camera, Heat Flux, Gas Temperature, Rate of Spread, Flame Height	Under zero-slope conditions, the flame front adopted a U-shape and the flame height as the average value of 50 instantaneous flame-height measurements from the images acquired by the visible video camera. Under 30°-slope conditions, this "statistical homogeneity" is not guaranteed, as the flame fluctuated strongly between two extreme shapes during the spread	[323]
Laboratory	Fuel bed: 0.85 m (l) x 0.45 m (w) Slope: 0° and 30°	Fuel load 0.4 kg/m^2 Fuel bed thickness: 5 cm Fuel density: 830 kg/m^3	Particle Image Velocimetry - PIV CCD camera, OH radical chemiluminescence (marker of heat release and flame topology), Rate of Fire Spread, Flame Length, Flame Angle, Flame Depth, Av. OH* level, Peak OH* level	Mechanisms governing upslope fire spread depends not only on the increased radiant heat transfer rate but also on convection induced by the aerodynamic effects, created by the interaction between the fire induced flow and the slope. The interaction between the slope and fire requires also more thoroughly investigations at a larger scale because fire front and associated flow develop three-dimensional features (V-shape) for wider fuel beds.	[53]
Field	Wooden shields exposed to grass fire during surface flame spread experiments 50 m by 10 m experimental site.	Spruce board wooden shields (various dimensions) exposed to grass fires. Site vegetation was meadow motley grass-thistle association. Areas of peat added.	Heat fluxes on shield external surface at various heights, air temperature, relative humidity, atmospheric pressure, wind speed, soil temperature & moisture content, FMC, fire spread rate, IR imagery (w. Thermocouples deployed for calibration)	Determined for the open grassland site, a necessary fuel cleared perimeter of 5 m width was required to ensure structure safety. Making fences permeable and adding fire retardants was required to reduce ignition risk. Pine tree timber constructions (0.2 m by 0.2 m, 36.7% MC) did not ignite in the absence of firebrands.	[59]

Table 2
Summary of the numerical studies on the flame contact and convection

Numerical conditions	Model information	Numerical investigations	Reference
Burner (1 m × 2 m) Fire Intensity: 5 MW/m Wind speed: 3 and 5 m/s Concrete structure (0.2 m × 2 m × 2 m or 5 m) at 5 m from the burner	CO to represent the pyrolysis gas 1-step chemical reaction A fraction of the fuel converted into soot RNG k-ε	Radiant, convective and total heat fluxes on the structure	[82]

(*continued on next page*)

Table 2 (*continued*)

Numerical conditions	Model information	Numerical investigations	Reference
Fire exposed structure in wind tunnel. Structures were Syporex blocks (2.04 m × 1.38 m x 0.07 m). Structure located at the end of wind tunnel at horizontal distance of 1 m from end of vegetation fuel bed (excelsior and Douglas Pine) Thermal-fluid structure interaction modelled using finite-volume blocking-off operation.	2 phase multiclass model k-ϵ turbulence model Finite volume blcoking-off operation Nonuniform grid of 86 × 33 × 18 cells Computational Domain: 15 m × 6 m x 1.2 m	Thermal impact of fire exposure of a structural element. Opposed flow prescribed burn (900 mˆ2 area)	[83]
Wind speed: 6, 8, 10, 12 and 14 m/s Wooden budling	3D conservation equations Multiphase approach SIMPLE algorithm	Effect of the fire intensity and wind speed on ignition of building due to forest fires	[88,89]
Infinitely wide fire front with finite depth Fire front is stationary 1m × 1m x 3(6) m building Surface and crown fires	Fire Dynamics Simulator 2D and 3D simulations	Effect of the 2D assumption is studied by performing a series of simulations in both two and three dimensions, and reporting the difference in the effects on structures	[84]
Grass fuel 20m fire width 5m × 5m × 2.5m structure	Fire Dynamics Simulator Contribution of conduction to the overall heat transfer is neglected Convection modelled using an empirical correlation for convective heat transfer to vertical circular cylinders Radiation is modelled by a piecewise function for the flaming and non-flaming regions	Comparison of the radiation heat load upon a structure using CFD modelling and AS 3959	[85]
3 m width fire bed at 20 m of the structure Fuel: methane with intensity of 6, 10, 14 and 18 MW/m Slope: 0–30° Cubic structure to model a structure: 6 m × 6 m x 6	FireFOAM CFD Solver 3D, multiphase, time dependent model Large Eddy simulation Computational domain: 50 m × 30 m x 25 m Grid: 7,800,000	Investigation of the effects of slope and fire intensity on an idealized building	[91,92,94,95]

Table 3
Summary of the laboratory experiments dealing with radiation (abbreviation HF corresponds to heat fluxes)

Experimental conditions	Vegetation	Energy quantity	Fire front geometry	ROS (cm/s)	Reference
Fire type: static fire Area: 0.07-4.9 m^2 Slope: 0° Location of heat flux measurements: at 2 m from the center of the fuel bed	Pinus halepensis needles, branches and dead leaves of Erica arborea, Quercus ilex and Quercus humilis Fuel diameter:0.3-2.5 m Fuel height: 0.2-0.73 m	Radiant HF: 0.6-3.2 kW/m^2			[106]
Fire type: fire propagation Area: 0.04-0.09 m^2 Slope: 0° Location of heat flux measurements: at the fuel bed end	Ponderosa pine needles	Flame emissivity: 0.16–0.28 Total HF: 42–103 kW/m^2 Radiant fraction: 0.1–0.4		0.10–0.64	[48]
Fire type: static fire Area: 0.012 m^2 Slope: 0° Fire Propagation Apparatus Sample holders with different percentage openings (0, 26 and 63%)	Needles of Pinus pinaster, Pinus halepensis and Pinus laricio	Peak of HRR: 5–18 kW			[115]
Fire type: static and propagation fires Area: 0.16 m^2 (static) and 6 m^2 (propagation) FTIR spectrometer at 2 m for static experiments and 3 m of the fuel for propagation experiments	Static: Excelsior wood wool (0.2 kg) and dry vine branches (0.5 kg) Propagation: Branches of Kermes oak (5 kg/m^2) with excelsior wood wool (1.5 kg/m^2) Fuel height: 0.7 m	Spectral intensity emitted by the flame			[120]
Fire type: static fire Area: 0.16 m^2 FTIR spectrometer at 2 m	Excelsior wood wool, vine branches, leaves of Quercus coccifera and needles of pinus halepensis Mass of excelsior: 0.2 kg Mass of vine branches: 0.5 -1 kg	Spectral intensity emitted by the flame Absorptivity: Q. coccifera (0.9-0.94) and P. halepensis (0.92-0.95)			[121]
Fire type: propagation fire Area: 0.5-4 m^2 FTIR spectrometer	Branches of Kermes oak (9 kg/m^2) with excelsior wood wool (2 kg/m^2)	Spectral intensity emitted by the flame Effective intensity: 1.2-43.4 kW/m^2.sr Effective emissivity: 0.41–0.74 Mean extinction coefficient: 0.15–0.53			[122]
Fire type: static fire Area: 0.012 - 0.098 m^2 Cone calorimeter and Large Scale Heat Release Apparatus	Needles of Pinus pinaster and Pinus laricio Mass: 13.52-116.25 g	Peak of HRR: 637.6-825 kW/m^2			[116]

(*continued on next page*)

Table 3 (*continued*)

Experimental conditions	Vegetation	Energy quantity	Fire front geometry	ROS (cm/s)	Reference
Fire type: fire propagation Area: 2–10 m^2 Slope: 0–30° Location of heat flux measurements: at 10 cm from the fuel bed	Needles of pinus halepensis Fuel height: 3.9-4.3 cm Fuel load: 1 kg/m^2	Radiant Energy 33–412 kJ/m^2 Radiant HF:1.3-9.9 kW/m^2 Integrated radiant HF: 25–315 kW/m	Height: 49–98 cm Angle: 20–103°	0.33–5.01	[108]
Fire type: fire propagation Thermocouples at 1 ft (30.5 cm) from the end of fuel bed Wide angle radiometer	Wood shaving (poplar hardwood) Fuel bed: 24 in. (60.9 cm) wide by 42 (106.7 cm) in long	Radiant heat flux: between 7.5 $Btu/h.ft^2$ (79 W/m^2) to 25 $Btu/h.ft^2$ (79 W/m^2) at 1 in. (2.5 cm) from the fire front Temperature in the fuel bed: Up to 1450 F (788°C)		0.25–0.47	[119]
Fire type: fire propagation Area: 1.68 m^2 Slope: 0° Location of heat flux measurements: at 3.5 m from the fuel bed	Needles and branches of ponderosa pine, Douglas-fire twigs and grass Fuel mass: 0.2-2.9 kg	Mean radiant HF: 0.124			[105]
Fire type: fire propagation Area: 6 m^2 Slope: 0–30° Location of heat flux measurements: at 20 cm from the fuel bed	Needles of Pinus sylvestnis var. mongolica Litv Fuel height:4 cm Fuel load: 0.7 kg/m^2	Radiant HF: 0.250-8.646 kW/m^2 Peak of convection: 0.063 to -4.123 kW/m^2		0.27–11.3	[109]
Fire type: static fire Mass loss calorimeter (50 kW/m^2) Outdoor wind tunnel	Gorse shrubland Fuel mass: 10 g (mass loss calorimeter) Fuel load: 1.6 and 3.1 kg/m^2 (wind tunnel)	Peak of HRR: 198.1-331.6 kW/m^2 Temperature increase: 1.1-27 °C/s			[110]
Fire type: Static fire Slope: 0° Location of heat flux measurements: at 2 m from the tree	Douglas-fir Trees of 2 and 5 m Fuel Height: 1.8-2.25 m Base: 1.4-1.8 m Mass: 8.1-15 kg	Radiant HF: 12–25 kW/m^2			[113]
Fire type: fire propagation Area: 4 m^2 Slope: 0° Location of heat flux measurements: at fuel bed end	Needles of pinus pinaster Fuel height:3.5-7 cm Fuel load: 0.6-1.2 kg/m^2	Mean HRR: 40.1-147.7 kW Radiant fraction of flame: 9.1-10.1% Radiant fraction of embers: 7.3-13.3% Convective fraction: 68.5-83.8%	Height: 24.2-72.9 cm Length: 25.3-75.6 cm	0.35–0.89	[52]
Fire type: Static fire Slope: 0° Large Scale Heat Release Apparatus Ignition with a radiant panel	Rockrose shrub Mass: 0.89-2.99 kg Fuel height: 1.1-1.4 m	Peak HRR: 100–257 kW			[114]
Fire type: fire propagation Area: 12 m^2 Slope: 0° Wind speed: 0–5 m/s Location of heat flux measurements: in fuel bed	Shrub of Quercus coccifera and straw in fire tunnel Straw: Fuel load: 1.5 kg/m^2 Fuel height: 10 cm Quercus coccifera Fuel load: 3-6 kg/m^2 Fuel height: 90 cm	Radiant HF: 2.6-6.8 kW/m^2	Height: 1.14-1.6 m Depth: 0.33-0.5 m Angle:0-57.1°		[107]
Fire type: Static fire Slope: 0° Gas temperature (GTR) calorimetry	Wood: red oak, Douglas fir, pine	Total heat of combustion16.4-17.9 kJ/g Convective heat of combustion: 7.8-8.7 k/g Radiative heat of combustion: 3.7-4.9 kJ/g Chemical heat of combustion: 12.4-13.0 kJ/g			[118]
Fire type: fire propagation Area: 4 m^2 Slope: 20° Location of heat flux measurements: at fuel bed end	Needles of pinus pinaster Fuel height:3.5-7 cm Fuel load: 0.6-1.2 kg/m^2	Peak HRR: 102.0-400.2 kW Peak radiant HF: 7.6-28.8 kW/m^2 Peak total HF: 9.1-34.3 kW/m^2 Radiant fraction of flame: 9.1-24.2% Radiant fraction of embers: 7.3-14.8% Convective fraction: 61.1-83.8%	Length: 38.7-93.3 cm Angle: 3.6-9.7°	0.88–1.76	[54]

Table 4
Summary of the field-scale experiments considering radiation heat transfer (abbreviation HF corresponds to heat fluxes).

Experimental conditions	Vegetation	Energy quantity	Fire front geometry	Flame duration (s)	ROS (m/s)	Reference
Fire type: prescribed burning Area: 5625–22 500 m^2 Slope: 0° Wind velocity: 2.8-6.94 m/s Location of heat flux measurements: in the fire at 3.1, 6.2, 9.2, 12.3 and 13.8 m above the ground	Pine, black spruce Fuel height: 13 m	Radiant HF: 110–290 kW/m^2	Height: 15–30 m		0.48–1.16	[128]
Fire type: prescribed burning Area: 5625–22 500 m^2	Pine, black spruce Fuel height: 1.5-13 m	Total HF: 7.8-150 kW/m^2		26–41	0.405–1.163	[58]

(*continued on next page*)

Table 4 (*continued*)

Experimental conditions	Vegetation	Energy quantity	Fire front geometry	Flame duration (s)	ROS (m/s)	Reference
Slope: 0° Wind velocity: 1.9-6.94 m/s Location of heat flux measurements: in the middle portion of the wall's front surface (2.44 m × 2.44 m) at 10, 20 or 30 m of fire	Stem density: 95–7427 no/ha	Frontal fire intensity: 34,321–93 476 kW/m				
Fire type: prescribed burning Area: 2400 m^2 Slope: 0° Wind velocity: 2 m/s Location of heat flux measurements: at 5, 10 and 15 m form the top of the parcel and at 2 and 4m above the ground	Strawberry tree, heather, cistus golden-chain, oak, olive tree Fuel height: 1.5-3.26m	Radiant HF: 1.5 - 7.5 kW/m^2 Fireline intensity: 19,000–20,500 kW/m			0.1–0.4	[129]
Fire type: prescribed burning Area: 64 ha Wind velocity: 3 m/s Location of heat flux measurements: in the fire on tower at 2, 10, 28 and 43 m above the ground	Grass Fuel load:1.08 kg/m^2	Radiant HF: 28.5 kW/m^2 Heat release rate: 11.4 kJ/m^2	Length:5.1 m		0.68	[130]
Fire type: prescribed burning and propagation in cut fuels Area: 60–1250 m^2 Slope: 0–26° Wind velocity: 0.9-3.6 m/s Location of heat flux measurements: in the fire	PCF: Remnants of dry shrubs Fuel height:0.5 m Fuel load:10 kg/m^2 PB: broom, strawberry tree, heather Fuel height:0.8-1.2 m Fuel load:8–10 kg/m^2	Total HF: 50–120 kW/m^2 Radiant HF: 30–50 kW/m^2	Height: 1.9-6.5 m Depth: 0.4-9.2 m Tilt angle: 51–80°	20–66	0.015–0.29	[132]
Fire type: prescribed burning and propagation in cut fuels Area: 25–1200 m^2 Slope: 0–25° Wind velocity: 0.5-3.3 m/s Location of heat flux measurements: at the vegetation top in the fire	PCF: Pine needles, oak branches, branches of strawberry tree Fuel height: 0.03-1.4m Fuel load: 0.5-25 kg/m^2 PB: Broom Fuel height: 0.8 m Fuel load: 10 kg/m^2	Total HF: 40–112 kW/m^2 Radiant HF: 25–51 kW/m^2	Height: 0.2-5.6 m Depth: 0.06-7.2 m Tilt angle: 40–90°	20–110	0.003–0.18	[131]
Fire type: prescribed burning Area: 1000–1400 m^2 Slope: 17–26° Wind velocity: 2-3.5 m/s Location of heat flux measurements: in the fire	Broom, strawberry tree, heather, white asphodel Fuel height: 0.3-1.2 m Fuel load: 1.4-7.4 kg/m^2	Total HF: 80–120 kW/m^2 Radiant HF: 13–55 kW/m^2 Fire intensity: 8345-31749 kW/m	Height: 0.3-1.2 m Length: 5.1-8.4 m Tilt angle: 22–63°	21–31	0.18-0.35 m/s	[133]
Fire type: prescribed burning Area: 2500 m^2 Slope: 13° Wind velocity: 3.6 m/s Location of heat flux measurements: in the fire at 0.6, 1.1 and 1.6 m above the ground	Heather, broom Fuel load: 1.15 (live) and 0.3 (dead) kg/m^2	Radiant HF: 10.1-169.6 kW/m^2 Fireline intensity: 543–14973 kW/m	Height: 0.5-6 m Depth: 1.2-45.5 m	21–135	0.04–0.35	[134]
Fire type: prescribed burning Slope: 0–37° Wind velocity: 0-1.5 m/s Location of heat flux measurements: 0.5m above ground level in the fire	Grass, pine needles litter, leaf litter, brush, sagebrush, pine	Radiant HF: 20–300 kW/m^2 Convective HF: 13–140 kW/m^2	Length: 0.39-30 m Depth: 0.68-40 m Tilt angle: 0–53°	4–50	0.05–0.8	[24]
Fire type: prescribed burning Area: 36 ha Slope: 5.7-11.3° Wind velocity: 0.5-1.5 m/s Location of heat flux measurements: in the fire	Grass with conifer litter, Pine, Douglas-fire	Radiant HF: 22–50 kW/m^2 Convective HF: 40–110 kW/m^2 Fire radiative energy: 302-3052 kJ/m^2	Height: 0.3-0.8 m	5–30	0.042–0.167	[25]
Fire type: prescribed burning Area: 2–454 ha Wind velocity: <8.9 m/s Location of heat flux measurements: In the fire on a tower at 5.5 m above the ground and on a tower of 10 m, remotely piloted aircraft system 2 space borne sensors (VIIRS and MODIS)	Pine, oak, grass Fuel load: 3.0-6.8 Mg/ha	Radiative fireline intensity: 4.2-57.7 kW/m Fire radiative power 0.8-888 MW	Flame perimeter:114–1197 m	1020–1740		[135]
Fire type: propagation in cut fuels Area: 64 m^2 Wind velocity: 0.45-2.02 m/s Location of heat flux measurements: on a fixed-wing aircraft	Leaf litter and milled, kiln-dried softwood lumber Fuel height:4.4-13.5 cm Fuel load:0.17-3.87 kg/m^2	Fireline intensity: 151–813 kW/m Fire radiated energy density:0.42-9.8 MJ/m^2 Radiant fraction: 0.13–0.22		8.7–89.7	0.009–0.133	[138]
Fire type: prescribed burning Area: 2–828 ha Location of heat flux measurements: In the fire on a tower at 5.5 m above the ground	Pine, oak, grass Fuel load: 2.42-10.8 Mg/ha	Radiant HF: 6–40 kW/m^2				[136]

(*continued on next page*)

Table 4 (*continued*)

Experimental conditions	Vegetation	Energy quantity	Fire front geometry	Flame duration (s)	ROS (m/s)	Reference
and on an 8.2 m tripod; outside the fire perimeter at 26 m above the ground, airborne LWIR imagery						
Fire type: propagation in cut fuels Area: 35 m^2 Slope: 0° Location of heat flux measurements: At 4.8 m from the fuel bed 21.6 and 30.56 m above the ground	Pine needles Fuel height: 0.063-0.136 m Fuel load: 0.634-1.376 kg/m^2	Radiant fraction: 0.15–0.26 Fire radiative power: 150–650 kW Fireline intensity: 207.5-2353.6 kW/m			0.013–0.156	[139]
Fire type: prescribed burning Area: 4.25-6.71 ha Slope: 0° Wind velocity: 1.8-3.9 m/s Location of heat flux measurements: on towers at 0.9 and 1.1 m above the ground in the fire	Pine, oak, huckleberry, blueberry Fuel height: 5–79 cm Fuel load:0.98-1.68 kg/m^2	Fireline intensity: 4 MW/m Radiant HF: 35–52 kW/m^2 Total incident radiative flux: 600–1300 kJ/m^2			0.13–0.19	[44]

Table 5
Summary of the numerical studies on radiation

Numerical conditions	Model information	Radiation model	Numerical investigations	Reference
Flat surface in Douglas-fir Different flame sizes: 5 × 2 m, 5 × 6 m, 5 × 15 m, 10 × 15 m, 30 × 20 m Different tree densities: no spacing, 2 m, 4 m and 8 m spacing	–	Solid flame model (rectangle) Flame temperature: 1200 K Flame emissivity: 1	Estimation of the structure ignition potential	[6]
Burner (1 m × 2 m) Fire Intensity: 5 MW/m Wind speed: 3 and 5 m/s Concrete structure (0.2 m × 2 m × 2 m or 5 m) at 5 m from the burner	CO to represent the pyrolysis gas 1-step chemical reaction A fraction of the fuel converted into soot RNG k-ε	Grey gas assumption Finite-volume method on an angular mesh	Radiant, convective and total heat fluxes on the structure	[82]
Front flame width: 20 m Flame height: 1 to 40 m	–	Solid flame model (rectangle) Flame emissivity: 1 Atmospheric transmissivity: 1 Flame temperature: 1200 K	Determination of the safety distances for wildland fires	Zárate et a. (2008)
10 m × 10 m × 6 m house Vegetation (coverage of 81%) modelled by titled cylinders with a radius of 1.5 and an emissive power of 57 kW/m^2 Fire front of 200 m wide with flame height of 1.5, 6, 9 and 12 m	Stochastic network model to simulate fire propagation Local wind field calculated with FLOWSTAR	Solid flame model (cylinder) Atmospheric transmittance and surface emissivity equal to 1 Monte Carlo method Number of facets for the cylinders: 40 × 40 Number of bundles for each square meter of the emitting surface: 10^4	Estimation of the clearing distance with Monte Carlo method	[174]
Different flame lengths: 5, 10, 15 and 20 m Receptor element at 1.8 m (radiation threshold of 4.7 kW/m^2) Safety distances determined for 13 fuels models under a wind speed of 8 m/s	-	Solid flame model (tilted rectangle) Flame temperature: 1200 K Flame emissivity: 1	Estimation of the fire impact to define acceptable safety distance	Rossi et al. (2011)
Wind speed: 3, 5, 10 and 15 m/s Wooden building 12 m × 15 m × 12 m and 20 m × 50 m × 20 m	3D conservation equations Multiphase approach	Diffusion approximation Grey gas assumption	Effect of the fire intensity and wind speed on ignition of building due to forest fires	[175]
Moisture content of trees: 20% Wind speed: 5.7 m/s Ambient temperature: 25°C 4 trees House with 4 walls and flat roof top	EcoSmart Fire software with subroutines (CalcTreeHRR, CalcTreeQ, CalcDamage, CoreFlux) HRR calculated from moisture content Flame height calculated from HRR	Solid flame model (cylinder) Flame temperature calculated from Froude number and flame diameter Extinction coefficient proportional to square root of Froude number and proportional to flame temperature Ground reflexion considered	Study the potential damage to a house during a fire at WUI with ornamental trees surrounding the construction	[176]
Row of 4 houses No slope Fuel load: 35 t/ha Ambient temperature: 308K Relative humidity: 25% Fire Danger index: 80 Flame width: 100 m	Rate of spread calculated from the fire danger index and the slope Flame length calculated from the rate of spread and the fuel load	Solid flame model (parallelepiped) Flame emissivity: 0.95 Flame temperature: 1095K	Effect of radiant heat flux from wildfires on structures in an urban environment	[177]

(*continued on next page*)

Table 5 (*continued*)

Numerical conditions	Model information	Radiation model	Numerical investigations	Reference
Flame length: 7.5 m (grassland fires), 13 m (shrubland fires) and 3.5 times the height of the vegetation (equal to 5, 10, 15, 20 and 25 m for crown fires) Atmospheric tank: 50 m^3 and 14,000 m^3 Pressurized tank: 15 m^3 and 200 m^3	Lumped model for the assessment of the response of storage tanks to fire exposure: target equipment discretised in thermal nodes for which material and energy balances are solved	Solid Flame model (tilted rectangle) Flame emissivity:1 Flame temperature: 1200 K	Proposal of a methodology for the evaluation of safety distances between storage tanks and vegetation that may be affected by a wildfire	Ricci et al. (2021)
3 m width fire bed at 20 m of the structure Fuel: methane with intensity of 10, 14 and 18 MW/m Slope: 0–30°	FireFOAM CFD Solver 3D, multiphase, time dependent model Large Eddy simulation Computational domain: 50 m × 30 m x 25 m Grid: 7,800,000 Cubic structure to model a structure: 6 m × 6 m x 6 m	Finite volume discrete ordinates model (fvDOM)	Investigation of the effects of slope and fire intensity on a idealized building	[95]
Canopy stratum of cork oaks, a shrub layer of plants of rockrose, tree heath and strawberry tree and a litter layer 2 vegetation distribution tested for the cleared area Wind speed: 25 and 45 km/h 2 ambient conditions	WFDS 3D, multiphase, time dependent model Large Eddy simulation Computational domain: 275 m × 80 m x 70 m Mesh size: 25 cm Boundary fuel model coupled with a linear pyrolysis sub-model for the thermal degradation of the solid-phase for litter and shrubs and fuel element model combined to an Arrhenius type model for solid-phase degradation including char oxidation for trees	Gases assimilated to gray medium Vegetative fuels assumed to be spherical, non-scattering and perfectly absorbing Radiative absorption coefficient function of species mass fractions, temperature and soot particulate A finite volume method used to solve the gray form of the RTE	Characterization of heat exposure conditions of a dwelling in common Mediterranean WUI scenarios	Perez-Ramirez et al. (2022)

Table 6
Summary of studies on the generation of firebrands

Research approach and scale	Study conditions	Vegetation/fuel	Measured quantities and values	Findings	Reference
Field-scale experiments	Prescribed fires 200 × 200 m plots Wind velocity: <25 km/h Average slope <5° Firebrand collection Bark consumption Surface FMC 5.6–9.6%	Jarrah forest of 3,5 and 22 year-old Fine fuel load 1.5 t/ha	Fire intensity 150–10,570 kW/m ROS 47–1364 m/h Flame height 0.3–14.2 m Bark consumption 0.2–25.1 mm Firebrand thickness 2–4 mm Spotting distance 11–164 m Firebrand density 0.15–39.7 #/m^2	Bark consumption will increase by a factor of at least three times and five times when fire intensity increased from 1000 kW/m to 3000 kW/m and from 3000 kW/m to 6000 kW/m respectively. Bark consumption on trunks increases with age (doubled for the 22-year-old forest compare to 5-year-old). The density of firebrands sharply decreases with distance from the firebreak.	[180]
Field-scale experiments	Prescribed fires 4.3 and 6.7 ha plots Average wind velocity 1.8 m/s Four different approaches were used to characterize firebrand generation: shrub layer consumption, bark consumption, firebrand collection, thermal analysis	Pitch pine and scattered Oaks. Understory vegetation consisted of scrub oaks, huckleberry and blueberry.	Fire intensity 500–3200 kW/m ROS 0.039–0.186 m/s Bark consumption 0.1–14 mm Firebrand thickness/diameter 1–6 mm Firebrand weight 5–100 mg Firebrand cross section area 5–50 mm^2 Firebrand distribution 60–238 pcs/m^2 Canopy consumption	The number of firebrands decreases with increasing firebrand area. The majority of firebrands are bark flakes. Shrub layer contribute to firebrand generation. The fire-induced draft is an important parameter for bark originated firebrand production and transport.	[178]
Post processing of field-scale experimental data	Development of a custom software in order to detect the location and the number of flying firebrands in a thermal image Wind velocity 0.1–5 m/s	Pitch pine and scattered Oaks. Understory vegetation consisted of scrub oaks, huckleberry and blueberry. Surface fuel load 0.83–1.68 kg/m^2	Firebrand distribution 12–960 pcs/m^2 Firebrand velocity 0.1–10.5 m/s 89% of firebrands have cross section area of 5–10 mm^2	The bark flakes were found to be not less than 70% of collected particles and the remaining particles were pine and shrub branches. Starting 13 m from fire front, an increasing number of firebrands is observed, starting from only a few to 180 per second.	[182]
Post processing of field-scale	Firebrand collection Diagnostics of firebrands and their characteristics on thermal	Pitch pine and scattered Oaks. Understory vegetation consisted of scrub oaks,	Fire intensity 180–12,5900 kW/m 2D firebrand flux 0.0075–0.036	Fireline intensity below 12,590 kW/m does not change significantly 2D firebrand flux	[183]

(*continued on next page*)

Table 6 (*continued*)

Research approach and scale	Study conditions	Vegetation/fuel	Measured quantities and values	Findings	Reference
experimental data	footages using developed software	huckleberry and blueberry. Surface fuel load 0.83–1.68 kg/m^2	pcs/m^2s 3D firebrand flux 0.029–4.91pcs/m^3s	for firebrands bigger than 20 mm^2, while occasional crowning can increase the firebrand flux in several times.	
Field-scale experiments	Prescribed fires 28 ha plot Temperature 13 °C Mean relative humidity 22% Wind velocity: 0.5–4.4 m/s Bark consumption Surface FMC 31 ± 11% Firebrand collection in aluminium cans	Pitch pine and scattered Oaks. Understory vegetation consisted of scrub oaks, huckleberry and blueberry	Firebrand flux 0.82–1.36 pcs/m^2s Fire intensity 7350 ± 3480 kW/m to 12,590 ± 5870 kW/m Surface fuel consumption 1.36 ± 0.64 kg/m^2 ROS 0.289 ± 0.014 m/s Mean flame height 2.4–5.0 m Firebrand density 335–536 pcs/m^2	There is a correlation between firebrand flux and fire intensity. Periods of high intensity firebrand showers occurred up to 100 m ahead of the fire front.	[186]
Field-scale experiments	6.25 ha plot Field-deployable emberometer designed to provide measurement of firebrand fluxes and information on both the geometry and the thermal conditions of firebrands	Pitch pine and scattered Oaks. Understory vegetation consisted of scrub oaks, huckleberry and blueberry	ROS 0.09–0.26 m/s Maximum firebrand density 300 pcs/m^2 About 9% of firebrands were “hot” (>100 C)	Temperature thresholds hot/cold were found to be material dependent. No correlation between particle size and temperature was observed.	[222]
Laboratory experiments (and developing empirical models)	Vertical combustion tunnel (TCV) is used. Airflow velocity: 0–6.5 m/s Particle orientation with respect to airflow range: ±90° Study on single particles	Pinus pinaster and Eucalyptus globulus	Mass loss Duration of combustion (flaming phase and burnout times)	Combustion time is shorter for Pine scales compared to Eucalyptus bark. Two combustion phases were identified (flaming and glowing). Mass loss increases with increasing the orientation angle and decreases with negative angles (against the airflow). Coefficient corresponding to mass loss in flaming combustion is one order of magnitude larger than that for glowing combustion.	[212]
Laboratory experiments	Two levels of FMC: air-dried and oven-dried. Fifty samples for each firebrand and FMC were tested. Furnace temperature: 1100 K	Needles of Pinus eldarica, P. halepensis, P. pinaster and P. pinea; Twigs of P. halepensis; Bark scales of P. halepensis; Cone scales of P. halepensis; Bark cubes of Q. suber.	Ignition success Mean time to ignition Weight loss Flaming and total combustion duration Gross heat of combustion	In all tests, all firebrands were ignited. (Ignition success 100%) The type of firebrand had a significant effect on time to ignition and flaming duration. FMC had significant effect on weight loss for all firebrand types, except for Q. suber bark cubes. Both flaming and smouldering duration differed significantly among the firebrands tested, regardless of FMC. Three firebrand groups are introduced in the context of spotting, based on the characteristics that are evaluated.	[213]
Laboratory experiments	Temperature: 1000 K, 1200 K Diameter: 2 mm, 6 mm Length: 125 mm FMC: 0.5%, 15% Firebrand type: dowel, natural Vertical wind tunnel Assumption of the 1-D convective heat transfer.	Douglas-fir, Western Juniper, Ponderosa pine, White oak.	Time required for firebrands to generate (s). Weight loss with thermogravimetric analysis.	Diameter and species type were found to be the most influential factors on firebrand generation time. Firebrand generation time for 2-mm diameter samples was almost insensitive to any other parameter, while for 6-mm of diameter, other parameters had significant contributions, suggesting the concept of a critical diameter.	[194]
Laboratory experiments	Full-scale wind tunnel experiments. FMC: 57–95%. 46 aluminium pans, 0.65-m long × 0.45-m wide downwind of vegetation in test station (14.3-m × 2.6-m) Three average wind speed: 5.36	Little Bluestem Grass, Chamise, Saw Palmetto, Loblolly Pine, Leyland Cypress	About 10,000 firebrands are assessed. Four statistical quantities (mean, standard deviation, skewness, median) are measured for three firebrand parameters: flying distance (m), projected area (cm2), mass (g).	Lognormal distribution found to be the best fit on the dataset. Strong correlation between mass and projected area existed, independent of fuel type and outside conditions. More massive and larger number of firebrands were	[324]

(*continued on next page*)

Table 6 (*continued*)

Research approach and scale	Study conditions	Vegetation/fuel	Measured quantities and values	Findings	Reference
	m/s, 11.17 m/s (14.3 m/s 3-s gust), 17.88 m/s (23 m/s 3-s gust).		Correlations between these three parameters are calculated.	generated by higher wind speeds. Firebrand mass and projected area varied in the following ranges: 0.02 g < mass <0.33 g, 0.71 cm^2 < projected area <2.49 cm^2.	
Laboratory experiments	Douglas-fir trees were burned in the absence of wind. Moisture content ranged between 10% and 50% at the time of ignition.	Three real-scale Douglas-fir trees (5.2m in height and 3m wide)	26 rectangular pans filled with water were used to collect firebrands. Each pan was 49.5 cm long by 29.5 cm wide. The arrangement of the pans was based on scoping experiments to determine the locations where the firebrands would land. The firebrands were subsequently dried, weighed and measured.	(i) Douglas-fir trees generated firebrands only for moisture content levels below 30% in the absence of wind, (ii) the vast majority of generated firebrands were cylindrical with an average size of 4 mm in diameter and 53 mm in length, and (iii) the surface area of the generated firebrands increased linearly with firebrand mass.	[191]
Experimental data collected after actual wildfire	The approximate size of assumed firebrand burn patterns, consisting of scorch marks, shallow char marks, and holes melted through plastic-type materials, were measured after the 2007 Angora fire (California, USA). Firebrand size distributions were estimated using image analysis software and compared to laboratory results to assess the possible overestimation of particle size due to progressive combustion or melting after firebrand landing.	White Fir—Jeffrey Pine forest with heavy understory. The vegetation fuels in the areas of residential development were discontinuous and varied widely from green grass lawns to ornamental landscaping and stands of conifer trees. Many of the building lots were undeveloped with managed vegetation. Pine needles and forest litter were common on and around surviving houses and in the surrounding unburned neighbourhoods.	Number and size distribution of burn patterns on affected items. A trampoline that was present in the area at the time of the fire was carried to the laboratory for analysis. Measurements on the trampoline were compared to other field observations and previous literature results.	More than 85% of the holes had an area less than 0.5 cm^2, with the largest being 2.02 cm^2. The hypothesis that the overall size distributions of burn pattern areas were representative of actual firebrand sizes was tested in the laboratory and corroborated.	[189]
Laboratory experiments	Firebrand generation from full-scale tree combustion was investigated in the absence of wind.	Douglas-fir trees, ranging in total height from 2.5 to 5.2 m and 3m maximum girth. The tree moisture content was varied	Firebrands were collected by pans filled with water. The firebrands were subsequently dried and the sizes were measured using callipers and the dry mass was determined using a precision balance.	Firebrands were cylindrical in shape. The average firebrand size measured from the 2.6-m Douglas-fir trees was 3 mm in diameter, 40 mm in length. The average firebrand size measured for the 5.2-m Douglas-fir trees was 4 mm in diameter with a length of 53 mm. The mass distribution of firebrands produced from two different tree sizes under similar tree moisture levels was similar. The surface area of the firebrands scaled with firebrand weight	[325]
Modelling	A simple mechanical firebrand breakoff model is presented for the formation of cylindrical firebrands similar to those collected from full scale tree burn experiments. Summarized a variety of statistics regarding the size and physical characteristics of firebrands (e.g., aspect ratio)	Full-scale Douglas-fir trees	Aspect ratios of firebrands and surface area or mass of trees, standard deviation of firebrand parameters such as height, mass, etc. Developed a Monte-Carlo simulation to capture measured distribution, characteristics of firebrands	The size distribution of firebrands is more dependent on the mechanics of combustion and limb failure than on a straight geometric relationship with the tree height. Geometric scaling analysis of firebrands indicated that the firebrand surface area scales on the firebrand mass raised to the 2/3rds power. The findings suggest that the size distribution of lab-scale firebrands might be similar as those for the field. Surface area and aspect ratio are only weekly correlated,	[195]
Laboratory experiments	Conducted burning experiments in a vertical wind tunnel, studied a variety of eucalyptus bark, varied moisture content, terminal velocities and burning behaviour evaluated. Wanted to	Eucalyptus bark	Ignition behaviour studied, velocity of firebrands (i.e., terminal velocity), burning behaviour, burnout time all measured,	Burning and smoldering behaviour reported is reported for varying samples and wind conditions, ignition by glowing versus flaming ignition was discussed, samples were ignited	[199]

(*continued on next page*)

Table 6 (*continued*)

Research approach and scale	Study conditions	Vegetation/fuel	Measured quantities and values	Findings	Reference
	understand terminal velocities and flight behaviour, multivariable statistical analysis conducted			and placed in wind tunnel and monitored.	
Real-scale laboratory experiments	Total tree height was 4.0 m and tree moisture content varied from 10% to 80%.	Three Korean Pine (Pinus koraiensis) trees.	Firebrands were collected using an array of pans filled with water. The firebrands were subsequently dried and the mass and size of more than 500 firebrands were measured. The Korean pine trees were also mounted on load cells during burning to determine the temporally resolved mass loss profiles	Korean pine trees do not produce significant numbers of firebrands if the MC is higher than 35% (in the absence of wind). All collected firebrands were cylindrical. The average firebrand size was 5 mm in diameter and 40 mm in length.	[326]

Table 7
Summary of studies on the transport of firebrands

Research approach and scale	Study conditions	Vegetation/fuel	Measured quantities and values	Findings	Reference
Numerical simulation	CFD modelling of firebrand transport and landing Firebrands transported by the plume are considered to be smouldering Combustion zone radius 2m	Twig firebrands were modelled as prolate ellipsoid	Convective plume formation Radial distribution of the axial plume velocity 0–16 m/s Firebrand length 5, 10, 15, 20 mm Firebrand trajectories Firebrand temperature 327–577 C	Temperature of larger firebrands at landing is higher compare to the small ones. Firebrands larger than 20 mm could not leave the combustion zone of 2 m radius fire.	[205]
Modelling	Performed detailed simulations of firebrand generation, transport, and deposition near a structure. Firebrand generation was modelled to provide distribution characteristics similar to what is reported in literature, the heat flux of deposited firebrands	Single trees were modelled	Calculated the distribution of firebrands relative to the structure, quantified the peak heat flux in an effort to understand the efficacy of the Australian Standard 3959.	The methodology is an example that can be applied. Ignition was not observed, but that was for the conditions specific to this study.	[204]
Modelling	Only fire line (the most intense segment of fire) is considered to represent the fire. It is assumed to be a straight infinitely long line. No shape and size for brands are assumed	Three surface fuel models: grass and litter, shrub and logging slash.	Mean wind speed (m/s) Minimum fire intensity (kW/m) Thermal strength (energy per unit length, kJ/m) Maximum firebrand height (m) Downwind drift distance (m)	Maximum firebrand height is proportional to square root of the thermal strength. Downwind lofting distance is found to be proportional to the product of mean windspeed and square root of the firebrand height.	[202]
Modelling and experiments	Measured and modelled the free fall characteristics of pseudo firebrands (i.e., nonreacting). Motivated by a need to understand how firebrand behave while being transported	Pseudo firebrands (non-reacting)	Data about the radial location of firebrands after being dropped from a tower	Argued that an improved transport model was developed, work supports that model should have a 6° of freedom model to consider firebrand aerodynamics, Important to consider lift and rotational forces	[203]

Table 8
Summary of studies on the deposition of firebrands and their ignition potential

Research approach and scale	Study conditions	Vegetation/fuel	Measured quantities and values	Findings	Reference
Laboratory experiments	Determination of smouldering time and thermal characteristics of bark firebrands Air flow rate 1,2,3 m/s Air flow temperature 80–85 C Horizontal and vertical arrangement of firebrands	Pine bark flakes Firebrand area 15 × 15, 20 × 20, 30 × 30 mm^2 Firebrand thickness 4–5 mm Initial firebrand mass 0.47–1.86 g	Mass loss 3.2–22.5% (horizontal) Mass loss 5–25% (vertical) Thickness expansion 76.9% ± 8.5% Smouldering time 32–109 s Maximum transport distance 146–218 m	Increase in the particle size leads to the decrease in their relative mass loss, and the rate change of the incident flow does not practically influence the mass loss change. The position of the particle plays an important role, the effect of which increases with increasing the particle size.	[219]
Laboratory experiments	Interaction of smouldering pine bark and twig firebrands with pine needle fuel beds	Pine bark flakes and twigs Bark firebrand area 15 × 15, 20 × 20, 30 × 30 mm^2 and	Smouldering and flaming ignition success	Increase in the flow rate led to increase in the probability of the fuel bed ignition.	[221]

(*continued on next page*)

Table 8 (*continued*)

Research approach and scale	Study conditions	Vegetation/fuel	Measured quantities and values	Findings	Reference
	Fuel bed density 60, 80 and 105 kg/m^3 Air flow rate and temperature: 1, 1.5, 2, 3 m/s and 40, 50, 60, 110 C respectively Number of firebrands 1–10 pcs	thickness 4–5 mm Pine twigs diameter 2 ÷ 4, 4 ÷ 6, 6 ÷ 8 mm and length 10 ± 1; 20 ± 2; 40 ± 2; 60 ± 2 mm		Higher number of firebrands increases success of ignition. Increase in the fuel bed density led to the decrease in the probability of ignition. Increase on 20° of air flow led to sharp increase of ignition success.	
Numerical simulation and laboratory experiments	3-D mathematical modelling and series of experiments of fuel bed ignition initiated by a single glowing firebrand Wind velocity: 2–3 m/s Fuel bed density 60, 80 and 105 kg/m^3 Bark firebrand MC 2.9 ± 0.2% Twig firebrand MC 3.5 ± 0.2% Fuel bed MC 9.3 ± 0.2%	Pine bark flakes and twigs Bark firebrand area 15 × 15, 20 × 20, 30 × 30 mm^2 and thickness 4–5 mm Pine twigs diameter 2 ÷ 4, 4 ÷ 6, 6 ÷ 8 mm and length 10 ± 1; 20 ± 2; 40 ± 2; 60 ± 2 mm	Ignition time 3.5–119.6 c Firebrand length vs ignition success	Irrespective of the pine bark sizes, fuel bed density or the airflow velocities, ignition by a single glowing bark firebrand was not observed. Single pine twigs ignited the fuel bed in the whole range of densities (60–105 kg/m^3) and with the airflow velocity of ≥2 m/s. Flame combustion of the fuel bed was observed only with firebrand length >10 cm.	[226]
Laboratory experiments (and developing empirical models)	Fuel bed sample 40 cm × 40 cm Air speed: 0, 1, 2 m/s 4% < FMC <21% Flaming brands made of bamboo, 2.37+-0.08 mm of diameter, terminal velocity of 3–4 m/s Glowing brands made of E. globulus, 20 × 15 x 1.3–2 mm, terminal velocity of 4 m/s Two wind tunnel speed configurations	Bamboo stick 50 mm long Bark of Eucalyptus globulus 50 mm long, 15 mm wide and ~2 mm in thickness Litter of dry-eucalypt forest	Ignition probability of fuel bed by flaming and glowing firebrands.	For flaming firebrands, fuel type does not influence the ignition probability, but wind speed (0 vs 1,2 m/s) and MC do. Flaming and glowing firebrands burned for ~9s and 2.5min, respectively. Results were found to be very sensitive to variation in parameters.	[214]
Numerical simulation	Firebrand is in glowing state. Energy loss to the surrounding is considered. Presence of moisture is considered. Dry fuel bed (worst case). Initial firebrand mass: 6.3 g Flaming while transport, 20% of mass upon landing (1.26 g). Firebrand emissivity: 0.6 No change in firebrand shape, just mass loss. Exponential effect of wind speed on mass loss. Extinction of firebrand when 90% mass burnt.	Disk firebrand of Doulas fir, 50 mm diameter and 6 mm thickness. Cylinder firebrand of Douglas-fir, 10 mm diameter and 70 mm length	Heat transfer from firebrand to fuel bed via conduction and radiation.	The temperature distribution and thermal penetration depth in the fuel bed are analysed. Higher relative contact pressure increases the maximum temperature in the fuel bed.	[225]
Laboratory experiments	Pile diameter: 6.35, 9.52,12.7 mm Pile mass: 0.5–100 g Number of firebrands for each mass: 10–202 No wind or 1.84 m/s	Birch firebrands. Fuel bed: 18 cm × 18 cm × 1.5 cm sheet of Superwool 607 and high temperature ceramic insulation board	Two measurement methods were compared, water-cooled heat flux gauge vs thin skin calorimeters. Peak heat flux of pile vs individual firebrand: 20–60 kW/m^2	Mass of a firebrand pile is introduced as a better metric compared to number of firebrands, as it does not need to account for variability in features of individual firebrands. Wind, pile mass and diameter were found influential. There was a critical pile mass above which piles did not produce higher heat fluxes. However, longer heating duration with increasing pile mass was observed.	[215]
Laboratory experiments	Eight full-scale experiments to study the impact of firebrand showers on decking assemblies under a continuous wind speed of 8 m/s	Sections of wood decking assemblies (1.2 m by 1.2 m) were constructed and attached to a re-entrant corner assembly. Douglas-fir wood pieces machined to dimensions of 7.9 mm (H) by 7.9 mm (W) by 12.7 mm (L) were used to produce firebrands.	The mass of firebrands as a function of projected area was determined for the firebrand showers directed at the decking assemblies. The time of flaming ignition was determined by visual inspection.	The mass of firebrands required for flaming ignitions was one order of magnitude lower than the firebrand mass reported in previous studies under a wind speed of 6 m/s [210] (O(10 g) vs. O(100 g)). Wind speed influences not only the spatial location and extent of the accumulated firebrands in stagnation points, but also the smouldering combustion	[209]

(*continued on next page*)

Table 8 (*continued*)

Research approach and scale	Study conditions	Vegetation/fuel	Measured quantities and values	Findings	Reference
				intensity of the accumulated firebrands.	
Laboratory experiments	Firebrands were simulated by machining wood (Pinus ponderosa) into small disks of uniform geometry and the size of the firebrands varied. Firebrands were allowed to impinge on fuel beds of shredded hardwood mulch, pine straw mulch, and cut grass. The moisture content of the fuel beds was varied.	Three different materials were used as test fuel beds for the ignition stud- ies: (1) shredded hardwood mulch; (2) pine straw mulch; and (3) cut grass.	The sizes of the firebrands, degree of air flow, and moisture content of the fuel beds were studied to determine ignition potential.	Single glowing firebrands were unable to ignite the fuel beds considered, over the range of moisture content and applied air flow tested. Flaming single firebrands were able to ignite all fuel beds tested, with the exception of hardwood fuel beds held at 11% moisture content. Multiple glowing firebrands were unable to ignite cut grass fuel beds and shredded hardwood mulch fuel beds held at 11% moisture. Ignition was only possible for other fuel beds provided large multiple glowing firebrands were used. Multiple flaming firebrands were unable to ignite hardwood fuel beds held at 11% moisture content, but were able to ignite grass fuel beds held at 11% moisture content.	[327]
Laboratory experiments	Experiments were performed to quantify firebrand accumulation. Full-scale walls of varying size were placed downstream of the NIST Continuous-Feed Firebrand Generator and the wind speed was varied in increments of 2 m/s up to 10 m/s.	Douglas-fir wood pieces, machined to dimensions of 7.9 mm (H) by 7.9 mm (W) by 12.7 mm (L) were used to produce firebrands. Two walls with dimensions of 1.32 m (H) by 2.44 m (W), and 2.44 m (H) by 2.44 m (W) were used. These were located at a distance of 7.5 m from the Continuous-Feed Firebrand Generator.	The firebrand size and mass distribution were determined as a function of wind speed. Separate experiments were conducted by placing an array of pans downstream of the firebrand generator.	For a given wall size exposed to specific firebrand size/mass distribution, it was observed that wind speed influences not only the spatial location and extent of the accumulated firebrands in the stagnation plane in front of the wall, but also the nature of the smouldering combustion intensity of the accumulated firebrands.	[328]
Laboratory experiments	The vulnerabilities of Japanese-style roof tile assemblies to firebrand exposures were investigated by using a continuous-feed firebrand generator with applied nominal wind speeds of 6 m/s and 9 m/s.	Roof tile assemblies were placed at 2.0 m from the NIST continuous-feed Dragon. Wood chips were used to simulate firebrands produced from structure combustion. A second set of experiments was performed adding debris under the roof tiles. Debris was simulated using fir and pine needles.	The number of firebrands that penetrated under the Japanese roof tiles was counted and their mass and area measured.	It was observed that Japanese-style roof tile assemblies were more vulnerable than concrete flat, concrete profile, and terracotta flat roof tiles for an applied wind speed of 6 m/s. When the experiments were performed with debris placed underneath the roof tiles, penetrated firebrands ignited debris. Flaming ignition was observed under 9 m/s where flame was observed to protrude from the tiles in an effort to reach necessary oxygen for combustion.	[329]
Review article	The paper article describes results/trends for embers made of metal, explains their potential physical state (e.g., liquid, solid) and size. Briefly describes firebrands and their burning behaviour, lists experiments and modelling efforts that consider ignition by firebrands		Ignition behaviour primarily measured	Review article regarding generation, transport of embers and subsequent spot fires	[330]
Review article	Review articles of many aspects of firebrand challenge/threat, the upward force (like internal pressure within a structural fires) is important, summarized reported ignitability of different fuels and firebrand types		Contains a review of many references	Review articles of many aspects of firebrand challenge/threat	[229]
Laboratory experiments	Particles (from different metals or pine cylinders) were heated in an oven and then dropped onto the fuel bed in a wind tunnel	Beds of cellulose or pine needles were evaluated.	Ignition probability when hot particles or firebrands are deposited on the fuel bed.	Maps of ignition (smouldering or flame) or non-igniting cases are reported for beds of cellulose. A variety of ignition sources are deposited. Hot spot theory is summarized, issues with the theory are noted, and they report	[228]

(*continued on next page*)

Table 8 (*continued*)

Research approach and scale	Study conditions	Vegetation/fuel	Measured quantities and values	Findings	Reference
				their own reduced order model to consider ignition.	
Laboratory experiments	High resolution heat flux distributions were measured for single firebrands using IR thermography and inverse heat transfer analysis	Oak wood firebrands, six firebrand geometries (cuboids with and without notches and cylinder)	Spatial and temporal variation in heat flux from a single firebrand to a surface	Peak heat fluxes 30–105 kW/m2. Firebrand geometry, wind speed and wind orientation relative to the firebrand affected the peak heat flux and the exposure duration. Cuboid shaped firebrands produced the higher heat fluxes than cylindrical shaped firebrands. Notches on the cuboid firebrands caused higher heat fluxes. The leading edge of the firebrand oriented parallel to the wind had the highest heat flux levels.	[217]
Laboratory experiments	Statistical assessment of different factors expected to have an impact on the heat flux from firebrand piles to a flat surface	Yellow Poplar, Eastern White Pine and Northern Red Oak wood firebrands. Firebrands: length of 12.5 mm, diameter of 9.5 mm. Natural (twigs) and artificial (dowels) firebrands. Live and dead	Statistical analysis was performed on the different experimental designs to determine the impact of the different factors on the firebrand pile heat flux	Wood moisture content, wood type, and density did not affect the heat flux. Higher heat fluxes are from the artificial firebrands. Wind speed and firebrand length have significant impact on heat flux while firebrand diameter and pile mass did not. Interaction between firebrand length and firebrand diameter (length times diameter) is significant. Reducing the number of firebrands in the pile impacted the heat flux.	[216]
Laboratory experiments and numerical simulation	The difference in burning behaviour and heat transfer between artificial and natural smouldering firebrands are explored through experiments and models	Firebrands were represented by twigs and dowels from northern red oak	Behaviour observation of firebrand types and how interactions of multiple elements in a pile versus individual firebrands impact the heat flux and total lifetime of the piles	Although individual firebrands had very similar peak heat fluxes, the heat flux of natural firebrand piles was lower than that of artificial firebrands. The deposited ash layer in natural firebrands was responsible for the reduced heat flux of the natural firebrand pile. The increase in surface area increases the surface losses of the natural firebrand.	[218]
Laboratory experiments and numerical simulation	An experimental and analytical effort to determine the variable relationships that control firebrand burning	Firebrands were represented by twigs from northern red oak, an average diameter of 5.25 mm and cut to a length of 50 mm	Quantification of the effects of firebrand burning behaviour under different wind conditions and with different firebrand configurations	An analytical model was developed to predict the time dependent burning of firebrands including ash accumulation in forced flow conditions. The heat and mass transfer Reynolds analogy model provided the best results for predicting char oxidation. Higher differences were predicted with arrays of firebrands, which was attributed to the complex flow field that develops around the firebrands.	[227]

Table 9
Summary of studies on the direct flame contact (or impingement)

Research approach and scale	Experimental design	Data collection method	Relevant Results and Observations	Reference
Laboratory experiments	Deck geometry comprising 5 redwood deck boards with 5 mm spacing attached to a vertical cement board wall Below-deck tests utilized a propane burner with fire size 40–80 kW/m^2. Above-deck tests utilized ASTM E2726 Class A brands	Large HRR hood to measure CO_2, CO and O_2 2 thermocouples were mounted to the deck and 12 were mounted in the center and spaced along the height of the cement board wall Two 25.4 mm (OD) water-cooled heat flux gauges, 152 mm and 508 mm above the deck surface	Under-deck Tests: - Larger burner thermal exposure resulted in faster ignition and sustained flaming -Peak heat release rate systematically decreased as thermal insult decreased Above-deck Tests: -For the same class A firebrand, peak heat flux measured on lower portion of wall	[238]

(*continued on next page*)

Table 9 (*continued*)

Research approach and scale	Experimental design	Data collection method	Relevant Results and Observations	Reference
			systematically increased as air flow velocity increased from 0 to 5 m/s -Deck orientation effects measured temperature along cement board	
Full-scale experiments	Redwood lattice fencing assembly (1.22 × 2.44 m) positioned on top of Japanese cypress wood chips and attached to a OSB stud wall (2.44 × 2.44 m) Firebrands were used to ignite mulching material which would smoulder and transition to flaming, igniting the fencing assembly The same fencing setup was used for three different air flow velocities: 4, 6, and 9 m/s	Set up was placed in front of a 4 m diameter fan and exposed to continuous firebrand attack using firebrand generator developed at NIST Flame height of ignited fencing assembly and vertical flame spread rates along the fencing assembly The size of firebrands generated from the burning fencing assembly	- The rate of flame height growth increased as the airflow rate increased from 4 to 6 m/s and then decreased as the airflow rate further increased to 9 m/s (without an OSB wall) - With the presence of a wall and a high air flow velocity (9 m/s), the rate of flame height growth rapidly increased - The enhanced oxygen supply as well as the formation of a stagnation zone enhanced recirculation in the area where the fencing assembly is burning.	[331]
Full-scale experiments	Western red cedar privacy fence (1.83 m tall and 2.44 m long) mounted on steel stands and placed on top of shredded hardwood mulch (0.05 m thick) was placed at a pre-defined spacing away from vertical wall of a wooden fence Four different gap spacings were used: 0, 0.3, 0.9, and 1.8 m The mulch and fence were exposed to a propane flame for 90 s An air flow velocity of 11 m/s (measured 1 m above the height of the ground) was straitened downstream of the privacy fence	Flame spread along the fence as well as spotting upstream of the ignition location The transient location of the flame for different gap sizes as well as the flame spread rate of the flame along the fence The flow structure in front of the vertical shed wall	- Flame spread rate along the fence was significantly affected by the gap spacing. -Larger gaps spacing corresponded to larger flame spread rates. -The location of the flame was affected by the gap size. -The only gap size of 0.3 m resulted in direct flame impingement with the shed wall -The formation of a vortex at the base of the shed wall was observed and it attributed to increase in the flame spread rate with increasing gap size. -The presence of the mulch bed is integral to sustain flaming combustion of the fence.	[332]
Full-scale experiments	Privacy fence (2.4 m long by 1.8 m tall) constructed using Western Red Cedar, California Redwood, and Vinyl with individual boards spaced 1.5 mm (on average) apart. The fence assembly was placed on a mulch bed (0.05m deep). Three different fence orientations were considered (0°, 45°, and 90°). The 0° configuration was mounted parallel to the air flow. Three air flow velocities were considered: 9, 13.5, and 18 m/s. Fence was ignited at the leading edge (the edge closest to the flow) using a propane burner at a flowrate of 20 L/min.	Four high-definition video cameras were placed around the fence to document the flame spread along the fence. Five thermocouples, mounted 0.61 m from one another, were used to document the flame spread Three water-cooled heat flux gauges and additional thermocouples were used to record the thermal exposure from the privacy fence to a wall of an adjoining structure.	-Flame spread rate along the fence was noted to be affected by both the orientation angle of the fence as well as the magnitude of the air flow -The "worst case" scenario indicative of the fastest horizontal flame spread rate was a 0° fence orientation exposed to an air flow velocity of 13.5 m/s. -The decrease in the horizontal flame spread rate when using 18 m/s as the air flow velocity can be attributed to the mulch, located underneath the fence assembly, being blown away -Visually noted that the bottom portion of a vertical wall was exposed to the highest heat flux due to the physical presence of the bulk of the flames located along the bottom third portion of the fence.	[239]
Full-scale experiments	Eleven full-scale car fires comprising a total of sixteen cars of different type were performed using a highly instrumented car park platform. A minimum separation distance between cars was 50 cm.	Calorimetry, thermocouples, heat flux gauges, load cell, gas analysis, infrared imagery and video recording.	-Flames can be "ejected" through the opening of the burning car during high intensity fire stages, which can result on flame impingement and subsequent ignition of adjacent car. -Burning spilt fuel and/or molten plastics emanated from one car to another produces pool fire with potential to fire spread via direct contact.	[236]
Full-scale experiments	Two full-scale car fires comprising a total of three cars (sedan type)	Thermocouples, infrared imagery and video recording.	-Flames can be "ejected" through the opening of the burning car during high intensity fire stages, which can result on flame impingement and subsequent ignition of adjacent car. - Burning spilt fuel and/or molten plastics emanated from one car to another produces pool fire with potential to fire spread via direct contact.	[237]
Full-scale experiments	Four experiments comprising several residential flammable items commonly involved in WUI fire scenarios.	Thermocouples, load cells, infrared imagery, gas analysis and video recording	- Peak of heat release rate and radiative heat fluxes over 2.5 MW and 20 kW/m^2 respectively shown potential for fire ignition of nearby flammable materials. - Flame heights (2.65 m–3.60 m) captured during the experiment suggested potential for ignition of elevated fuel (e.g. dead vegetation, roofing systems, rolling shutters, etc.) in the main structure via direct flame impingement. - Increase of effective burning area via fuel melting during the combustion process increases fire spread potential via flame	[241]

(*continued on next page*)

Table 9 (*continued*)

Research approach and scale	Experimental design	Data collection method	Relevant Results and Observations	Reference
			impingement. Some of the fuels almost doubled their burning surface area.	

Table 10
Summary of the experimental studies on radiation (HFG is the heat flux gauge, TSC is the thin skin calorimeter)

Fire room dimensions (L x W x H)	Fuel and HRR range	Heat flux gauge type	Maximum radiative heat flux on the target wall or outside the room	Reference
Small-scale experiments				
0.5 m × 0.5 m x 0.5 m (thermally thick)	Propane HRR 11–32 kW, Target wall	Steel plate HFGs and Gardon HFGs	13 kW/m^2 - 47 kW/m^2 0.1m–0.3m separation distance	[242]
0.5 m × 0.5 m x 0.5 m (thermally thick)	Propane HRR 20–50 kW Target wall	Steel plate HFGs and Gardon HFGs	4 kW/m^2 -61 kW/m^2 0.1m–0.5m separation distance	[243]
6 m × 3 m x 0.7 m (industrial premise) (thermally thick)	Wood cribs HRR 2.5–3.8 MW	Schmidt Boelter HFGs	1 kW/m^2 to 46 kW/m^2 5m and 50m separation distance	[244]
0.4 m × 0.4 m x 0.4 m (thermally thick)	Propane HRR 3–90 kW	Radiometer	up to 1.04 kW/m^2 (side direction) radiation fraction: 0.08 to 0.28 (ejecting flames)	[245]
0.6 m × 0.6 m x 0.9 m (thermally thin)	Polypropylene + Heptane (accelerant) HRR 50–95 kW Fuel load 24–80 MJ/m^2	TSC	2 kW/m^2 (front door and side wall) 0.1m–0.3m separation distance	[247]
0.6 m × 0.6 m x 0.9 m (thermally thin)	Polypropylene + Heptane (accelerant) HRR 100–120 kW Fuel load 80 MJ/m^2	TSC and Schmidt Boelter HFGs	5–15 kW/m^2 (front door, side wall, and back wall) 0.1m–0.3m separation distance	[248]
Full-scale experiments				
2.64 × 3.64 x 2.93/3.0 m (thermally thick) [Lab/External - unknown]	15, 25, 40 kg/m^3 pine cribs	Watercooled Radiometer (Medtherm 64)	12–47 kW/m^2 at 2m distance	[249]
3.7 m × 4.3 m x 2.4 m (thermally thick)	Typical living room furniture Fuel load 19.7 kg/m^2 Target wall	Schmidt Boelter HFGs	up to 140 kW/m^2 at 1.8m separation distance and 4.9m high	[250]
5.95 m × 4.4 m x 2.75 m (thermally thick)	Propane (flowrates unknown) or wood cribs (38 kg/m^2) HRR not informed Target wall	Radiometer	12.67 kW/m^2 - 28.75 kW/m^2 2.4m–4m separation distance	[246]
4 m × 3 m x 2.75 m (thermal thickness not applicable)	Propane HRR 1–5 MW Target wall	Gardon HFGs	3 kW/m^2 - 20 kW/m^2 3m–5m separation distance	[251]
3 m × 4 m x 3 m (thermally thick)	Propane HRR 2–4 MW Target wall	Gardon HFGs	7.44 kW/m^2 - 19.24 kW/m^2 3m–4m separation distance	[252]
3.0 × 3.0 × 2.3m 3 × steel clad 3 × timber clad [Outside with wind] (thermally thin)	Pine 45 kg/m^2 and cardboard lining 770 MJ/m^2 steel clad 1315 MJ/m^2 timber clad HRR - unspecified	TSCs calibrated against a water-cooled HFG	**Timber** -Door: 145–260 kW/m^2 1m from door: 150–273 kW/m^2 Window: 164–196 kW/m^2 **Steel** -Door: 133–156 kW/m^2 1m: 59–79 kW/m^2 2m: 35–55 kW/m^2 Window: 160–200 kW/m^2	[253]
3.0 × 3.0 × 2.3m 1 steel clad 1 timber clad [Outside with wind] (thermally thin)	Pine 45 kg/m^2 and cardboard lining 770 MJ/m^2 steel clad 1315 MJ/m^2 timber clad HRR - unspecified	TSCs calibrated against a water-cooled HFG	**Timber dwelling** Door: 106 kW/m^2 (average 93 kW/m^2) 1m door average: 43 kW/m^2 Window average: 88 kW/m^2 1m window average - 50 kW/m^2 **Steel dwelling** Door - 213 kW/m^2 (steady state 95 kW/m^2) 1m steady state: 32 kW/m^2. Window: 132 kW/m^2, (steady state 80 kW/m^2)	[254]
not applicable	HFGs tested against prescribed heat fluxes Diesel pool fire	FOA-013-01 and RAP 12.M.2	20 kW/m^2 and 40 kW/m^2 30 kW/m^2, 1.5 kW/m^2, and 1.0 kW/m^2 at 2m, 4m, and 6m, respectively (pool fire)	[255]
3.6 m × 2.4 m x 2.2 m 14 steel clad, 6 timber clad [outside with wind]	Timber cribs 392 MJ/m^2	TSC (calibrated by water-cooled HFG)	50–100 kW/m^2 no flame impingement; 100–250 kW/m^2 with flame impingement 2.2 m and 1.2m distance and side panels	[256]

(*continued on next page*)

Table 10 (*continued*)

Fire room dimensions (L x W x H)	Fuel and HRR range	Heat flux gauge type	Maximum radiative heat flux on the target wall or outside the room	Reference
3.6 m × 2.4 m x 2.4 m 4 with differentiating thermal thicknesses and amount of leakage (Laboratory)	2 timber cribs 25 kg/m^2 - 438 MJ/m^2 HRR 3.25–3.8 MW	TSCs (calibrated by water-cooled HFG)	Next to wall: 1–22.5 kW/m^2 2m away from door, 1.6m high: 11.5–15.5 kW/m^2	[257]
3.6 m × 2.4 m x 2.4 m (Laboratory) (thermally thin)	2 timber cribs 25 kg/m^2 - 438 MJ/m^2 HRR 3.25–3.8 MW	Calculated from temperatures at door using Lee and Davidson approach [278]	46 kW/m^2 radiation of flame (approx. 0.65–0.85m from door) 1 m–4 m from the dwelling, the radiation heat flux decreases from 36 kW/m^2 to 5 kW/m^2	[258]
3.6 m × 2.4 m x 2.3 m External experiment with wind 2 experiments 2 dwellings (fire origin and target dwelling) (thermally thin)	2 timber cribs 30 kg/m^2 - 510 MJ/m^2 HRR 4.5–6.5 MW	TSCs (calibrated by water-cooled HFG)	1m opposite door: peak 48 kW/m^2 (33 kW/m^2 average) 2m opposite door: 62 kW/m^2 2m from window: 28 kW/m^2 (average 22 kW/m^2) 4m from window: 17 kW/m^2 (average 14 kW/m^2) 1.75m opposite door: (average 27 kW/m^2) 1.5 m opposite door: 66 kW/m^2 2m from window: 22 kW/m^2 (average 19 kW/m^2) 4m from window: 14 kW/m^2 (average 11 kW/m^2)	[260]
3.6 m × 2.4 m x 2.3 m 3 external experiments with wind 2 dwellings (fire origin and target dwelling) (thermally thin)	2 timber cribs 30 kg/m^2 - 510 MJ/m^2 HRR - 5–8.7 MW	TSCs (calibrated by water-cooled HFG)	2m high 2m from target dwelling: 39–59 kW/m^2 (average 31–39 kW/m^2)	[261]
3.6 m × 2.4 m x 2.4 m 2 steel clad - offset 1m openings facing each other Laboratory experiment (thermally thin)	timber cribs @ 25 kg/m^2 - 438 MJ/m^2 HRR - 3.8 MW (single), 7 MW (double)	TSCs (calibrated by water-cooled HFG)	1m away from door: 15–25 kW/m^2 2.5m from alley and 2.5m high: 35 kW/m^2 at wall collapse	[259]
3.6 m × 2.4 m x 2.4 m 8 with different ventilation conditions and fuel crib locations Laboratory experiment (thermally thin)	timber cribs 25 kg/m^2 - 438 MJ/m^2 HRR - 3.25–3.8 MW	TSCs (calibrated by water-cooled HFG)	2.0m–3.0m from door: 5–15 kW/m^2 2.0m–3.0m from window: 5–12 kW/m^2	[267]

Table 11
Summary of the numerical studies on radiation from fires (FDS = Fire Dynamics Simulator; HPC = High Performance Computer)

Fire room dimensions (L x W x H)	Modelling approach	Mesh size and wind condition	Fuel and HRR	Computing hardware	Reference
Single dwelling*: *numerical modelling					
3 m × 3 m x 2.3m (thermally thin)	FDS and Ozone	Mesh: δx = 5 cm (FDS) Wind: outdoors (atmospheric wind)	FDS: Fuel: Timber cribs and timber/cardboard cladding HRR: total HRR not informed (HRR for cardboard and timber was prescribed from FPA HRRPUA x time curves) Ozone: Prescribed HRRPUA of 1138.37 kW/m2	University of Edinburgh and Stellenbosch University's HPCs	[254]
0.6 m × 0.9 m x 0.6 m (thermally thin)	FDS	Mesh: δx = 5 cm Wind: in-lab (still air)	Fuel: Polypropylene + Heptane (accelerant) HRR (prescribed): 50–95 kW	University of Edinburgh's HPC	[247]
0.6 m × 0.9 m x 0.6 m (thermally thin)	FDS	Mesh: δx = 5 cm and 2.5 cm Wind: in-lab (still air)	Fuel: Polypropylene + Heptane (accelerant) HRR (prescribed): 100–120 kW	University of Edinburgh's HPC	[248]
0.6 m × 0.9 m x 0.6 m (thermally thin and thermally thick)	FDS	Mesh: δx = 5 cm Wind: in-lab, wind (0–3 m/s)	Fuel: Propane HRR (prescribed): 25–67.5 kW	University of Edinburgh's HPC	[266]
3.6 m × 2.4 m x 2.3 m (thermally thin)	B-Risk	Mesh: not applicable. Wind: outdoors (atmospheric wind)	Fuel: timber cribs HRR (prescribed): max 8.7 MW	Not informed	[261]
Fire spread between structures*: *numerical modelling					
3 m × 3 m x 2.3 m (thermally thin) [3 dwellings side-by-side in a row]	FDS	Mesh: δx = 10 cm Wind: outdoors (atmospheric wind)	Fuel: timber (cribs and walls) + cardboard linings HRR (prescribed): HRRPUA = 1314 kW/m^2 (estimated from FPA curves and correlations)	Stellenbosch University's HPC	[269]

(*continued on next page*)

Table 11 (*continued*)

Fire room dimensions (L x W x H)	Modelling approach	Mesh size and wind condition	Fuel and HRR	Computing hardware	Reference
3.6 m × 2.4 m x 2.3 m (thermally thin) [2 dwellings facing each other]	Analytical model [radiation from gases, flames and hot walls]	Mesh: not applicable. Wind: outdoors (atmospheric wind)	Fuel: timber cribs HRR: 4.5–6.5 MW	Not informed	[260]
Urban areas [model tested in an area with 2500 buildings]	Analytical model [Inside-building sub-model: one-zone model. Fire spread sub-model: thermal radiation, fire plumes, and firebrands from the building on fire to neighbouring buildings]	Mesh: not applicable. Wind: outdoors (atmospheric wind)	Not informed	Not informed	[274]
3.6 m × 2.4 m x 2.2 m (thermally-thin) [20 dwellings in a 4 × 5 matrix configuration]	B-Risk	Mesh: not applicable. Wind: outdoors (atmospheric wind)	Fuel: timber (cribs and walls) + cardboard linings HRR: max 3.7 MW (prescribed from correlations)	Not informed	[275]

References

[1] S.L. Manzello, R. Blanchi, M.J. Gollner, D. Gorham, S. McAllister, E. Pastor, E. Planas, P. Reszka, S. Suzuki, Summary of workshop large outdoor fires and the built environment, Fire Saf. J. 100 (2018), https://doi.org/10.1016/j.firesaf.2018.07.002.

[2] K. Haynes, K. Short, G. Xanthopoulos, D. Viegas, L.M. Ribeiro, R. Blanchi, Wildfires and WUI fire fatalities, in: S.L. Manzello (Ed.), Encyclopedia of Wildfires and Wildland-Urban Interface (WUI) Fires, Springer International Publishing, Cham), 2020, pp. 1–16.

[3] S.L. Manzello, S. Suzuki, Y. Hayashi, Enabling the study of structure vulnerabilities to ignition from wind driven firebrand showers: a summary of experimental results, Large Outdoor Fires 54 (2012) 181–196.

[4] safety, ITF, Large Outdoor Fires and the Built Environment — Global Overview of Different Approaches to Standardization, ISO, 2022, p. 19.

[5] S.E. Caton, R.S.P. Hakes, D.J. Gorham, A. Zhou, M.J. Gollner, Review of pathways for building fire spread in the wildland urban interface Part I: exposure conditions, Fire Technol. 53 (2017) 429–473.

[6] J.D. Cohen, B.W. Butler, Modeling potential structure ignitions from flame radiation exposure with implications for wildland/urban interface fire management, in: Proceedings of the 13th Fire and Forest Meteorology Conference, International Association of Wildland Fire, 1998, pp. 81–86.

[7] J.H. McGuire Sfpe, Fire and the spatial separation of buildings, Fire Technol. 1 (1965) 278–287.

[8] W.E. Mell, S.L. Manzello, A. Maranghides, D. Butry, R.G. Rehm, The wildland-urban interface fire problem - current approaches and research needs, Int. J. Wildland Fire 19 (2010) 238–251.

[9] A. Maranghides, W. Mell, A case study of a community affected by the Witch and Guejito wildland fires, Fire Technol. 47 (2011) 379–420.

[10] J. Leonard, R. Blanchi, Investigation of Bushfire Attack Mechanisms Involved in House Loss in the ACT Bushfire 2003, Highett, Vic, 2005.

[11] A. Westhaver, Why Some Homes Survived: Learning from the Fort McMurray Wildland/urban Interface Fire Disaster, Institute for Catastrophic Loss Reduction Toronto, ON, Canada), 2017.

[12] D.X. Viegas, M. Figueiredo Almeida, L.M. Ribeiro, J. Raposo, M.T. Viegas, R. Oliveira, D. Alves, C. Pinto, H. Jorge, A. Rodrigues, D. Lucas, O complexo de incêndios de Pedrógão Grande e concelhos limítrofes, iniciado a 17 de junho de 2017, 2017.

[13] S. Quarles, P. Leschak, K. Worley, R. Brown, C. Iskowitz, C. Iskowitz, Lessons Learned from Waldo Canyon: FAC Mitigation Assessment Team Report, 2013.

[14] J.E. Leonard, L. Macindoe, K.B. Watson, I.D. Bennetts, M.H. Kelly, T.G. Clayton, D. Baines, Victorian 2009 Bushfire Research Response – Final Report, Bushfire CRC, 2009.

[15] A. Sekizawa, O. Goto, Challenges in Fire Protection for Cultural Property Buildings Based on the Lessons from the Shurijo Castle Fire, Fire Technology, 2022.

[16] S. Suzuki, S.L. Manzello, Characteristics of firebrands collected from actual urban fires, Fire Technol. 54 (2018) 1533–1546.

[17] S. Suzuki, S.L. Manzello, Firebrands generated in Shurijo Castle fire on October 30th, 2019, Fire Technol. 58 (2022) 777–791.

[18] A. Steen-Hansen, K. Storesund, R. Fjellgaard Mikalsen, J.P. Stensaas, A.G. Bøe, K. Hox, R.H. Gabrielsen, S. Lacasse (Eds.), The Large Fire in Lærdal, January 2014. How Did the Fire Spread and what Restricted the Fire Damage?, Natural Disasters and Societal Safety Symposium, Fagtrykk Trondheim AS, Oslo, 2015.

[19] Committee, SA, Australian Standard–Construction of Buildings in Bushfire-Prone Areas AS 3959-2018, 2018.

[20] Council, IC, 2021 International Wildland-Urban Interface Code, 2021.

[21] S.L. Manzello, S. McAllister, S. Suzuki, Large outdoor fires and the built environment: objectives and goals of permanent IAFSS working group, Fire Saf. J. 98 (2018) 1–2.

[22] E. Pastor, Direct flame contact, in: S.L. Manzello (Ed.), Encyclopedia of Wildfires and Wildland-Urban Interface (WUI) Fires, Springer International Publishing, Cham), 2020, pp. 221–226.

[23] W.R. Anderson, E.A. Catchpole, B.W. Butler, Convective heat transfer in fire spread through fine fuel beds, Int. J. Wildland Fire 19 (2010) 284–298.

[24] D. Frankman, B.W. Webb, B.W. Butler, D. Jimenez, J.M. Forthofer, P. Sopko, K. S. Shannon, J.K. Hiers, R.D. Ottmar, D. Frankman, B.W. Webb, B.W. Butler, D. Jimenez, J.M. Forthofer, P. Sopko, K.S. Shannon, J.K. Hiers, R.D. Ottmar, Measurements of convective and radiative heating in wildland fires, Int. J. Wildland Fire 22 (2012) 157–167.

[25] D. Frankman, B.W. Webb, B.W. Butler, D. Jimenez, M. Harrington, D. Frankman, B.W. Webb, B.W. Butler, D. Jimenez, M. Harrington, The effect of sampling rate on interpretation of the temporal characteristics of radiative and convective heating in wildland flames, Int. J. Wildland Fire 22 (2012) 168–173.

[26] B. Butler, C. Hardy, A Study of the Impact of Slope and Wind on Firefighter Safety Zone Effectiveness - Final Report to the Joint Fire Science Program, USDA Forest Service, Rocky Mountain Research Station, Missoula Fire Sciences Laboratory, Missoula, MT, 2014.

[27] B. Butler, R. Parsons, W. Mell, Recent Findings Relating to Firefighter Safety Zones, 2015.

[28] J.R. Gallacher, B. Ripa, B.W. Butler, T.H. Fletcher, Lab-scale observations of flame attachment on slopes with implications for firefighter safety zones, Fire Saf. J. 96 (2018) 93–104.

[29] H. Pearce, M. Finney, T. Strand, M. Katurji, C. Clements, New Zealand Field-Scale Fire Experiments to Test Convective Heat Transfer in Wildland Fires, 2019, 2019/05/01/.

[30] J. Fayad, L. Rossi, N. Frangieh, C. Awad, G. Accary, F.-J. Chatelon, F. Morandini, T. Marcelli, V. Cancellieri, D. Cancellieri, D. Morvan, A. Pieri, G. Planelles, R. Costantini, S. Meradji, J.-L. Rossi, Numerical study of an experimental high-intensity prescribed fire across Corsican Genista salzmannii vegetation, Fire Saf. J. 131 (2022), 103600.

[31] M.A. Finney, J. Forthofer, I.C. Grenfell, B.A. Adam, N.K. Akafuah, K. Saito, 'A study of flame spread in engineered cardboard fuelbeds: Part I: correlations and observations, in: Seventh International Symposium on Scale Modeling (ISSM-7); Hirosaki, Japan, International Scale Modeling Committee, 2013, p. 10, 6-9 August, 2013.

[32] M.A. Finney, J.D. Cohen, J.M. Forthofer, S.S. McAllister, M.J. Gollner, D. J. Gorham, K. Saito, N.K. Akafuah, B.A. Adam, J.D. English, Role of buoyant flame dynamics in wildfire spread, Proc. Natl. Acad. Sci. USA 112 (2015) 9833–9838.

[33] B.J. Stocks, M.E. Alexander, R.A. Lanoville, Overview of the international crown fire modelling experiment (ICFME), Can. J. For. Res. 34 (2004) 1543–1547.

[34] C.B. Clements, B. Davis, D. Seto, J. Contezac, A. Kochanski, J.B. Fillipi, N. Lareau, B. Barboni, B. Butler, S. Krueger, R. Ottmar, R. Vihnanek, W.E. Heilman, J. Flynn, M.A. Jenkins, J. Mandel, C. Teske, D. Jimenez, J. O'Brien, B. Lefer, Overview of the 2013 FireFlux II grass fire field experiment, in: D.X. Viegas (Ed.), Advances in Forest Fire Research. Coimbra, vols. 392–400, Coimbra University Press, Portugal, 2014, pp. 392–400.

[35] R.D. Ottmar, J.K. Hiers, B.W. Butler, C.B. Clements, M.B. Dickinson, A.T. Hudak, J.J. O'Brien, B.E. Potter, E.M. Rowell, T.M. Strand, T.J. Zajkowski, R.D. Ottmar, J. K. Hiers, B.W. Butler, C.B. Clements, M.B. Dickinson, A.T. Hudak, J.J. O'Brien, B. E. Potter, E.M. Rowell, T.M. Strand, T.J. Zajkowski, Measurements, datasets and preliminary results from the RxCADRE project – 2008, 2011 and 2012, Int. J. Wildland Fire 25 (2015) 1–9.

[36] C.B. Clements, A.K. Kochanski, D. Seto, B. Davis, C. Camacho, N.P. Lareau, J. Contezac, J. Restaino, W.E. Heilman, S.K. Krueger, B. Butler, R.D. Ottmar, R. Vihnanek, J. Flynn, J.-B. Filippi, T. Barboni, D.E. Hall, J. Mandel, M.A. Jenkins, J. O'Brien, B. Hornsby, C. Teske, C.B. Clements, A.K. Kochanski, D. Seto, B. Davis, C. Camacho, N.P. Lareau, J. Contezac, J. Restaino, W.E. Heilman, S.K. Krueger, B. Butler, R.D. Ottmar, R. Vihnanek, J. Flynn, J.-B. Filippi, T. Barboni, D.E. Hall, J. Mandel, M.A. Jenkins, J. O'Brien, B. Hornsby, C. Teske, The FireFlux II

experiment: a model-guided field experiment to improve understanding of fire–atmosphere interactions and fire spread, Int. J. Wildland Fire 28 (2019) 308–326.
[37] B. Butler, D. Jimenez, J. Forthofer, P. Sopko, K. Shannon, J. Reardon, In-situ characterization of wildland fire behavior, in: Dale D. Wade, Mikel L. Robinson (Eds.), Proceedings of 3rd Fire Behavior and Fuels Conference, International Association of Wildland Fire, Birmingham, AL, 2010, p. 11, 25-29 *October 2010*; *Spokane, WA*.
[38] B. Butler, C. Teske, D. Jimenez, J. O'Brien, P. Sopko, C. Wold, M. Vosburgh, B. Hornsby, E. Loudermilk, B. Butler, C. Teske, D. Jimenez, J. O'Brien, P. Sopko, C. Wold, M. Vosburgh, B. Hornsby, E. Loudermilk, Observations of energy transport and rate of spreads from low-intensity fires in longleaf pine habitat – RxCADRE 2012, Int. J. Wildland Fire 25 (2015) 76–89.
[39] T.L. Clark, L. Radke, J. Coen, D. Middleton, Analysis of small-scale convective dynamics in a crown fire using infrared video camera imagery, J. Appl. Meteorol. Climatol. 38 (1999) 1401–1420.
[40] M.B. Dickinson, C.E. Wold, B.W. Butler, R.L. Kremens, D. Jimenez, P. Sopko, J. J. O'Brien, The wildland fire heat budget—using Bi-directional probes to measure sensible heat flux and energy in surface fires, Sensors 21 (2021).
[41] W.L. Fons, Analysis of fire spread in light forest fuels, J. Agric. Res. 72 (3) (1946) 92–121, 72, 92-121.
[42] G.M. Byram, Combustion of forest fuels, in: G.M. Byram, W.R. Krumm (Eds.), Forest Fire - Control and Use, McGraw-Hill Book Co., New York, 1959, pp. 61–89.
[43] J.E. Vehrencamp, An Investigation of Fire Behavior in a Natural Atmospheric Environment, Univ. Calif. at Los Angeles, Engr. Dept. No. 55-50, 1955.
[44] E.V. Mueller, N. Skowronski, J.C. Thomas, K. Clark, M.R. Gallagher, R. Hadden, W. Mell, A. Simeoni, Local measurements of wildland fire dynamics in a field-scale experiment, Combust. Flame 194 (2018) 452–463.
[45] J.M.C. Mendes-Lopes, J.M.P. Ventura, J.M.P. Amaral, Flame characteristics, temperature–time curves, and rate of spread in fires propagating in a bed of Pinus pinaster needles, Int. J. Wildland Fire 12 (2003) 67–84.
[46] B.M. Wotton, J.S. Gould, W.L. McCaw, N.P. Cheney, S.W. Taylor, B.M. Wotton, J. S. Gould, W.L. McCaw, N.P. Cheney, S.W. Taylor, Flame temperature and residence time of fires in dry eucalypt forest, Int. J. Wildland Fire 21 (2011) 270–281.
[47] J.S. Gould, W.L. McCaw, N.P. Cheney, Project Vesta: Findings, Extension and Validation for South Eastern Australia Eucalypt Forests, 2004.
[48] H.E. Anderson, Heat Transfer and Fire Spread, Res. Pap. INT-RP-69 vol. 20, U.S. Department of Agriculture, Forest Service, Intermountain Forest and Range Experiment Station, Ogden, Utah, 1969, p. 69.
[49] S. Fehrmann, W. Jahn, J. de Dios Rivera, Permeability comparison of natural and artificial Pinus radiata forest litters, Fire Technol. 53 (2017) 1291–1308.
[50] S. Figueroa, JdD. Rivera, W. Jahn, Influence of permeability on the rate of fire spread over natural and artificial Pinus radiata forest litter, Fire Technol. 55 (2019) 1085–1103.
[51] E.V. Mueller, M.R. Gallagher, N. Skowronski, R.M. Hadden, Approaches to modeling bed drag in pine forest litter for wildland fire applications, Transport Porous Media 138 (2021) 637–660.
[52] F. Morandini, Y. Perez-Ramirez, V. Tihay, P.-A. Santoni, T. Barboni, Radiant, convective and heat release characterization of vegetation fire, Int. J. Therm. Sci. 70 (2013) 83–91.
[53] F. Morandini, X. Silvani, D. Honoré, G. Boutin, A. Susset, R. Vernet, Slope effects on the fluid dynamics of a fire spreading across a fuel bed: PIV measurements and OH* chemiluminescence imaging, Exp. Fluid 55 (2014) 1788.
[54] V. Tihay, F. Morandini, P.-A. Santoni, Y. Perez-Ramirez, T. Barboni, Combustion of forest litters under slope conditions: burning rate, heat release rate, convective and radiant fractions for different loads, Combust. Flame 161 (2014) 3237–3248.
[55] F. Morandini, X. Silvani, J.-L. Dupuy, A. Susset, Fire spread across a sloping fuel bed: flame dynamics and heat transfers, Combust. Flame 190 (2018) 158–170.
[56] H.C. Tran, J.D. Cohen, R.A. Chase, 'MODELING ignition of structures in wildland/urban interface fires, 1992/09/24/25, in: Proceedings, 1st International Fire and Materials Conference, UK: Inter Science Communications Limited, Arlington, VA. London, 1992.
[57] J.D. Cohen, Structure ignition assessment model (SIAM)1, in: David R. Weise, Robert E. Martin (Eds.), t, Echnical Coordinators. The Biswell Symposium: Fire Issues and Solutions in Urban Interface and Wildland Ecosystems; February 15-17, 1994; Walnut Creek, California. Gen. Tech. Rep. PSW-GTR-158, vol. 158, Pacific Southwest Research Station, Forest Service, U.S. Department of Agriculture, Albany, CA, 1995, pp. 85–92.
[58] J.D. Cohen, Relating flame radiation to home ignition using modeling and experimental crown fires, Can. J. For. Res. 34 (2004) 1616–1626.
[59] A.M. Grishin, A.I. Filkov, E.L. Loboda, V.V. Reyno, A.V. Kozlov, V.T. Kuznetsov, D.P. Kasymov, S.M. Andreyuk, A.I. Ivanov, N.D. Stolyarchuk, A field experiment on grass fire effects on wooden constructions and peat layer ignition, Int. J. Wildland Fire 23 (2014).
[60] R.O. Weber, Modelling fire spread through fuel beds, Prog. Energy Combust. Sci. 17 (1991) 67–82.
[61] R.R. Linn, F.H. Harlow, FIRETEC: A Transport Description of Wildfire behavior.' 1997/12/01/. Research Org.: Los Alamos National Lab. (LANL), Los Alamos, NM (United States)), 1997. Available at:.
[62] O. Séro-Guillaume, J. Margerit, Modelling forest fires. Part I: a complete set of equations derived by extended irreversible thermodynamics, Int. J. Heat Mass Tran. 45 (2002) 1705–1722.
[63] W. Mell, M.A. Jenkins, J. Gould, P. Cheney, A physics-based approach to modelling grassland fires, Int. J. Wildland Fire 16 (2007) 1–22.
[64] Y. Wang, P. Chatterjee, J.L. de Ris, Large eddy simulation of fire plumes, Proc. Combust. Inst. 33 (2011) 2473–2480.
[65] D. Morvan, G. Accary, S. Meradji, N. Frangieh, O. Bessonov, A 3D physical model to study the behavior of vegetation fires at laboratory scale, Fire Saf. J. 101 (2018) 39–52.
[66] V. Babrauskas, Ignition Handbook, Principles and Applications to Fire Safety Engineering, Fire Investigation. Risk Management and Forensic Science, Fire Science Publishers, 2003.
[67] F.A. Williams, Urban and wildland fire phenomenology, Prog. Energy Combust. Sci. 8 (1982) 317–354.
[68] R. Ball, A.C. McIntosh, J. Brindley, Feedback processes in cellulose thermal decomposition: implications for fire-retarding strategies and treatments, Combust. Theor. Model. 8 (2004) 281–291.
[69] C. Di Blasi, Comparison of semi-global mechanisms for primary pyrolysis of lignocellulosic fuels, J. Anal. Appl. Pyrol. 47 (1998) 43–64.
[70] C.P. Bankston, B.T. Zinn, R.F. Browner, E.A. Powell, Aspects of the mechanisms of smoke generation by burning materials, Combust. Flame 41 (1981) 273–292.
[71] R.A. Susott, Characterization of the thermal properties of forest fuels by combustible gas analysis, For. Sci. 28 (1982) 404–420.
[72] G.Q. James, Principles of Fire Behavior, 2016.
[73] F.C. Beall, H.W. Eickner, Thermal Degradation of Wood Components: a Review of the Literature, USDA Forest Service No, 1970. FPL 130.
[74] F. Shafizadeh, Introduction to pyrolysis of biomass, J. Anal. Appl. Pyrol. 3 (1982) 283–305.
[75] F.A. Albini, R. Baughman, Estimating Windspeeds for Predicting Wildland Fire Behavior, USDA Forest Service, Ogden, UT, 1979. Intermountain Forest and Range Experiment Station. No. Research Paper INT-RP-221.
[76] J.M. Forthofer, B.W. Butler, C.W. McHugh, M.A. Finney, L.S. Bradshaw, R. D. Stratton, K.S. Shannon, N.S. Wagenbrenner, A comparison of three approaches for simulating fine-scale surface winds in support of wildland fire management. Part II. An exploratory study of the effect of simulated winds on fire growth simulations, Int. J. Wildland Fire 23 (2014) 982–994.
[77] A. Cardil, M. Salis, D. Spano, G. Delogu, D. Molina Terrén, Large wildland fires and extreme temperatures in Sardinia (Italy), iFor, Biogeosci. For. 7 (2014) 162–169.
[78] A. Cardil, C.S. Eastaugh, D.M. Molina, Extreme temperature conditions and wildland fires in Spain, Theor. Appl. Climatol. 122 (2015) 219–228.
[79] B.E. Potter, The role of released moisture in the atmospheric dynamics associated with wildland fires, Int. J. Wildland Fire 14 (2005) 77–84.
[80] J.L. Dupuy, Slope and fuel load effects on fire behavior: laboratory experiments in pine needles fuel beds, Int. J. Wildland Fire 5 (1995) 153–164.
[81] R.R. Linn, J.L. Winterkamp, D.R. Weise, C. Edminster, A numerical study of slope and fuel structure effects on coupled wildfire behaviour, Int. J. Wildland Fire 19 (2010) 179–201.
[82] B. Porterie, S. Nicolas, J.L. Consalvi, J.C. Loraud, F. Giroud, C. Picard, Modeling thermal impact of wildland fires on structures in the urban interface. Part 1: radiative and convective components of flames representative of vegetation fires, Numer. Heat Tran., Part A: Applications 47 (2005) 471–489.
[83] B. Porterie, J.-L. Consalvi, J.-C. Loraud, F. Giroud, C. Picard, Dynamics of wildland fires and their impact on structures, Combust. Flame 149 (2007) 314–328.
[84] S. Hostikka, J. Mangs, E. Mikkola, Comparison of two and three dimensional simulations of fires at wildland urban interface, Fire Saf. Sci. 9 (2009) 1353–1364.
[85] N. Khan, D. Sutherland, R. Wadhwani, K. Moinuddin, Physics-based simulation of heat load on structures for improving construction standards for bushfire prone areas, Front. Mech. Eng. 5 (2019) 35.
[86] N. Masoudvaziri, F. Szasdi Bardales, O.K. Keskin, A. Sarreshtehdari, K. Sun, N. Elhami-Khorasani, Streamlined wildland-urban interface fire tracing (SWUIFT): modeling wildfire spread in communities, Environ. Model. Software 143 (2021), 105097.
[87] A. Maranghides, E. Link, S. Nazare, S. Hawks, J. McDougald, S. Quarles, D. Gorham, WUI Structure/Parcel/Community Fire Hazard Mitigation Methodology, 2022.
[88] V. Perminov, V. Marzaeva, Mathematical modeling of the impact of forest fires on buildings and structures, MATEC Web Conf 209 (2018), 00021.
[89] V. Perminov, K.O. Fraynova, A. Lukianov, Numerical modeling of the process of thermal impact of wildfires on buildings located near forests, Mater. Sci. Forum 970 (2019) 82–87.
[90] M. Ghodrat, F. Shakeriaski, D.J. Nelson, A. Simeoni, Existing improvements in simulation of fire–wind interaction and its effects on structures, Fire 4 (2021) 27.
[91] A. Edalati-nejad, M. Ghodrat, A. Simeoni, Numerical investigation of the effect of sloped terrain on wind-driven surface fire and its impact on idealized structures, Fire 4 (2021) 94.
[92] M. Ghaderi, M. Ghodrat, J.J. Sharples, LES simulation of wind-driven wildfire interaction with idealized structures in the wildland-urban interface, Atmosphere 12 (2021) 21.
[93] M. Ghodrat, F. Shakeriaski, D.J. Nelson, A. Simeoni, Experimental and numerical analysis of formation and flame precession of fire whirls: a review, Fire 4 (2021).
[94] A. Edalati-nejad, M. Ghodrat, S.A. Fanaee, A. Simeoni, Numerical simulation of the effect of fire intensity on wind driven surface fire and its impact on an idealized building, Fire 5 (2022) 17.
[95] M. Ghodrat, A. Edalati-Nejad, A. Simeoni, Collective effects of fire intensity and sloped terrain on wind-driven surface fire and its impact on a cubic structure, Fire 5 (2022) 208.

[96] W.G. Page, B.W. Butler, An empirically based approach to defining wildland firefighter safety and survival zone separation distances. International, Journal of Wildand Fire 26 (2017) 665–667.
[97] J.R. Curry, W.L. Fons, Forest-fire behavior studies, Mech. Eng. 62 (1940) 219–225, 219-225 62.
[98] J.S. Barrows, Fire Behavior in Northern Rocky Mountain Forests, USDA Forest Service, Missoula, MT: US, 1951. Rocky Mountain Forest and Range Experiment Station No. Research Paper RM-28.
[99] W.L. Fons, Forest fire modeling, Heat-mass Transfer and Thermodynamics (1963) 164–175.
[100] G. Byram, H. Clements, M. Bishop, R. Nelson, Project Fire Model-An Experimental Study of Model Fires, USDA Forest Service, Southeastern Forest Experiment Station, Southern Forest Fire Laboratory No. Final Report, Macon, Georgia, 1966. June 1, 1966.
[101] R.C. Rothermel, A Mathematical Model for Predicting Fire Spread in Wildland Fuels, USDA Forest Service. Intermountain Forest and Range Experiment Station, Odgen, UT, 1972.
[102] W. Parker, Development of a Model for the Heat-Release Rate of Wood. A Status Report, Final report. National Bureau of Standards, Center for Fire Research, Washington, DC (USA), 1985.
[103] V. Babrauskas, W.J. Parker, Ignitability measurements with the cone calorimeter, Fire Mater. 11 (1987) 31–43.
[104] A. Tewarson, Flammability parameters of materials: ignition, combustion, and fire propagation, J. Fire Sci. 12 (1994) 329–356.
[105] P.H. Freeborn, M.J. Wooster, W.M. Hao, C.A. Ryan, B.L. Nordgren, S.P. Baker, C. Ichoku, Relationships between energy release, fuel mass loss, and trace gas and aerosol emissions during laboratory biomass fires, J. Geophys. Res. Atmos. 113 (2008).
[106] A. Àgueda, E. Pastor, Y. Pérez, E. Planas, Experimental study of the emissivity of flames resulting from the combustion of forest fuels, Int. J. Therm. Sci. 49 (2010) 543–554.
[107] J.-L. Rossi, K. Chetehouna, A. Collin, B. Moretti, J.-H. Balbi, Simplified flame models and prediction of the thermal radiation emitted by a flame front in an outdoor fire, Combust. Sci. Technol. 182 (2010) 1457–1477.
[108] J.L. Dupuy, J. Maréchal, Slope effect on laboratory fire spread: contribution of radiation and convection to fuel bed preheating, Int. J. Wildland Fire 20 (2011) 289.
[109] N. Liu, J. Wu, H. Chen, L. Zhang, Z. Deng, K. Satoh, D. Viegas, J. Raposo, Upslope spread of a linear flame front over a pine needle fuel bed: the role of convection cooling, Proc. Combust. Inst. 35 (2014).
[110] J. Madrigal, E. Marino, M. Guijarro, C. Hernando, C. Díez, Evaluation of the flammability of gorse (Ulex europaeus L.) managed by prescribed burning, Ann. For. Sci. 69 (2012) 387–397.
[111] T. Barboni, L. Leonelli, P.-A. Santoni, V. Tihay-Felicelli, Influence of particle size on the heat release rate and smoke opacity during the burning of dead Cistus leaves and twigs, J. Fire Sci. 35 (2017) 259–283.
[112] K. Meerpoel-Pietri, V. Tihay-Felicelli, Y. Quilichini, T. Barboni, P.-A. Santoni, 'Experimental study of flammability of two decking slabs with a cone calorimeter, in: Mediterranean Combustion Symposium 11, 2019, 2019/06/16/20. Tenerife, Spain).
[113] W. Mell, A. Maranghides, R. McDermott, S.L. Manzello, Numerical simulation and experiments of burning douglas fir trees, Combust. Flame 156 (2009) 2023–2041.
[114] F. Morandini, P.A. Santoni, J.B. Tramoni, W.E. Mell, Experimental investigation of flammability and numerical study of combustion of shrub of rockrose under severe drought conditions, Fire Saf. J. 108 (2019), 102836.
[115] P. Bartoli, A. Simeoni, H. Biteau, J.L. Torero, P.A. Santoni, Determination of the main parameters influencing forest fuel combustion dynamics, Fire Saf. J. 46 (2011) 27–33.
[116] N. Chiaramonti, E. Romagnoli, P.A. Santoni, T. Barboni, Comparison of the combustion of pine species with two sizes of calorimeter: 10 g vs. 100 g, Fire Technol. 53 (2017) 741–770.
[117] J-w Wang, J. Fang, J-f Guan, Y. Zeng, Y-m Zhang, Flame volume and radiant fraction of jet diffusion methane flame at sub-atmospheric pressures, Fuel 167 (2016) 82–88.
[118] A. Tewarson, Generation of heat and chemical compounds in fires, in: SFPE Handbook of Fire Protection Engineering, 2002.
[119] J.B. Fang, F.R. Steward, Flame spread through randomly packed fuel particles, Combust. Flame 13 (1969) 392–398.
[120] P. Boulet, G. Parent, A. Collin, Z. Acem, B. Porterie, J.P. Clerc, J.L. Consalvi, A. Kaiss, Spectral emission of flames from laboratory-scale vegetation fires, Int. J. Wildland Fire 18 (2009) 875–884.
[121] P. Boulet, G. Parent, Z. Acem, A. Collin, O. Séro-Guillaume, On the emission of radiation by flames and corresponding absorption by vegetation in forest fires, Forest Fires 46 (2011) 21–26.
[122] P. Boulet, G. Parent, Z. Acem, A. Kaiss, Y. Billaud, B. Porterie, Y. Pizzo, C. Picard, Experimental investigation of radiation emitted by optically thin to optically thick wildland flames, Journal of Combustion (2011), 137437, 2011.
[123] J.-L. Dupuy, J. Maréchal, D. Morvan, Fires from a cylindrical forest fuel burner: combustion dynamics and flame properties, Combust. Flame 135 (2003) 65–76.
[124] S.B. Show, Climate and forest fires in Northern California, J. For. 17 (1919) 965–979.
[125] J.R. Curry, W.L. Fons, Rate of spread of surface fires in the ponderosa pine type of California, J. Agric. Res. 57 (1938) 239–267.
[126] N.P. Cheney, J. Gould, W. Anderson, The influence of fuel, weather and fire shape variables on fire-spread in grasslands, Int. J. Wildland Fire 3 (1993) 31–44.
[127] N. Cheney, J. Gould, Fire growth in grassland fuels, Int. J. Wildland Fire 5 (1995) 237–247.
[128] B.W. Butler, J. Cohen, D.J. Latham, R.D. Schuette, P. Sopko, K.S. Shannon, D. Jimenez, L.S. Bradshaw, Measurements of radiant emissive power and temperatures in crown fires, Can. J. For. Res. 34 (2004) 1577–1587.
[129] P.A. Santoni, A. Simeoni, J.L. Rossi, F. Bosseur, F. Morandini, X. Silvani, J. H. Balbi, D. Cancellieri, L. Rossi, Instrumentation of wildland fire: characterisation of a fire spreading through a Mediterranean shrub, Fire Saf. J. 41 (2006) 171–184.
[130] C.B. Clements, S. Zhong, S. Goodrick, J. Li, B.E. Potter, X. Bian, W.E. Heilman, J. J. Charney, R. Perna, M. Jang, D. Lee, M. Patel, S. Street, G. Aumann, Observing the dynamics of wildland grass fires: FireFlux - a field validation experiment, Bull. Am. Meteorol. Soc. 88 (2007) 1369–1382.
[131] X. Silvani, F. Morandini, Fire spread experiments in the field: temperature and heat fluxes measurements, Fire Saf. J. 44 (2009) 279–285.
[132] X. Silvani, F. Morandini, J.-F. Muzy, Wildfire spread experiments: fluctuations in thermal measurements, Int. Commun. Heat Mass Tran. 36 (2009) 887–892.
[133] F. Morandini, X. Silvani, Experimental investigation of the physical mechanisms governing the spread of wildfires, Int. J. Wildland Fire 19 (2010) 570–582.
[134] M.G. Cruz, B.W. Butler, D.X. Viegas, P. Palheiro, Characterization of flame radiosity in shrubland fires, Combust. Flame 158 (2011) 1970–1976.
[135] M.B. Dickinson, A.T. Hudak, T. Zajkowski, E.L. Loudermilk, W. Schroeder, L. Ellison, R.L. Kremens, W. Holley, O. Martinez, A. Paxton, B.C. Bright, J. J. O'Brien, B. Hornsby, C. Ichoku, J. Faulring, A. Gerace, D. Peterson, J. Mauceri, Measuring radiant emissions from entire prescribed fires with ground, airborne and satellite sensors – RxCADRE 2012, Int. J. Wildland Fire 25 (2016) 48.
[136] A.T. Hudak, M.B. Dickinson, B.C. Bright, R.L. Kremens, E.L. Loudermilk, J. J. O'Brien, B.S. Hornsby, R.D. Ottmar, Measurements relating fire radiative energy density and surface fuel consumption – RxCADRE 2011 and 2012, Int. J. Wildland Fire 25 (2016) 25.
[137] M.G. Cruz, R.J. Hurley, R. Bessell, A.L. Sullivan, Fire behaviour in wheat crops – effect of fuel structure on rate of fire spread, Int. J. Wildland Fire 29 (2020) 258.
[138] R.L. Kremens, M.B. Dickinson, A.S. Bova, Radiant flux density, energy density and fuel consumption in mixed-oak forest surface fires, Int. J. Wildland Fire 21 (2012) 722–730.
[139] J.M. Johnston, M.J. Wooster, R. Paugam, X. Wang, T.J. Lynham, L.M. Johnston, Direct estimation of Byram's fire intensity from infrared remote sensing imagery, Int. J. Wildland Fire 26 (2017) 668–684.
[140] D.X. Viegas, M.G. Cruz, L.M. Ribeiro, A.J. Silva, A. Ollero, B.C. Arrue, R. Dios, F. Gomez-Rodriguez, L. Merino, A.I. Miranda, P. Santos, 'Gestosa fire spread experiments, in: Proceedings of the 4th International Conference on Forest Fire Research, 2002, 2002. Luso, Portugal).
[141] P.A. Martins Fernandes, Fire spread prediction in shrub fuels in Portugal, For. Ecol. Manag. 144 (2001) 67–74.
[142] E. Bilgili, B. Saglam, Fire behavior in maquis fuels in Turkey, For. Ecol. Manag. 184 (2003) 201–207.
[143] M. De Luis, M.J. Baeza, J. Raventós, J.C. González-Hidalgo, Fuel characteristics and fire behaviour in mature Mediterranean gorse shrublands, Int. J. Wildland Fire 13 (2004) 79–87.
[144] P.-A. Santoni, F. Morandini, T. Barboni, Steady and unsteady fireline intensity of spreading fires at laboratory scale, Open Therm. J. 4 (2010) 212–219.
[145] I.K. Knight, M. Dando, N.B.F.R. Unit, Radiation above Bushfires, National Bushfire Research Unit, 1989.
[146] A.L. Sullivan, P.F. Ellis, I.K. Knight, A review of radiant heat flux models used in bushfire applications, Int. J. Wildland Fire 12 (2003) 101–110.
[147] D. Morvan, J.L. Dupuy, Modeling the propagation of a wildfire through a Mediterranean shrub using a multiphase formulation, Combust. Flame 138 (2004) 199–210.
[148] F. Pimont, J.L. Dupuy, R.R. Linn, Coupled slope and wind effects on fire spread with influences of fire size: a numerical study using FIRETEC, Int. J. Wildland Fire 21 (2012) 828–842.
[149] Y. Perez-Ramirez, W.E. Mell, P.A. Santoni, J.B. Tramoni, F. Bosseur, Examination of WFDS in modeling spreading fires in a furniture calorimeter, Fire Technol. 53 (2017) 1795–1832.
[150] D. Morvan, N. Frangieh, Wildland fires behaviour: wind effect versus Byram's convective number and consequences upon the regime of propagation, Int. J. Wildland Fire 27 (2018) 636–641.
[151] X. Sánchez-Monroy, W. Mell, J. Torres-Arenas, B.W. Butler, Fire spread upslope: numerical simulation of laboratory experiments, Fire Saf. J. 108 (2019), 102844.
[152] J.E. Hilton, J.E. Leonard, R. Blanchi, G.J. Newnham, K. Opie, A. Power, C. Rucinski, W. Swedosh, Radiant heat flux modelling for wildfires, in: The 22nd International Congress on Modelling and Simulation Held in Tasmania, Australia, vol. 175, 2020, pp. 62–80. December 3–8, 2017.
[153] J.R. Howell, M.P. Mengüç, K. Daun, R. Siegel, Thermal Radiation Heat Transfer, 2020.
[154] W.W. Yuen, RAD-NNET, a neural network based correlation developed for a realistic simulation of the non-gray radiative heat transfer effect in three-dimensional gas-particle mixtures, Int. J. Heat Mass Tran. 52 (2009) 3159–3168.
[155] M.F. Modest, The treatment of nongray properties in radiative heat transfer: from past to present, J. Heat Tran. 135 (2013).
[156] A. Selamet, V.S. Arpaci, Rayleigh limit—penndorf extension, Int. J. Heat Mass Tran. 32 (1989) 1809–1820.
[157] L. Wang, M.F. Modest, D.C. Haworth, S.R. Turns, Modeling nongray gas-phase and soot radiation in luminous turbulent nonpremixed jet flames, Combust. Theor. Model. 9 (2005) 673–691.

[158] W.W. Yuen, C.L. Tien, A simple calculation scheme for the luminous-flame emissivity, Symposium (International) on Combustion 16 (1977) 1481–1487.
[159] M.F. Modest, Radiative Heat Transfer, Academic Press, 2013.
[160] M. Alberti, R. Weber, M. Mancini, A. Fateev, S. Clausen, Validation of HITEMP-2010 for carbon dioxide and water vapour at high temperatures and atmospheric pressures in 450-7600cm-1 spectral range, J. Quant. Spectrosc. Radiat. Transfer 157 (2015) 14–33.
[161] L.S. Rothman, I.E. Gordon, R.J. Barber, H. Dothe, R.R. Gamache, A. Goldman, V. I. Perevalov, S.A. Tashkun, J. Tennyson, HITEMP, the high-temperature molecular spectroscopic database, XVIth Symposium on High Resolution Molecular Spectroscopy (HighRus-2009) 111 (2010) 2139–2150.
[162] W. Grosshandler, A Narrow-Band Model for Radiation Calculations in a Combustion Environment, National Institute of Standards and Technology (NIST), Gaithersburg, MD No, 1993. NIST Technical Note, 1402.
[163] F. Liu, Numerical solutions of three-dimensional non-grey gas radiative transfer using the statistical narrow-band model, J. Heat Tran. 121 (1999) 200–203.
[164] L. Pierrot, A. Soufiani, J. Taine, Accuracy of narrow-band and global models for radiative transfer in H2O, CO2, and H2O CO2 mixtures at high temperature, XVIth Symposium on High Resolution Molecular Spectroscopy (HighRus-2009) 62 (1999) 523–548.
[165] H.C. Hottel, Radiant heat transmission, in: W.H. McAdams (Ed.), Heat Transmission, McGraw-Hill, New York, 1954.
[166] T.F. Smith, Z.F. Shen, J.N. Friedman, Evaluation of coefficients for the weighted sum of gray gases model, J. Heat Tran. 104 (1982) 602–608.
[167] N. Crnomarković, M. Sijercic, S. Belosevic, D. Tucakovic, T. Zivanovic, Numerical investigation of processes in the lignite-fired furnace when simple gray gas and weighted sum of gray gases models are used, Int. J. Heat Mass Tran. 56 (2013) 197–205.
[168] H.C. Hottel, Radiative Transfer, McGraw-Hill, New York), 1967.
[169] D.K. Edwards, Molecular gas band radiation, in: T.F. Irvine, J.P. Hartnett (Eds.), Advances in Heat Transfer, vol. 12, Elsevier, 1976, pp. 115–193.
[170] A. Soufiani, J. Taine, High temperature gas radiative property parameters of statistical narrow-band model for H2O, CO2 and CO, and correlated-K model for H2O and CO2, Int. J. Heat Mass Tran. 40 (1997) 987–991.
[171] W.W. Yuen, W.C. Tam, W.K. Chow, Assessment of radiative heat transfer characteristics of a combustion mixture in a three-dimensional enclosure using RAD-NETT (with application to a fire resistance test furnace), Int. J. Heat Mass Transfer 68 (2014) 383–390.
[172] W.C. Tam, W. Yuen, Assessment of Radiation Solvers for Fire Simulation Models Using RADNNET-ZM, Asia-Oceania Symposium on Fire Science and Technology, 2018, 2018/10//. Singapore.
[173] S. Sen, I.K. Puri, Thermal radiation modeling in fl ames and fi res, in: M. Faghri, B. Sunden (Eds.), Transport Phenomena in Fires, vol. 31, WIT Press, 2008, pp. 301–325.
[174] Y. Billaud, A. Kaiss, J.L. Consalvi, B. Porterie, Monte Carlo estimation of thermal radiation from wildland fires, Int. J. Therm. Sci. 50 (2011) 2–11.
[175] K.O. Fryanova, V.A. Perminov, Impact of forest fires on buildings and structures, Magazine of Civil Engineering 75 (2017) 15–22.
[176] M.A. Dietenberger, C.R. Boardman, EcoSmart fire as structure ignition model in wildland urban interface: predictions and validations, Fire Technol. 53 (2017) 577–607.
[177] G. Penney, S. Richardson, Modelling of the radiant heat flux and rate of spread of wildfire within the urban environment, Fire 2 (2019).
[178] M. El Houssami, E. Mueller, J.C. Thomas, A. Simeoni, A. Filkov, N. Skowronski, M.R. Gallagher, K. Clark, R. Kremens, Experimental procedures characterising firebrand generation in wildland fires, Fire Technol. 52 (2016) 731–751.
[179] S.L. Manzello, S. Suzuki, M.J. Gollner, A.C. Fernandez-Pello, Role of firebrand combustion in large outdoor fire spread, Prog. Energy Combust. Sci. 76 (2020), 100801.
[180] J.S. Gould, W.L. McCaw, N.P. Cheney, P.F. Ellis, I.K. Knight, A.L. Sullivan, Project Vesta: Fire in Dry Eucalypt Forest: Fuel Structure, Fuel Dynamics and Fire Behaviour, CSIRO Publishing, 2008.
[181] N. Skowronski, A. Simeoni, K. Clark, W. Mell, M. Gallagher, E. Mueller, R. Kremens, M.E. Houssami, A. Filkov, C. Thomas, Evaluation and Optimization of Fuel Treatment Effectiveness with an Integrated Experimental/Modeling Approach, 2016. Final Project Report No. 12-1-03-11, Joint Fire Science Program. Available at: https://www.firescience.gov/projects/12-1-03-11/project/12-1-03-11_final_report.pdf. (Accessed 11 April 2021).
[182] A. Filkov, S. Prohanov, E. Mueller, D. Kasymov, P. Martynov, M. El Houssami, J. Thomas, N. Skowronski, B. Butler, M. Gallagher, W. Mell, R. Kremens, R. M. Hadden, A. Simeoni, Investigation of firebrand production during prescribed fires conducted in a pine forest, Proc. Combust. Inst. 36 (2017) 3263–3270.
[183] A. Filkov, S. Prohanov, Particle tracking and detection software for firebrands characterization in wildland fires, Fire Technol. 55 (2019) 817–836.
[184] S. Prohanov, A. Filkov, D. Kasymov, M. Agafontsev, V. Reyno, Determination of firebrand characteristics using thermal videos, Fire 3 (2020) 68.
[185] R. Hadden, N. Skowronski, M. Gallagher, C. Thomas, E. Mueller, Measurement of firebrands generated during fires in pine-dominated ecosystems in relation to fire behavior and intensity. Joint Fire Science Program, Available at: https://www.firescience.gov/projects/15-1-04-55/project/15-1-04-55_final_report.pdf, 2020. (Accessed 11 April 2021).
[186] J.C. Thomas, E.V. Mueller, S. Santamaria, M. Gallagher, M. El Houssami, A. Filkov, K. Clark, N. Skowronski, R.M. Hadden, W. Mell, A. Simeoni, Investigation of firebrand generation from an experimental fire: development of a reliable data collection methodology, Fire Saf. J. 91 (2017) 864–871.
[187] S. Pokswinski, M.R. Gallagher, N.S. Skowronski, E.L. Loudermilk, J.J. O'Brien, J. K. Hiers, Diurnal pine bark structure dynamics affect properties relevant to firebrand generation, Fire 3 (2020).
[188] S. Rissel, K. Ridenour, Ember production during the bastrop complex fire, Fire Management Today 72 (2013) 7–13.
[189] S.L. Manzello, E.I.D. Foote, Characterizing firebrand exposure from wildland-urban interface (WUI) fires: results from the 2007 Angora fire, Fire Technol. 50 (2014) 105–124.
[190] S.L. Manzello, A. Maranghides, W.E. Mell, Firebrand generation from burning vegetation<xref ref-type="fn" rid="FN1">1</xref&gt, Int. J. Wildland Fire 16 (2007) 458–462.
[191] S.L. Manzello, T.G. Cleary, J.R. Shields, A. Maranghides, W. Mell, J.C. Yang, Experimental investigation of firebrands: generation and ignition of fuel beds, Fire Saf. J. 43 (2008) 226–233.
[192] F. Hedayati, B. Bahrani, A. Zhou, S.L. Quarles, D.J. Gorham, A framework to facilitate firebrand characterization, Front. Mech. Eng. 5 (2019).
[193] A. Zhou, S. Quarles, D.R. Weise, Fire Ember Production from Wildland and Structural Fuels, North Carolina State University No. JFSP Project, Raleigh, NC, 2019. No. 15-1-04-4.
[194] T.R. Hudson, D.L. Blunck, Effects of fuel characteristics on ember generation characteristics at branch-scales, Int. J. Wildland Fire 28 (2019) 941–950.
[195] A. Tohidi, N. Kaye, W. Bridges, Statistical description of firebrand size and shape distribution from coniferous trees for use in Metropolis Monte Carlo simulations of firebrand flight distance, Fire Saf. J. 77 (2015) 21–35.
[196] B.W. Barr, O.A. Ezekoye, Thermo-mechanical modeling of firebrand breakage on a fractal tree, Proc. Combust. Inst. 34 (2013) 2649–2656.
[197] A. Maranghides, D. McNamara, R. Vihnanek, J. Restaino, C. Leland, A Case Study of a Community Affected by the Waldo Fire Event Timeline and Defensive Actions, 2015.
[198] M.G. Cruz, A.L. Sullivan, J.S. Gould, N.C. Sims, A.J. Bannister, J.J. Hollis, R. J. Hurley, Anatomy of a catastrophic wildfire: the black Saturday kilmore East fire in Victoria, Australia, For. Ecol. Manag. 284 (2012) 269–285.
[199] P.F. Ellis, The Aerodynamic and Combustion Characteristics of Eucalypt Bark—A Firebrand Study, Ph.D. Dissertation, Australian National University, Canberra, 2000.
[200] W.G. Page, N.S. Wagenbrenner, B.W. Butler, D.L. Blunck, An analysis of spotting distances during the 2017 fire season in the Northern Rockies, USA, Can. J. For. Res. 49 (2018) 317–325.
[201] M.A. Storey, O.F. Price, R.A. Bradstock, J.J. Sharples, Analysis of variation in distance, number, and distribution of spotting in Southeast Australian wildfires, Fire 3 (2020).
[202] F.A. Albini, Potential Spotting Distance from Wind-Driven Surface Fires, 1983. No. INT-309.
[203] A. Tohidi, N.B. Kaye, Aerodynamic characterization of rod-like debris with application to firebrand transport, J. Wind Eng. Ind. Aerod. 168 (2017) 297–311.
[204] A. Wickramasinghe, N. Khan, K. Moinuddin, Physics-based Simulation of Firebrand and Heat Flux on Structures in the Context of AS3959, 2020.
[205] O.V. Matvienko, A.I. Filkov, Simulation of firebrands transport generated by the seat of fire, Proc. SPIE-Int. Soc. Opt. Eng. 9680 (2015).
[206] A. Tohidi, N.B. Kaye, Comprehensive wind tunnel experiments of lofting and downwind transport of non-combusting rod-like model firebrands during firebrand shower scenarios, Fire Saf. J. 90 (2017) 95–111.
[207] P.J. Richards, N. Williams, B. Laing, M. McCarty, M. Pond, Numerical calculation of the three-dimensional motion of wind-borne debris, J. Wind Eng. Ind. Aerod. 96 (2008) 2188–2202.
[208] S.L. Manzello, J.R. Shields, T.G. Cleary, A. Maranghides, W.E. Mell, J.C. Yang, Y. Hayashi, D. Nii, T. Kurita, On the development and characterization of a firebrand generator, Fire Saf. J. 43 (2008) 258–268.
[209] S.L. Manzello, S. Suzuki, Experimental investigation of wood decking assemblies exposed to firebrand showers, Fire Saf. J. 92 (2017) 122–131.
[210] S.L. Manzello, S. Suzuki, Exposing decking assemblies to continuous wind-driven firebrand showers, Fire Saf. Sci. 11 (2014) 1339–1352.
[211] S. Suzuki, S.L. Manzello, Investigating coupled effect of radiative heat flux and firebrand showers on ignition of fuel beds, Fire Technol. 57 (2021) 683–697.
[212] M. Almeida, D.X. Viegas, A.I. Miranda, V. Reva, Effect of particle orientation and of flow velocity on the combustibility of Pinus pinaster and Eucalyptus globulus firebrand material, Int. J. Wildland Fire 20 (2011) 946–962.
[213] A. Ganteaume, M. Guijarro, M. Jappiot, C. Hernando, C. Lampin-Maillet, P. Pérez-Gorostiaga, J.A. Vega, Laboratory characterization of firebrands involved in spot fires, Ann. For. Sci. 68 (2011) 531–541.
[214] P.F.M. Ellis, The likelihood of ignition of dry-eucalypt forest litter by firebrands, Int. J. Wildland Fire 24 (2015) 225–235.
[215] R.S.P. Hakes, H. Salehizadeh, M.J. Weston-Dawkes, M.J. Gollner, Thermal characterization of firebrand piles, Fire Saf. J. 104 (2019) 34–42.
[216] E. Bearinger, B.Y. Lattimer, J.L. Hodges, C. Rippe, A. Kapahi, Statistical assessment of parameters affecting firebrand pile heat transfer to surfaces, Front. Mech. Eng. 7 (2021).
[217] E.D. Bearinger, J.L. Hodges, F. Yang, C.M. Rippe, B.Y. Lattimer, Localized heat transfer from firebrands to surfaces, Fire Saf. J. 120 (2021), 103037.
[218] S. Wong, J.L. Hodges, B.Y. Lattimer, Impact of ash layer retention on heat transfer in piles of vegetation and structure firebrands, Fire Saf. J. 134 (2022), 103694.
[219] V. Fateev, M. Agafontsev, S. Volkov, A. Filkov, Determination of smoldering time and thermal characteristics of firebrands under laboratory conditions, Fire Saf. J. 91 (2017) 791–799.
[220] A. Filkov, D. Kasymov, V. Zima, O. Matvienko, Experimental investigation of surface litter ignition by bark firebrands, AIP Conf. Proc. 1698 (2016).

[221] D.P. Kasymov, A.I. Filkov, D.A. Baydarov, O.V. Sharypov, Interaction of smoldering branches and pine bark firebrands with fuel bed at different ambient conditions, Proc. SPIE-Int. Soc. Opt. Eng. 10035 (2016).
[222] S. Zen, J.C. Thomas, E.V. Mueller, B. Dhurandher, M. Gallagher, N. Skowronski, R.M. Hadden, Development of a Field Deployable Firebrand Flux and Condition Measurement System, Fire Technology, 2020.
[223] K. Kempná, Investigation of Wooden Structures Ignition by Firebrand Accumulation, Vysoká škola báňská - Technical University Ostrava, 2015.
[224] K. Meerpoel-Pietri, V. Tihay-Felicelli, P.-A. Santoni, Determination of the critical conditions leading to the ignition of decking slabs by flaming firebrands, Fire Saf. J. 120 (2021), 103017.
[225] A. Warey, Influence of thermal contact on heat transfer from glowing firebrands, Case Stud. Therm. Eng. 12 (2018) 301–311.
[226] O.V. Matvienko, D.P. Kasymov, A.I. Filkov, O.I. Daneyko, D.A. Gorbatov, Simulation of fuel bed ignition by wildland firebrands, Int. J. Wildland Fire (2018) 550–561.
[227] B.Y. Lattimer, E. Bearinger, S. Wong, J.L. Hodges, Evaluation of models and important parameters for firebrand burning, Combust. Flame 235 (2022), 111619.
[228] A.C. Fernandez-Pello, C. Lautenberger, D. Rich, C. Zak, J. Urban, R. Hadden, S. Scott, S. Fereres, Spot fire ignition of natural fuel beds by hot metal particles, embers, and sparks, Combust. Sci. Technol. 187 (2015) 269–295.
[229] E. Koo, P.J. Pagni, D.R. Weise, J.P. Woycheese, Firebrands and spotting ignition in large-scale fires, Int. J. Wildland Fire 19 (2010) 818–843.
[230] R.S.P. Hakes, S.E. Caton, D.J. Gorham, M.J. Gollner, A review of pathways for building fire spread in the wildland urban interface Part II: response of components and systems and mitigation strategies in the United States, Fire Technol. 53 (2017) 475–515.
[231] L. Noordijk, T. Lemaire, Modelling of fire spread in car parks, Heron 50 (2005) 209–218.
[232] A. Sargeant, J. Leonard, S. Brown, R. Blanchi, Civilian Passenger Vehicle Burnover Experimentation. Australasian Fire Authorities Council No. AFAC, 2006. "Guidance for People in Vehicles during Bushfires, 2006.
[233] Sargeant Leonard, JBRBSA, Civilian passenger vehicle burnover experimentation, in: The Joint AFAC/Bushfire CRC Conference 2007, 2007.
[234] M.Z.M. Tohir, M. Spearpoint, C. Fleischmann, Prediction of time to ignition in multiple vehicle fire spread experiments, Fire Mater. 42 (2018) 69–80.
[235] M. Sodangi, Building Information Modelling—Development and Validation of Implementation Framework for Improving Performance of Subcontractors, 2019.
[236] Building Research Establishment, Fire Spread in Car Parks (BD2552), 2010. London. Available at: http://webarchive.nationalarchives.gov.uk/20120919132719/http://www.communities.gov.uk/documents/planningandbuilding/pdf/1795610.pdf.
[237] X.H. Jiang, G.Q. Zhu, H. Zhu, D.Y. Li, Full-scale experimental study of fire spread behavior of cars, Procedia Eng. 211 (2018) 297–305.
[238] L.E. Hasburgh, D.S. Stone, S.L. Zelinka, Laboratory investigation of fire transfer from exterior wood decks to buildings in the wildland–urban interface, Fire Technol. 53 (2017) 517–534.
[239] E.L. Johnsson, A. Maranghides, Effects of Wind Speed and Angle on Fire Spread along Privacy Fences, National Institute of Standards & *Technology*, 2016, pp. 1–28.
[240] D. Caballero, J. Sjöström, Deliverable D5. Inventory of pattern scenarios, Available at: https://wuiview.webs.upc.edu/download/WUIVIEW_D5.1_F.zip, 2019. Accessed 31/08/2022.
[241] P. Vacca, E. Planas, C. Mata, J.A. Muñoz, F. Heymes, E. Pastor, Experimental analysis of real-scale burning tests of artificial fuel packs at the Wildland-Urban Interface, Saf. Sci. 146 (2022), 105568.
[242] A. Yanagisawa, D. Goto, Y. Ohmiya, M.A. Delichatsios, Y. Lee, K. Wakatsuki, Effect of a facing wall on façade flames, Fire Saf. Sci. 9 (2008) 801–811.
[243] Y.-P. Lee, M.A. Delichatsios, Y. Ohmiya, K. Wakatsuki, A. Yanagisawa, D. Goto, Heat fluxes on opposite building wall by flames emerging from an enclosure, Proc. Combust. Inst. 32 (2009) 2551–2558.
[244] H. Ingason, A. Lönnermark, Fire spread between industrial premises, Fire Saf. Sci. 10 (2011) 1305–1317.
[245] F. Ren, L. Hu, X. Sun, K. Hu, Experimental study on flame radiation fraction of facade fire ejected from opening of a compartment, Appl. Therm. Eng. 129 (2018) 573–576.
[246] H. Cheng, G. Hadjisophocleous, Experimental study and modeling of radiation from compartment fires to adjacent buildings, Fire Saf. J. 53 (2012) 43–62.
[247] M. Beshir, Y. Wang, F. Centeno, R. Hadden, S. Welch, D. Rush, Semi-empirical model for estimating the heat release rate required for flashover in compartments with thermally-thin boundaries and ultra-fast fires, Fire Saf. Sci.: Proceedings of the 13th International Symposium 120 (2021), 103124.
[248] M. Beshir, K. Omar, F.R. Centeno, S. Stevens, L. Gibson, D. Rush, Experimental and numerical study for the effect of horizontal openings on the external plume and potential fire spread in informal settlements, Appl. Sci. 11 (2021).
[249] C.-Y. Lin, Study of exposure fire spread between buildings by radiation, J. Chin. Inst. Eng. 23 (2000) 493–504.
[250] A. Maranghides, E.L. Johnsson, Residential Structure Separation Fire Experiments, 2008. NIST No. NIST Technical Note 1600.
[251] D. Glennie, G S Vallerent Hadjisophocleous, C. Florence (Eds.), Calculation of Radiant Heat Flux from Compartment Fires in Various Ventilation Conditions, 2013, 2013. Available at: http://www.matec-conferences.org/10.1051/matecconf/20130902006, 2021/10/29/13:18:40.
[252] M. Turco, P. Lhotsky, G. Hadjisophocleous, Investigation into the use of a water curtain over openings to prevent fire spread, MATEC Web of Conferences 46 (2016), 04001.
[253] A. Cicione, R.S. Walls, C. Kahanji, Experimental study of fire spread between multiple full scale informal settlement dwellings, Fire Saf. J. 105 (2019) 19–27.
[254] A. Cicione, M. Beshir, R.S. Walls, D. Rush, Full-scale informal settlement dwelling fire experiments and development of numerical models, Fire Technol. 56 (2020) 639–672.
[255] V. Nyzhnyk, O. Tarasenko, O. Kyrychenko, S. Kosiarum, S. Pozdieiev, The criteria of estimating risks of spreading fire to adjacent building facilities, IOP Conf. Ser. Mater. Sci. Eng. 708 (2019), 012064.
[256] N. de Koker, R.S. Walls, A. Cicione, Z.R. Sander, S. Löffel, J.J. Claasen, S.J. Fourie, L. Croukamp, D. Rush, 20 dwelling large-scale experiment of fire spread in informal settlements, Fire Technol. 56 (2020) 1599–1620.
[257] Y. Wang, M. Beshir, A. Cicione, R. Hadden, M. Krajcovic, D. Rush, A full-scale experimental study on single dwelling burning behavior of informal settlement, Fire Saf. Sci.: Proceedings of the 13th International Symposium 120 (2021), 103076.
[258] Y. Wang, L. Gibson, M. Beshir, D. Rush, Determination of critical separation distance between dwellings in informal settlements fire, Fire Technol. 57 (2021) 987–1014.
[259] Y. Wang, M. Beshir, R. Hadden, A. Cicione, M. Krajcovic, L. Gibson, D. Rush, Laboratory experiment of fire spread between two informal settlement dwellings, Int. J. Therm. Sci. 171 (2022), 107195.
[260] A. Cicione, R. Walls, Z. Sander, N. Flores, V. Narayanan, S. Stevens, D. Rush, The effect of separation distance between informal dwellings on fire spread rates based on experimental data and analytical equations, Fire Technol. 57 (2021) 873–909.
[261] A. Cicione, R. Walls, S. Stevens, Z. Sander, N. Flores, V. Narayanan, D. Rush, An Experimental and Numerical Study on the Effects of Leakages and Ventilation Conditions on Informal Settlement Fire Dynamics, Fire Technology, 2021.
[262] C. Barnett, Fire separation between external walls of buildings, Fire Saf. Sci. 2 (1989) 841–850.
[263] Y. Wang, C. Bertrand, M. Beshir, C. Kahanji, R. Walls, D. Rush, Developing an experimental database of burning characteristics of combustible informal dwelling materials based on South African informal settlement investigation, Fire Saf. J. 111 (2020), 102938.
[264] K.B. McGrattan, S. Hostikka, J.E. Floyd, Fire Dynamics Simulator (Version 6), User's Guide, NIST special publication, 2014.
[265] J. Cadorin, D. Pintea, J. Franssen, The Design Fire Tool OZone V2. 0-Theoretical Description and Validation on Experimental Fire Tests, Rapport interne SPEC/2001_01 University of Liege, 2001.
[266] F.R. Centeno, M. Beshir, D. Rush, Influence of wind on the onset of flashover within small-scale compartments with thermally-thin and thermally-thick boundaries, Fire Saf. J. 117 (2020), 103211.
[267] C.K. Lemmertz, R.P. Helfenstein, M. Beshir, D. Rush, W.J. Von Arnswaldt, F. R. Centeno, Semi-empirical correlations for predicting hot gas layer temperature in pre-flashover compartment fires considering fire source location, J. Braz. Soc. Mech. Sci. Eng. 44 (2022) 195.
[268] C. Wade, G. Baker, K. Frank, R. Harrison, M. Spearpoint, B-RISK 2016 User Guide and Technical Manual, 2016, p. 144.
[269] A. Cicione, R.S. Walls, Towards a simplified fire dynamic simulator model to analyse fire spread between multiple informal settlement dwellings based on full-scale experiments, Fire Mater. 45 (2021) 720–736.
[270] M.J. Hurley, D. Gottuk Jr., K. H Harada, E. Kuligowski, M. Puchovsky, J. Torero Jr., C. W Wieczorek, SFPE Handbook of Fire Protection Engineering, fifth ed., 2016.
[271] M. Beshir, M. Mohamed, S.A. Kouritem, C.K. Lemmertz, F.R. Centeno, D. Rush, Investigating numerically the effect of wind on fire spread between two informal settlements dwellings, Fire Technol. (2023).
[272] D. Rush, G. Luoyi, A. Trimble, M. Beshir, L. Gibson, Modelling the Influence of Wind on Fire Spread within Informal Settlements, 12th Asia-Oceania Symposium on Fire Science and Technology, AOSFST 2021, 2021.
[273] L. Gibson, A. Cicione, S. Stevens, D. Rush, The influence of wind and the spatial layout of dwellings on fire spread in informal settlements in Cape Town, Comput. Environ. Urban Syst. 91 (2022), 101734.
[274] K. Himoto, T. Tanaka, Development and validation of a physics-based urban fire spread model, Fire Saf. J. 43 (2008) 477–494.
[275] A. Cicione, L. Gibson, C. Wade, M. Spearpoint, R. Walls, D. Rush, Towards the development of a probabilistic approach to informal settlement fire spread using ignition modelling and spatial metrics, Fire 3 (2020).
[276] C. Wade, G.B. Baker, K. Frank, R. Harrison, M. Spearpoint, B-RISK 2016 User Guide and Technical Manual, BRANZ, 2016.
[277] V. Babrauskas, Heat release rates, in: SFPE Handbook of Fire Protection Engineering, Springer, 2016, pp. 799–904.
[278] S.W. Lee, R.A. Davidson, Physics-based simulation model of post-earthquake fire spread, J. Earthq. Eng. 14 (2010) 670–687.
[279] F.J. Vodvarka, Firebrand Field Studies-Final Report, IIT Research Institute, 1969.
[280] Y. Wang, J. Sun, L. He, Q. Wang, D. Rush, Experimental study on fallout behaviour of tempered glass façades with different frame insulation conditions in an enclosure fire, Proc. Combust. Inst. 37 (2019) 3889–3898.
[281] Y. Wang, M. Beshir, L. Gibson, S. Stevens, L. Bisby, D. Rush, How "informal" is an informal settlement fire? SFPE Europe 2 (2020).
[282] Y. Hasemi, N. Yasui, N. Itagaki, Ji Izumi, T. Osaka, T. Kaku, T. Naruse, I. Hagiwara, K. Kagiya, Ji Suzuki, Full-scale Fire Tests of 3-story Wooden School

Building, World Conference on Timber Engineering, Canada., Quebec City, 2014, 2014.
[283] S. Suzuki, S.L.J. Manzello, Firebrand production from building components fitted with siding treatments, Fire Saf. J. vol. 80 (2016) 64–70.
[284] S.L. Manzello, S. Suzuki, T.J.F. Naruse, materials, Quantifying Wind-driven Firebrand Production from Roofing Assembly Combustion, vol. 43, 2019, pp. 3–7.
[285] P.J. Pagni, Thermal Glass Breakage, Fire Safety Science-Proceedings of the Seventh International Symposium, 2002, IAFSS, Worcester, Massachusetts, USA), 2002.
[286] S.L. Manzello, R.G. Gann, S.R. Kukuck, K.R. Prasad, W.W. Jones, An experimental determination of a real fire performance of a non-load bearing glass wall assembly, Fire Technol. 43 (2007) 77–89.
[287] Y. Wang, Q. Wang, Y. Su, J. Sun, L. He, K.M. Liew, Fracture behavior of framing coated glass curtain walls under fire conditions, Fire Saf. J. 75 (2015) 45–58.
[288] S. Suzuki, A review on structure ignitions by firebrands, Bulletin of Japan Association for Fire Science and Engineering 67 (2017) 49–55.
[289] A. Green, N.B. Kaye, On the use of sprays to intercept airborne embers during wildfires, Fire Saf. J. 108 (2019), 102842.
[290] J.C. Yang, S.L. Manzello, A dimensional analysis on firebrand penetration through a mesh screen, Fuel 160 (2015) 114–116.
[291] A. Sharifian, J. Hashempour, A novel ember shower simulator for assessing performance of low porosity screens at high wind speeds against firebrand attacks, J. Fire Sci. 34 (2016) 335–355.
[292] J. Hashempour, AJJofs Sharifian, Effective Factors on the Performance of Woven Wire Screens against Leaf Firebrand Attacks, vol. 35, 2017, pp. 303–316.
[293] S. Loder, Wildfire protection tests focus on the details of construction: researchers seek to reduce the damage caused by windblown embers, Eng. News Rec. 283 (2) (2019).
[294] T. Nishino, K. Himoto, T. Tanaka, Development of a probabilistic model of spotting fires by firebrands considering resident firefighting, Bulletin of Japan Association for Fire Science Engineering 60 (2010) 11–20.
[295] E. Koo, R.R. Linn, P.J. Pagni, C.B. Edminster, Modelling firebrand transport in wildfires using HIGRAD/FIRETEC, Int. J. Wildland Fire 21 (2012) 396–417.
[296] J. Dold, K. Scott, J. Sanders, The Processes Driving an Ember Storm, SPEIC14 – towards Sustainable Combustion, 2014, 2014/11/19/21. Lisboa, Portugal.
[297] L.A. Sanabria, I.A. French, R.P. Cechet, Building Fire Impact Model, MODSIM 2013 Conference Proceedings, 2013, 2013.
[298] S.L. Lee, J.M. Hellman, Firebrand trajectory study using an empirical velocity-dependent burning law, Combust. Flame 15 (1970) 265–274.
[299] H. Huang, R. Ooka, S. Kato, Y. Hayashi, A numerical study of firebrands scattering in urban fire based on CFD and firebrands aerodynamics measurements, J. Fire Sci. 25 (2007) 355–378.
[300] K. Himoto, T. Tanaka, Transport of disk-shaped firebrands in a turbulent boundary layer, J Fire Safety Science 8 (2005) 433–444.
[301] E. Koo, P. Pagni, R. Linn, 'Using FIRETEC to describe firebrand behavior in wildfires, in: The Tenth International Symposium of Fire and Materials.', 2007, 2007.
[302] N. Sardoy, J.-L. Consalvi, B. Porterie, A.C. Fernandez-Pello, Modeling transport and combustion of firebrands from burning trees, Combust. Flame 150 (2007) 151–169.
[303] Y.D. Kim, Y. Hayashi, C.Y.J. Tri, S.J. Baek, A Numerical Study on Travel Distances of Firebrands by Wind, 7th Asia-Pacific Conference on Wind Engineering, APCWE-VII, Taipei, Taiwan, 2009, 2009.
[304] C.M. Thomas, J.J. Sharples, J.P. Evans, The terminal-velocity assumption in simulations of long-range ember transport, Math. Comput. Simulat. 175 (2020) 96–107.
[305] A. Tohidi, N.B. Kaye, 'The sensitivity of modeled flight distance to the lofting to transport transition criterion in coupled ember flight models, in: Proceedings of the 12th Americas Conference on Wind Engineering, 2013. Seattle.' 2013.
[306] B. Nader, J.-B. Filippi, P. Bisgambiglia, A DEVS Fire Jumps Model and Associated Simulations Using ForeFire, SummerSim, 2010, 2010.
[307] M. Hamada, On the Rate of Fire Spread, Disaster Research, vol. 1, Non-life Insurance Rating Organization of Japan, 1951, pp. 35–44.
[308] T.I. Zohdi, A machine-learning framework for rapid adaptive digital-twin based fire-propagation simulation in complex environments, Comput. Methods Appl. Mech. Eng. 363 (2020), 112907.
[309] R.A. Anthenien, S.D. Tse, A. Carlos Fernandez-Pello, On the trajectories of embers initially elevated or lofted by small scale ground fire plumes in high winds, Fire Saf. J. 41 (2006) 349–363.
[310] M. Janssens, Use of Bench-Scale Piloted Ignition Data for Mathematical Fire Models, 1989, 1989/09//undefined.
[311] M. Janssens, Fundamental Thermophysical Characteristics of Wood and Their Role in Enclosure Fire Growth, Doctoral Dissertation thesis, Ghent University, 1991.
[312] NIST 'National Fire Research Laboratory, Available at: https://www.nist.gov/el/fire-research-division-73300/national-fire-research-laboratory-73306. July 19.
[313] National Research and Development Agency 'Building Research Institute, Available at: https://www.kenken.go.jp/english/index.html. July 19.
[314] Suncorp, CSIRO, James Cook University, Room 11 Architects 'one house.', Available at: https://ecos.csiro.au/one-house-to-save-many/. July 19.
[315] University of Corsica, Explorii platform, Available at: https://feuxdeforet.universita.corsica/article.php?id_site=33&id_menu=0&id_rub=412&id_cat=0&id_art=5730&lang=fr. July 19.
[316] A. Maranghides, D. McNamara, R. Vihnanek, J. Restaino, C. Leland, A Case Study of a Community Affected by the Waldo Fire Event Timeline and Defensive Actions, NIST Technical Note No. 1910, 2015.
[317] A.C. Miranda, H.S. Miranda, IdFO. Dias, BFdS. Dias, Soil and air temperatures during prescribed cerated fires in Central Brazil, J. Trop. Ecol. 9 (1993) 313–320.
[318] J.P. Hidalgo, C. Maluk, A. Cowlard, C. Abecassis-Empis, M. Krajcovic, J.L. Torero, A Thin Skin Calorimeter (TSC) for quantifying irradiation during large-scale fire testing, Int. J. Therm. Sci. 112 (2017) 383–394.
[319] aL. Sullivan, A review of wildland fire spread modelling, 1990-present 3: mathematical analogues and simulation models, Int. J. Wildland Fire (2009) 1–42.
[320] W. Mell, A. Maranghides, R. McDermott, S.L. Manzello, Numerical simulation and experiments of burning douglas fir trees, Combust. Flame 156 (2009) 2023–2041.
[321] J.D. Walker, B.J. Stocks, Thermocouple errors in forest fire research, Fire Technol. 4 (1968) 59–62.
[322] C.W. Philpot, No. Res. Note PSW-RN-090, in: Temperatures in a Large Natural-Fuel Fire, U.S. Department of Agriculture, Forest Service, Pacific Southwest Forest and Range Experiment Station, Berkeley, CA, 1966.
[323] X. Silvani, F. Morandini, J.L. Dupuy, A. Susset, R. Vernet, O. Lambert, Measuring velocity field and heat transfer during natural fire spread over large inclinable bench, Exp. Therm. Fluid Sci. 92 (2018) 184–201.
[324] B. Bahrani, Characterization of Firebrands Generated from Selected Vegetative Fuels in Wildland Fires, The University of North Carolina at Charlotte, 2020.
[325] S.L. Manzello, A. Maranghides, W.E. Mell, Firebrand generation from burning vegetation, Int. J. Wildland Fire 16 (2007) 458–462.
[326] S.L. Manzello, A. Maranghides, J.R. Shields, W.E. Mell, Y. Hayashi, D. Nii, Mass and size distribution of firebrands generated from burning Korean pine (Pinus koraiensis) trees, Fire Mater. 33 (2009) 21–31.
[327] S.L. Manzello, T.G. Cleary, J.R. Shields, J.C. Yang, Ignition of mulch and grasses by firebrands in wildlandurban interface fires, Int. J. Wildland Fire 15 (2006) 427–431.
[328] S. Suzuki, S.L. Manzello, Experimental investigation of firebrand accumulation zones in front of obstacles, Fire Saf. J. 94 (2017) 1–7.
[329] S. Suzuki, S.L. Manzello, Experimental study on vulnerabilities of Japanese-Style tile roof assemblies to firebrand exposures, Fire Technol. 56 (2020) 2315–2330.
[330] A.C. Fernandez-Pello, Wildland fire spot ignition by sparks and firebrands, Fire Saf. Sci. 91 (2017) 2–10.
[331] S. Suzuki, S.L. Manzello, Understanding structure ignition vulnerabilities using mock-up sections of attached wood fencing assemblies, Fire Mater. 43 (2019) 675–684.
[332] K.M. Bulter, E. Johnsson, M. Fernandez, M. Zarzecki, E. Auth, Flame spread along fences near a structure in a wind, in: Fire Safety - International Conference on Research and Advanced Technology in Fire Safety2, 2017.